Supporting information

Acceptor-Donor-Acceptor (A-D-A) Derivatives Based on Dibenzochrysene

Félix Gagnon,[a] *Chloé Dindault,*[b] *Eve Paradis,*[a] *Guillaume Wantz*[b] *and Jean-François Morin*[a,]*

[a] Département de Chimie and Centre de Recherche sur les Matériaux Avancés (CERMA), Université Laval, Pavillon A.-Vachon. 1045 Ave de la Médecine, Québec, G1V 0A6, Canada

[b] Univ. Bordeaux, CNRS, Bordeaux INP, IMS, UMR 5218, F-33400 Talence, France

Corresponding author: jean-francois.morin@chm.ulaval.ca

TABLE OF CONTENTS

APPARATUS **3**

GENERAL METHODS **4**

EXPERIMENTAL SECTION **5**

COMPOUND 3 5

COMPOUND 4 6

COMPOUND 5 7

COMPOUND 6 8

COMPOUND 7 9

COMPOUND 8 10

COMPOUND 9 12

COMPOUND 10 13

COMPOUND 11 14

NMR SPECTRA **16**

UV-VIS SPECTROSCOPY **34**

ELECTROCHEMISTRY **37**

THERMOGRAVIMETRIC ANALYSIS **46**

DIFFERENTIAL SCANNING CALORIMETRY **47**

COMPUTATIONAL CHEMISTRY **49**

ORGANIC SOLAR CELLS DEVICES **65**

REFERENCES **73**

Apparatus

NMR spectra were recorded using a Bruker AC-300 spectrometer at 300 MHz or Varian Inova AS400 spectrometer (Varian, Palo Alto, USA) at 400 MHz or an Agilent DD2 500 MHz. Signals are reported as s (singlet), d (doublet), t (triplet), dd (doublet of doublets), dt (doublet of triplets), m (multiplet) and coupling constants (*J*) are reported in hertz (Hz). The chemical shifts are reported in ppm (δ) relative to the residual solvent peak. High-resolution mass spectra (HRMS) were recorded using an Agilent 6210 time-of-flight (TOF) LCMS apparatus equipped with an ESI and APPI ion source (Agilent Technologies, Toronto, Canada). UV-visible spectra of compounds in solution were recorded on a Varian diode-array spectrophotometer (model Cary 7000) using 10 mm path length quartz cells. UV-visible spectra of compounds in thin film were recorded on a SAFAS-monaco UVmc2 spectrophotometer on glass substrates. Fluorescence spectra of compounds in solution were recorded on a Cary Eclipse Varian fluorimeter using 10 mm path length quartz cells. Cyclic voltammograms (CVs) were recorded on a BioLogic SP-50e Single-channel potentiostat using platinum wires as working and counter electrodes at a scan rate of 50 $mV \cdot s^{-1}$ and an Ag/Ag^+ (0.01 M of $AgNO_3$ in dichloromethane) reference electrode in an anhydrous and nitrogen-saturated solution of 0.1 M of tetrabutylammonium hexafluorophosphate ([*n*-Bu_4N][PF_6]) in dry dichloromethane. In these conditions, for a freshly prepared reference electrode, the half-wave oxidation potential ($E_{½}$) of ferrocene should be around 0.475 V versus Ag/Ag^+.[1, 2] The highest occupied molecular orbital (HOMO) and the lowest unoccupied molecular orbital (LUMO) were determined from the peaks obtained in differential pulse voltammetry (DPV) at a scan rate of 10 mV s^{-1}. The ferrocene/ferrocenium couple was established at 4.8 V below the vacuum level.[3-6]

$$E_{HOMO} = -[(E^{½}_{ox\ vs\ Ag/Ag^{+}}) - (E^{½}_{Ferrocene\ vs\ Ag/Ag^{+}}) + 4.8]$$

$$E_{LUMO} = -[(E^{½}_{red\ vs\ Ag/Ag^{+}}) - (E^{½}_{Ferrocene\ vs\ Ag/Ag^{+}}) + 4.8]$$

Thermogravimetric analysis (TGA) spectra were recorded using a Mettler TGA/SDTA-851e/SF/1100 °C instrument equipped with a MT1 model balance. The balance was protected by a constant flow of PP nitrogen at a flow of 20 mL/minute. 2 mg of samples were weighted and heated from 50 °C to 800 °C at 20 °C/minute. Differential scanning calorimetry (DSC) thermograms were recorded on a Mettler Toledo DSC 823 calorimeter using N_2 flow with a heating ramp rate of 10 °C/minute. Prior to T_c measurements, the thermal history was erased with a heating scan at 20 °C/minute followed by a cooling scan at -10 °C/minute.

General Methods

Chemical reagents were purchased from Sigma–Aldrich Co. Canada, Oakwood Products, Inc., 1PlusChem Inc. or Brilliant Matters and were used as received. Vat Orange 1 was purchased from Hangzhou Chungyo Chemical Co. Ltd. and was washed using *N*,*N*-dimethylformamide prior to use.

Experimental Section

Compounds **1** and **2**,[7] 1-bromo-4-(octyloxy)benzene,[8] 4-octyloxyaniline[9] and 5-iodothiophene-2-carbaldehyde[10] were synthesized according to reported procedures.

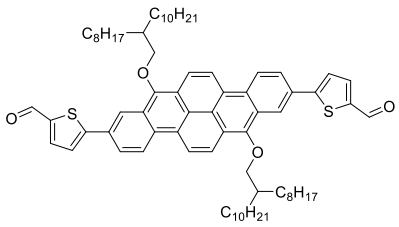

Compound 3: A high-pressure vessel equipped with a magnetic stir bar was charged with compound **2** (1.00 g, 0.8715 mmol), dichlorobis(triphenylphosphine)palladium(II) (62 mg, 0.087 mmol), triphenylphosphine (46 mg, 0.17 mmol) and potassium carbonate (482 mg, 3.49 mmol). The vessel was put under vacuum for 15 minutes before 5-bromothiophene-2-carbaldehyde (666 mg, 3.49 mmol) was added. Then, the vessel was purged using three vacuum-nitrogen cycles before the addition of degassed toluene (29 mL) and degassed water (1.7 mL). The pressure vessel cap was screwed, and the mixture was vigorously stirred at 110 °C for 72 hours. After cooling to room temperature, the mixture was washed three times with water and the organic layer was dried with magnesium sulfate. The solvent was removed under reduced pressure and the resulting solid was purified using column chromatography (silica gel, hexanes followed with ethyl acetate:hexanes 1:4 and hot chloroform as eluent) to provide compound **3** as an orange solid (784 mg, 80 %).

^{1}H NMR (400 MHz, chloroform-*d*) δ 9.94 (s, 2H), 8.96 (d, *J* = 9.2 Hz, 2H), 8.85 (d, *J* = 1.9 Hz, 2H), 8.81 (d, *J* = 9.9 Hz, 2H), 8.48 (d, *J* = 9.5 Hz, 2H), 8.01 (d, *J* = 8.8 Hz, 2H), 7.81 (d, *J* = 3.9 Hz, 2H), 7.63 (d, *J* = 3.9 Hz, 2H), 4.18 (d, *J* = 5.3 Hz, 4H), 2.26 – 2.11 (m, 2H), 1.87 (dq, *J* = 14.2, 7.4 Hz, 4H), 1.78 – 1.65 (m, 4H), 1.61 – 1.51 (m, 12H), 1.50 – 1.43 (m, 8H), 1.42 – 1.20 (m, 36H), 0.88 (dd, *J* = 8.8, 7.3 Hz, 12H).

^{13}C NMR (126 MHz, carbon disulfide:dimethyl sulfoxide-d_6 (4:1)) δ 180.44, 152.52, 149.70, 142.61, 136.55, 129.72, 127.59, 125.03, 124.82, 124.25, 124.16, 123.48, 123.33, 122.19, 121.78, 120.59, 119.58, 78.76, 39.30, 31.66, 31.65, 31.18, 29.95, 29.51, 29.49, 29.47, 29.44, 29.15, 26.97, 22.63, 22.62, 13.97, 13.96.

HRMS (APPI+): $C_{74}H_{98}O_4S_2$ $[M]^+$ 1114.6907 m/z, found 1114.6973 m/z, diff 5.97 ppm.

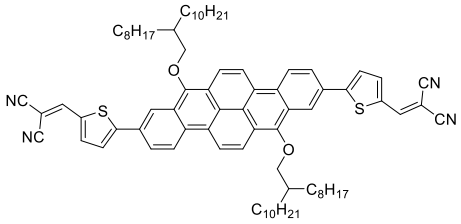

Compound 4: In a dried round bottom flask equipped with a magnetic stir bar, compound **3** (100 mg, 89.6 μmol) and propanedinitrile (29 mg, 448 μmol) were added. The vessel was put under vacuum for 15 minutes and purged using three vacuum-nitrogen cycles before the addition of degassed anhydrous toluene (89 mL). The mixture was stirred for 10 minutes at 50 °C before triethylamine (1.25 μL, 8.96 μmol) was added. The mixture was stirred for an additional 16 hours at 50 °C before acetic anhydride (2 mL, 21 mmol) was added. After an additional 24 hours at 50 °C, the mixture was washed three times with water and the solvent was removed under reduced pressure. The resulting solid was triturated in methanol to provide the desired compound **4** as a dark brown solid (100 mg, 93 %).

^{1}H NMR (500 MHz, carbon disulfide:dimethyl sulfoxide-d_6 (4:1)) δ 9.06 (d, J = 9.2 Hz, 2H), 8.87 (d, J = 9.8 Hz, 2H), 8.83 (d, J = 2.0 Hz, 2H), 8.56 (s, 2H), 8.47 (d, J = 9.4 Hz, 2H), 8.13 (dd, J = 9.0, 1.9 Hz, 2H), 7.99 (d, J = 4.2 Hz, 2H), 7.78 (d, J = 4.0 Hz, 2H), 4.22 (d, J = 5.7 Hz, 4H), 2.24 (p, J = 6.1 Hz, 2H), 1.90 (dq, J = 13.9, 6.8 Hz, 4H), 1.75 (dq, J = 13.1, 6.1 Hz, 4H), 1.63 – 1.54 (m, 8H), 1.53 – 1.45 (m, 8H), 1.45 – 1.24 (m, 40H), 0.95 (dt, J = 9.2, 7.0 Hz, 12H).

^{13}C NMR (126 MHz, carbon disulfide:dimethyl sulfoxide-d_6 (4:1)) δ 154.46, 150.95, 149.94, 140.67, 134.79, 129.16, 127.78, 125.21, 124.82, 124.70, 124.45, 123.57, 123.31, 122.30, 121.88, 120.72, 120.09, 113.38, 112.53, 79.07, 75.72, 39.12, 31.65, 31.63, 31.04, 29.85, 29.48, 29.43, 29.15, 29.13, 26.80, 22.60, 13.94.

HRMS (APPI+): $C_{80}H_{98}N_4O_2S_2$ $[M]^+$ 1210.7131 m/z, found 1210.7186 m/z, diff 4.53 ppm.

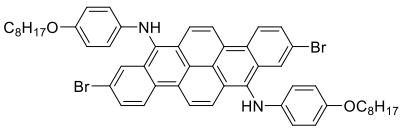

Compound 5: A dried round bottom flask equipped with a magnetic stir bar was charged with 2,9-dibromodibenzo[*b,def*]chrysene-7,14-dione (1.00 g, 2.04 mmol), 4-octyloxyaniline (993 mg, 4.49 mmol) and 1,4-diazabicyclo[2.2.2]octane (1.37 g, 12.24 mmol). The flask was vacuumed for 15 minutes and purged using three vacuum-nitrogen cycles before the addition of degassed anhydrous toluene (136 mL). The reaction was cooled down to 0 °C before titanium(IV) chloride (9.18 mL, 9.18 mmol) was added. The mixture was stirred for 16 hours at 105 °C before it was cooled down at room temperature and diluted with chloroform. The reaction was filtered under vacuum and the solvent was removed under reduced pressure. The resulting solid was triturated in cold methanol, filtered and dried under vacuum. This imine intermediate and sodium tetrahydroborate (617 mg, 16.3 mmol) were added to a dried round bottom flask equipped with a magnetic stir bar. The flask was vacuumed for 15 minutes and purged using three vacuum-nitrogen cycles before it was cooled down to 0 °C and degassed anhydrous tetrahydrofuran (68 mL) was added. The mixture was stirred for 15 minutes at 0 °C before methanol (1 mL) was added dropwise. The mixture was then stirred for 16 hours while warming up to room temperature before it was quenched with a saturated solution of ammonium chloride. The mixture was extracted with chloroform and the combined organic layers were washed with distilled water and brine (three times) and dried with magnesium

sulfate. The solvent was removed under reduced pressure and the resulting solid was triturated with cold methanol, filtered and dried under vacuum to provide the desired compound **5** as a red solid (1.19 g, 65 %).

^{1}H NMR (500 MHz, carbon disulfide:dimethyl sulfoxide-d_6 (4:1)) δ 8.94 (dd, J = 9.3, 1.8 Hz, 2H), 8.85 (dd, J = 9.9, 1.8 Hz, 2H), 8.72 (d, J = 2.1 Hz, 2H), 8.46 (d, J = 9.5 Hz, 2H), 8.20 (d, J = 4.4 Hz, 2H), 7.81 (dd, J = 9.0, 2.1 Hz, 2H), 6.68 – 6.51 (m, 8H), 3.84 (t, J = 6.5 Hz, 4H), 1.74 (dq, J = 8.8, 6.4 Hz, 4H), 1.54 – 1.28 (m, 20H), 1.04 – 0.90 (m, 6H).

^{13}C NMR (126 MHz, carbon disulfide:dimethyl sulfoxide-d_6 (4:1)) δ 151.21, 141.68, 132.34, 129.47, 128.29, 126.58, 126.30, 126.02, 125.14, 124.56, 124.45, 123.85, 121.73, 120.18, 114.83, 114.64, 67.43, 31.59, 29.24, 29.19, 29.08, 25.91, 22.61, 13.97.

HRMS (APPI+): $C_{52}H_{54}Br_2N_2O_2$ $[M]^+$ 896.2552 m/z, found 896.2587 m/z, diff 3.88 ppm.

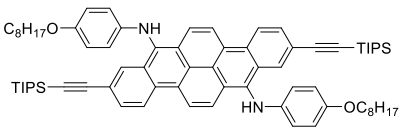

Compound 6: A dried round bottom two-neck flask equipped with a magnetic stir bar was charged with compound **5** (4,00 g, 4.45 mmol), dichlorobis(triphenylphosphine)palladium(II) (187 mg, 267 µmol) and copper(I) iodide (42 mg, 222 µmol). The flask was vacuumed for 15 minutes and purged using three vacuum-nitrogen cycles before the addition of degassed anhydrous tetrahydrofuran (89 mL) and *N*-(propan-2-yl)propan-2-amine (18 mL). The mixture was degassed for 10 minutes with nitrogen before triisopropylsilylacetylene (3.25 g, 17.8 mmol) was added. The reaction was degassed for 5 minutes before being heated at reflux for 16 hours. The reaction was cooled down at room temperature, quenched with a saturated aqueous solution of ammonium chloride and extracted three times with chloroform. The combined organic layers were dried with magnesium sulfate, filtered under

vacuum and the solvent was removed under reduced pressure. The resulting solid was purified through column chromatography (silica gel, hexanes:dichloromethane 3:2 as the eluent) before being precipitated in methanol and filtered under vacuum to provide the desired compound **6** as a red solid (3.31 g, 67 %).

^{1}H NMR (400 MHz, chloroform-*d*) δ 8.87 (d, *J* = 9.0 Hz, 2H), 8.76 (d, *J* = 10.0 Hz, 2H), 8.52 (d, *J* = 1.7 Hz, 2H), 8.37 (d, *J* = 9.6 Hz, 2H), 7.75 (dd, *J* = 8.8, 1.6 Hz, 2H), 6.66 (d, *J* = 9.0 Hz, 4H), 6.59 (d, *J* = 9.1 Hz, 4H), 6.00 (s, 2H), 3.83 (t, *J* = 6.5 Hz, 4H), 1.73 (dt, *J* = 14.6, 6.6 Hz, 4H), 1.53 – 1.40 (m, 4H), 1.39 – 1.25 (m, 16H), 1.19 (d, *J* = 2.2 Hz, 42H), 0.99 – 0.85 (m, 6H).

^{13}C NMR (126 MHz, chloroform-*d*) δ 152.84, 141.92, 132.25, 129.16, 128.67, 128.01, 127.78, 126.67, 125.59, 125.47, 123.84, 122.69, 121.49, 116.00, 115.77, 107.77, 92.70, 77.40, 68.72, 31.97, 29.59, 29.53, 29.40, 26.24, 22.80, 18.91, 14.24, 11.57.

HRMS (APPI+): $C_{74}H_{96}N_2O_2Si_2$ $[M]^+$ 1100.701 m/z, found 1100.7079 m/z, diff 6.25 ppm.

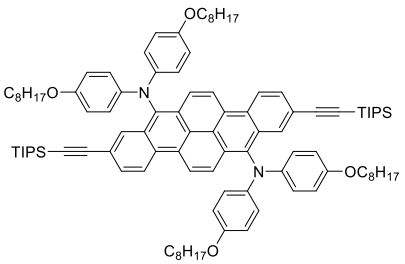

Compound 7: A dried round bottom flask equipped with a magnetic stir bar was charged with compound **6** (3.00 g, 4.45 mmol), 1-bromo-4-(octyloxy)benzene (1.63 g, 5.72 mmol), tris(dibenzylideneacetone)dipalladium (374 mg, 408 µmol), tri-*tert*-butylphosphanium tetrafluoroborate (237 mg, 816 µmol) and sodium *tert*-butanoate (1.31 g, 13.6 mmol). The flask was vacuumed for 15 minutes and purged using three vacuum-nitrogen cycles before the addition of degassed anhydrous toluene (151 mL). The reaction was stirred for 16 hours at 90 °C before it was cooled at room temperature. A saturated aqueous solution of ammonium chloride was added, followed by ethyl acetate. The resulting mixture was washed three

times with distilled water and brine and the aqueous layer was extracted three times with chloroform. The combined organic layers were dried with magnesium sulfate, filtered under vacuum and the solvent was removed under reduced pressure. The resulting solid was purified through column chromatography (silica gel, hexanes:dichloromethane 4:1 as the eluent) before being triturated in methanol and filtered to provide the desired compound **7** as a purple solid (3.21 g, 78 %).

^{1}H NMR (500 MHz, chloroform-*d*) δ 8.87 (d, *J* = 8.7 Hz, 2H), 8.84 (d, *J* = 10.1 Hz, 2H), 8.60 (d, *J* = 1.8 Hz, 2H), 8.47 (d, *J* = 9.5 Hz, 2H), 7.74 (dd, *J* = 8.9, 1.7 Hz, 2H), 7.04 (d, *J* = 9.0 Hz, 8H), 6.73 (d, *J* = 9.3 Hz, 8H), 3.86 (tt, *J* = 6.6, 3.2 Hz, 8H), 1.79 – 1.65 (m, 8H), 1.40 (qd, *J* = 7.5, 3.6 Hz, 8H), 1.35 – 1.20 (m, 32H), 1.14 (d, *J* = 2.0 Hz, 42H), 0.91 – 0.83 (m, 12H).

^{13}C NMR (126 MHz, chloroform-*d*) δ 153.87, 142.32, 136.95, 130.46, 129.71, 129.44, 128.96, 128.90, 126.82, 126.10, 124.89, 123.76, 123.70, 121.89, 121.76, 115.47, 107.80, 92.40, 68.44, 31.96, 29.53, 29.51, 29.38, 26.22, 22.80, 18.88, 14.23, 11.50.

HRMS (APPI+): $C_{102}H_{136}N_2O_4Si_2$ $[M]^+$ 1509.0039 m/z, found 1509.0142 m/z, diff 6.84 ppm.

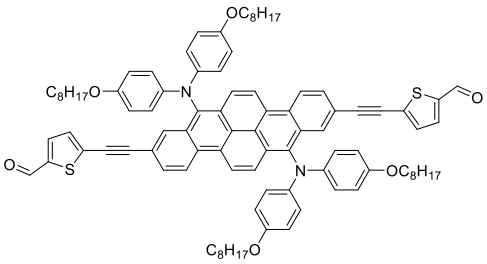

Compound 8: A dried round bottom flask equipped with a magnetic stir bar was charged with compound **7** (3,00 g, 1.99 mmol) and degassed anhydrous tetrahydrofuran (99 mL). Once compound **7** solubilized, a tetrabutylammonium fluoride (TBAF) solution (15.9 mL, 15.9 mmol, 1 M in tetrahydrofuran) was added. The mixture was stirred 16 hours at room temperature before chloroform was added. The organic layer was washed with distilled water and dried with magnesium sulfate. The solvent was

removed under reduced pressure and the resulting solid was triturated using methanol and filtered under vacuum. The desilylated intermediate was immediately charged in a dried round bottom flask equipped with a magnetic stir bar, and 5-iodothiophene-2-carbaldehyde (1.42 g, 5.97 mmol), dichlorobis(triphenylphosphine)palladium (II) (167 mg, 238 μmol) and copper(I) iodide (37 mg, 199 μmol) were added. The flask was vacuumed for 15 minutes and purged using three vacuum-nitrogen cycles before degassed anhydrous toluene (66 mL) and distilled triethylamine (15 mL) were added. The mixture was degassed for 10 minutes and stirred for 16 hours at 50 °C before it was cooled at room temperature. A saturated aqueous solution of ammonium chloride was added and the resulting mixture was extracted three times with chloroform. The combined organic layers were dried with magnesium sulfate and the solvent was removed under reduced pressure. The resulting solid was purified using column chromatography (silica gel, hexanes:dichloromethane 1:1, followed by hexanes:ethyl acetate 4:1 as the eluent) before it was triturated in methanol and filtered under vacuum to provide the desired compound **8** as a burgundy solid (2.42 g, 86 %).

^{1}H NMR (500 MHz, chloroform-*d*) δ 9.87 (s, 2H), 8.95 (d, *J* = 9.4 Hz, 2H), 8.87 (d, *J* = 10.0 Hz, 2H), 8.66 (d, *J* = 1.7 Hz, 2H), 8.50 (d, *J* = 9.7 Hz, 2H), 7.81 (dd, *J* = 8.9, 1.7 Hz, 2H), 7.67 (d, *J* = 3.9 Hz, 2H), 7.34 (d, *J* = 3.9 Hz, 2H), 7.07 (d, *J* = 9.2 Hz, 8H), 6.75 (d, *J* = 9.2 Hz, 8H), 3.86 (t, *J* = 6.7 Hz, 8H), 1.81 – 1.67 (m, 8H), 1.45 – 1.36 (m, 8H), 1.36 – 1.18 (m, 32H), 0.96 – 0.79 (m, 12H).

^{13}C NMR (126 MHz, chloroform-*d*) δ 182.50, 153.91, 144.19, 141.98, 137.17, 136.12, 132.92, 132.88, 130.69, 129.90, 129.44, 129.26, 128.37, 127.02, 126.34, 125.10, 124.30, 123.89, 121.52, 120.56, 115.52, 98.71, 83.46, 68.47, 31.94, 29.51, 29.50, 29.36, 26.20, 22.78, 14.23.

HRMS (APPI+): $C_{94}H_{100}N_2O_6S_2$ $[M]^+$ 1416.7023 m/z, found 1416.7096 m/z, diff 5.17 ppm.

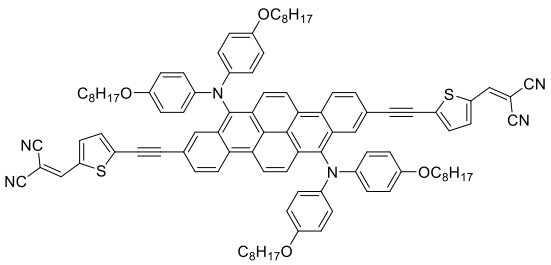

Compound 9: A dried round bottom flask equipped with a magnetic stir bar was charged with compound **8** (300 mg, 211 μmol) and malononitrile (69 mg, 1.06 mmol). The flask was vacuumed for 15 minutes and purged using three vacuum-nitrogen cycles before the addition of degassed anhydrous toluene (52 mL). The mixture was stirred for 10 minutes at 60 °C before triethylamine (0.3 mL, 2.1 mmol) was added. The mixture was stirred for 72 hours at 60 °C. Then, acetic anhydride (2.0 mL, 21 mmol) was added, and the mixture was stirred for an additional 24 hours at 60 °C. After it was cooled to room temperature, the mixture was diluted with ethyl acetate and washed twice with saturated aqueous solutions of ammonium chloride, a saturated aqueous solution of sodium bicarbonate and brine. The organic layer was dried with magnesium sulfate and the solvent was removed under reduced pressure. The resulting solid was triturated in methanol and filtered under vacuum, purified through column chromatography (silica gel, dichloromethane as the eluent) before it was triturated in methanol and filtered to provide the desired compound **9** as a dark brown solid (113 mg, 35 %).

^{1}H NMR (500 MHz, carbon disulfide:dimethyl sulfoxide-d_6 (4:1)) δ 9.09 (d, J = 9.2 Hz, 2H), 8.95 (d, J = 10.0 Hz, 2H), 8.62 – 8.55 (m, 4H), 8.47 (d, J = 9.5 Hz, 2H), 7.90 (d, J = 4.3 Hz, 2H), 7.85 (dd, J = 8.9, 1.8 Hz, 2H), 7.42 (d, J = 4.0 Hz, 2H), 7.01 (d, J = 9.2 Hz, 8H), 6.71 (d, J = 9.2 Hz, 8H), 3.86 (t, J = 6.4 Hz, 8H), 1.74 (p, J = 6.4 Hz, 8H), 1.53 – 1.23 (m, 40H), 1.02 – 0.87 (m, 12H).

^{13}C NMR (126 MHz, carbon disulfide:dimethyl sulfoxide-d_6 (4:1)) δ 153.06, 150.83, 140.80, 139.20, 136.28, 136.24, 132.67, 132.58, 129.68, 128.98, 128.62, 128.43, 127.51, 126.18, 125.52,

124.43, 124.22, 123.35, 120.67, 119.57, 114.72, 113.15, 112.39, 100.24, 83.51, 76.94, 67.27, 31.54, 29.13, 29.08, 29.03, 25.83, 22.57, 13.93.

HRMS (APPI+): $C_{100}H_{100}N_6O_4S_2$ $[M]^+$ 1512.7247 m/z, found 1512.7337 m/z, diff 5.89 ppm.

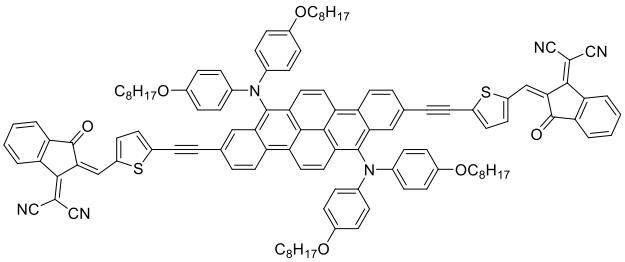

Compound 10: A dried round bottom flask equipped with a magnetic stir bar was charged with compound **8** (150 mg, 106 µmol) and 2-(3-oxoinden-1-ylidene)propanedinitrile (41 mg, 212 µmol). The flask was vacuumed for 15 minutes and purged using three vacuum-nitrogen cycles before the addition of degassed anhydrous toluene (5.2 mL). After solubilization, boron trifluoride diethyl etherate (neat, 0.13 mL, 1.06 mmol) was added dropwise, followed by acetic anhydride (0.1 mL). The mixture was stirred for 2 hours at room temperature before it was added directly on a silica gel column (chloroform as the eluent). The resulting solid was triturated in a methanol:diethyl ether mixture and filtered under vacuum. The solid was then triturated again in hexanes and filtered under vacuum. Finally, the solid was precipitated in ethanol using ethyl acetate as the good solvent and filtered under vacuum to provide the desired compound **10** as a dark purple solid (123 mg, 66 %).

^{1}H NMR (400 MHz, chloroform-*d*) δ 8.98 (d, *J* = 9.1 Hz, 2H), 8.89 (d, *J* = 10.0 Hz, 2H), 8.86 (s, 2H), 8.72 (d, *J* = 7.2 Hz, 2H), 8.69 (s, 2H), 8.52 (d, *J* = 9.2 Hz, 2H), 7.97 (d, *J* = 7.5 Hz, 2H), 7.87 – 7.76 (m, 8H), 7.43 – 7.38 (m, 2H), 7.09 (d, *J* = 9.2 Hz, 8H), 6.77 (d, *J* = 9.2 Hz, 8H), 3.88 (t, *J* = 6.5 Hz, 8H), 1.80 – 1.63 (m, 8H), 1.46 – 1.36 (m, 8H), 1.26 (d, *J* = 10.9 Hz, 32H), 0.85 (t, *J* = 7.0 Hz, 12H).

^{13}C NMR (126 MHz, carbon disulfide:dimethyl sulfoxide-d_6 (4:1)) δ 186.21, 158.53, 153.07, 143.64, 140.85, 139.24, 137.56, 136.82, 136.30, 136.11, 135.82, 134.81, 134.11, 132.59, 129.71, 128.99, 128.56, 128.39, 127.59, 126.17, 125.51, 124.60, 124.42, 124.16, 123.78, 123.33, 120.72, 119.85, 114.74, 113.31, 113.15, 101.15, 84.62, 70.59, 67.28, 31.54, 29.13, 29.10, 29.03, 25.83, 22.57, 13.93.

HRMS (APPI+): $C_{118}H_{108}N_6O_6S_2$ $[M]^+$ 1768.7772 m/z, found 1782.7892 m/z, diff 6.78 ppm.

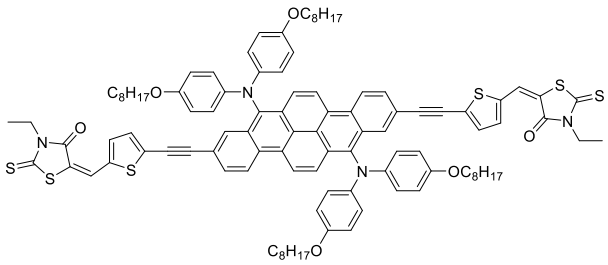

Compound 11: A dried round bottom flask equipped with a magnetic stir bar was charged with compound **8** (300 mg, 211 μmol) and 3-ethyl-2-sulfanylidene-1,3-thiazolidin-4-one (170 mg, 1.06 mmol). The flask was vacuumed for 15 minutes and purged using three vacuum-nitrogen cycles before the addition of degassed anhydrous toluene (52 mL). The reaction was stirred 10 minutes at 60 °C before piperidine (0.2 mL, 2.12 mmol) was added. The mixture was stirred for 72 hours at 60 °C. Then, acetic anhydride (2.0 mL, 21 mmol) was added, and the mixture was stirred for 24 hours at 60 °C. The mixture was diluted with ethyl acetate and washed twice with saturated aqueous solutions of ammonium chloride, a saturated aqueous solution of sodium bicarbonate and brine. The organic layer was dried with magnesium sulfate and the solvent was removed under reduced pressure. The resulting solid was triturated in methanol and purified through column chromatography (silical gel, dichloromethane as the eluent). The solid was triturated in methanol and filtered under vacuum to provide the desired compound **11** as a dark brown metallic solid with green reflection (267 mg, 74 %).

^{1}H NMR (500 MHz, Chloroform-*d*) δ 8.95 (d, *J* = 8.9 Hz, 2H), 8.87 (d, *J* = 9.7 Hz, 2H), 8.65 (s, 2H), 8.56 – 8.46 (m, 2H), 7.86 – 7.78 (m, 4H), 7.38 – 7.29 (m, 4H), 7.07 (d, *J* = 7.5 Hz, 8H), 6.76 (d, *J* = 7.5 Hz, 8H), 4.30 – 4.13 (m, 4H), 3.87 (t, *J* = 6.4 Hz, 8H), 1.72 (p, *J* = 6.6 Hz, 8H), 1.44 – 1.35 (m, 8H), 1.35 – 1.17 (m, 38H), 0.85 (t, *J* = 6.1 Hz, 12H).

^{13}C NMR (126 MHz, carbon disulfide:chloroform-*d* (3:1)) δ 190.60, 166.39, 153.68, 141.51, 139.42, 136.89, 133.34, 133.30, 130.60, 130.43, 129.62, 129.03, 128.84, 128.04, 126.69, 126.13, 125.03, 124.12, 123.70, 123.49, 122.51, 121.27, 120.61, 115.27, 99.39, 84.23, 68.02, 39.79, 32.08, 29.66, 29.63, 29.55, 26.36, 23.06, 14.39, 12.32.

HRMS (APPI+): $C_{104}H_{110}N_4O_6S_6$ $[M]^+$ 1702.675 m/z, found 1702.6828 m/z, diff 4.62 ppm.

NMR Spectra

Compound 3

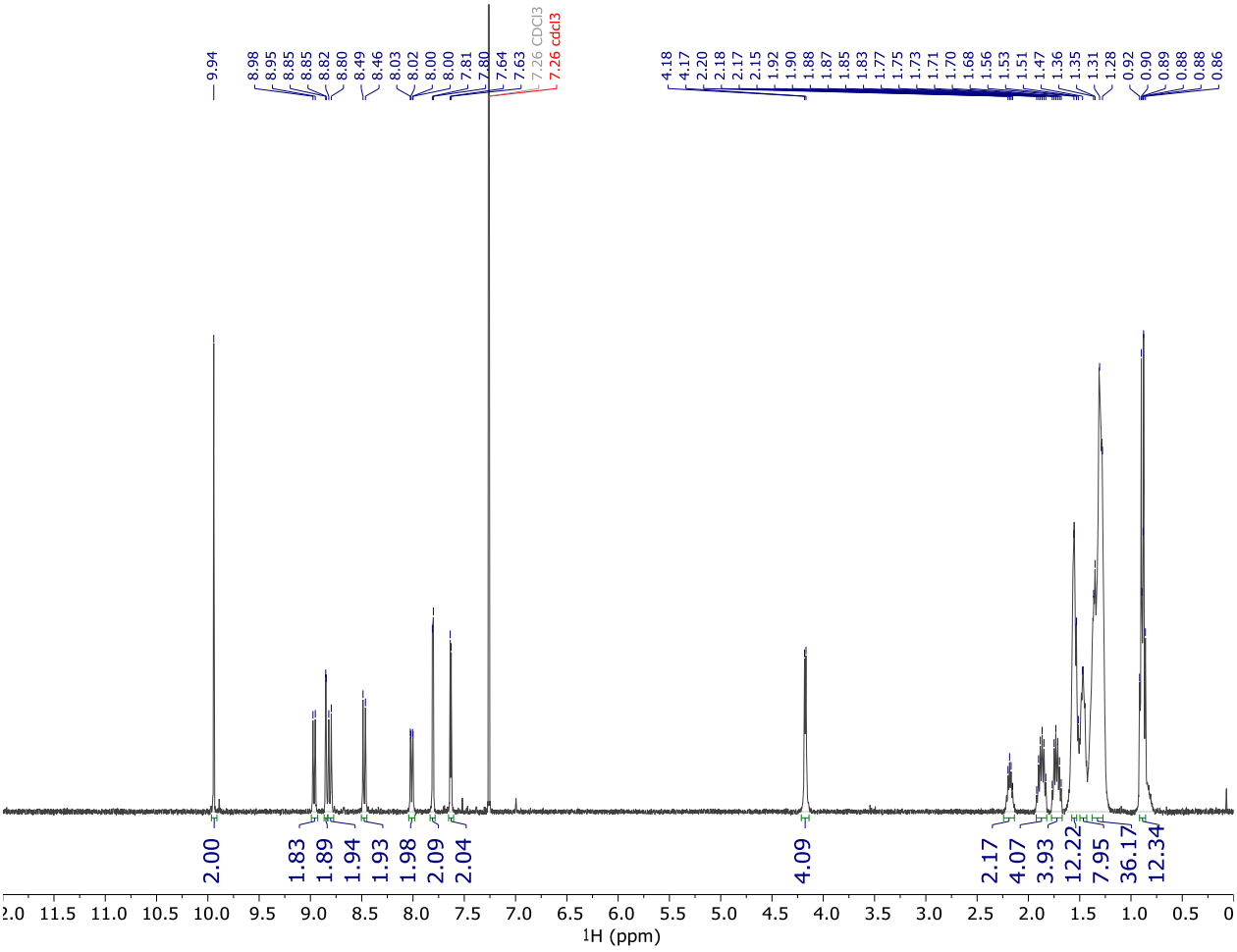

Figure S1: ^{1}H NMR spectrum of compound **3** in chloroform-*d* at 400 MHz.

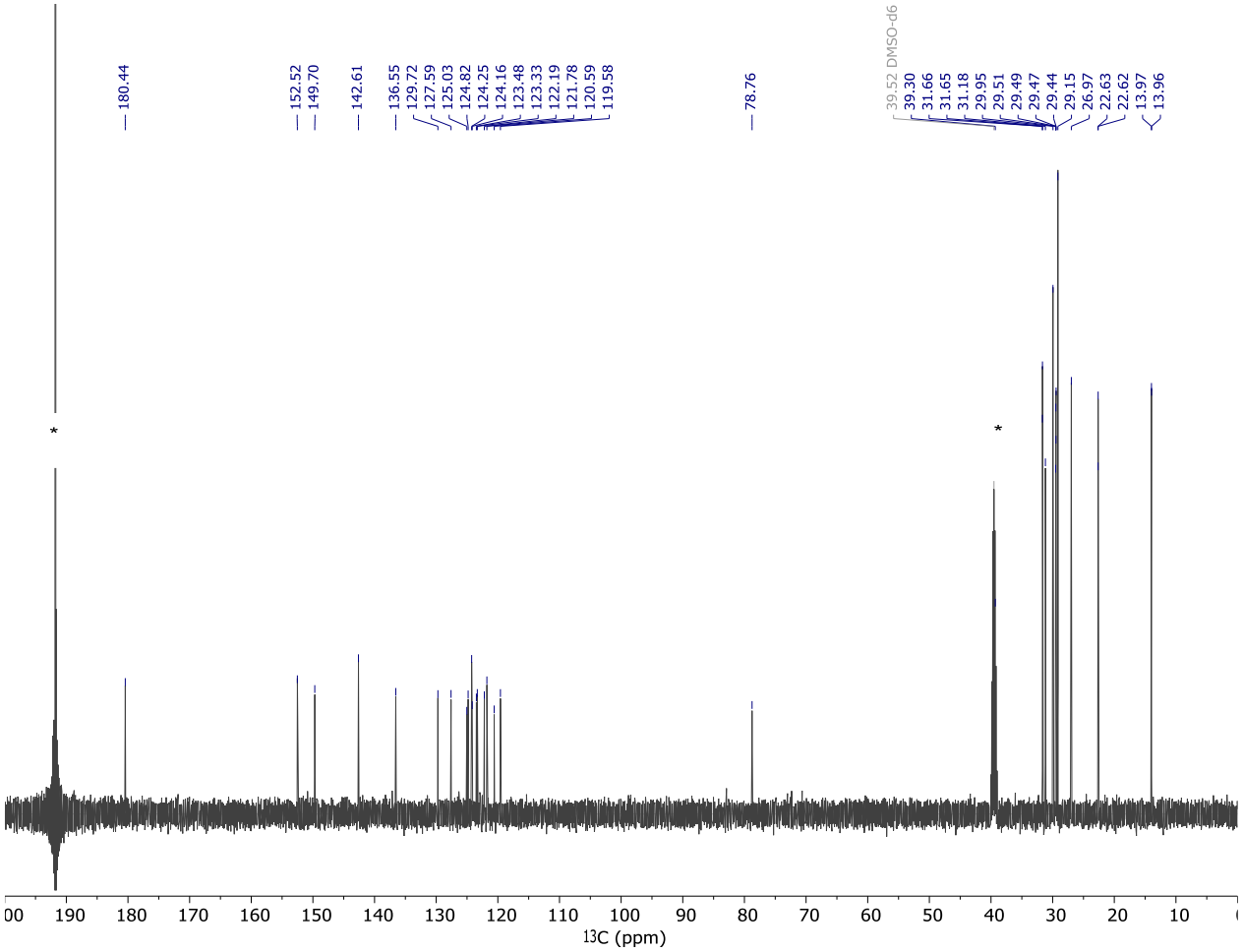

Figure S2: ^{13}C NMR spectrum of compound **3** in carbon disulfide:dimethyl sulfoxide-d_6 (4:1) at 126 MHz. Carbon disulfide peak at 191.78 ppm and dimethyl sulfoxide-d_6 at 39.52 ppm.

Compound 4

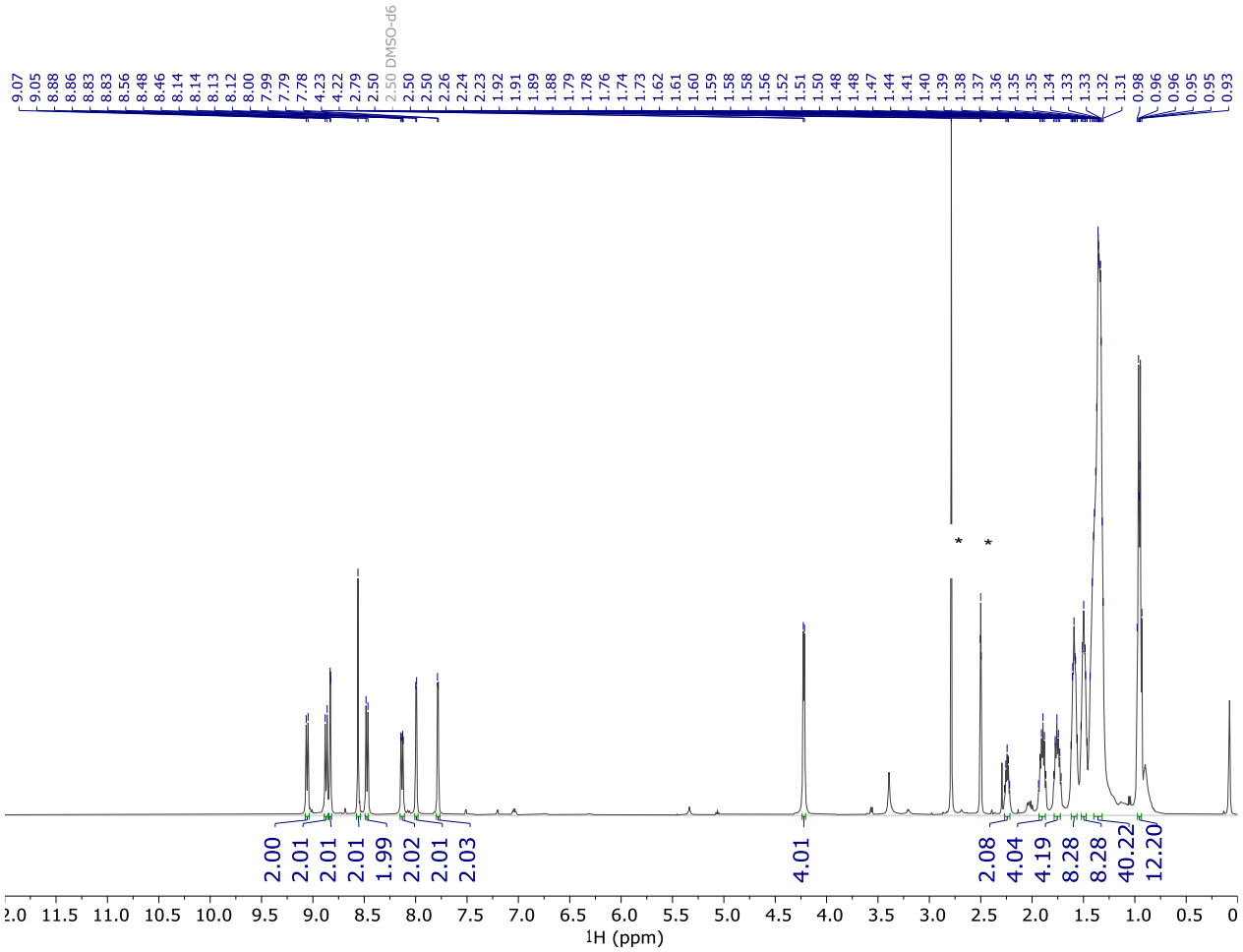

Figure S3: ^{1}H NMR spectrum of compound **4** in carbon disulfide:dimethyl sulfoxide-d_6 (4:1) at 500 MHz. Dimethyl sulfoxide-d_6 peak at 2.50 ppm and water at 2.79 ppm.

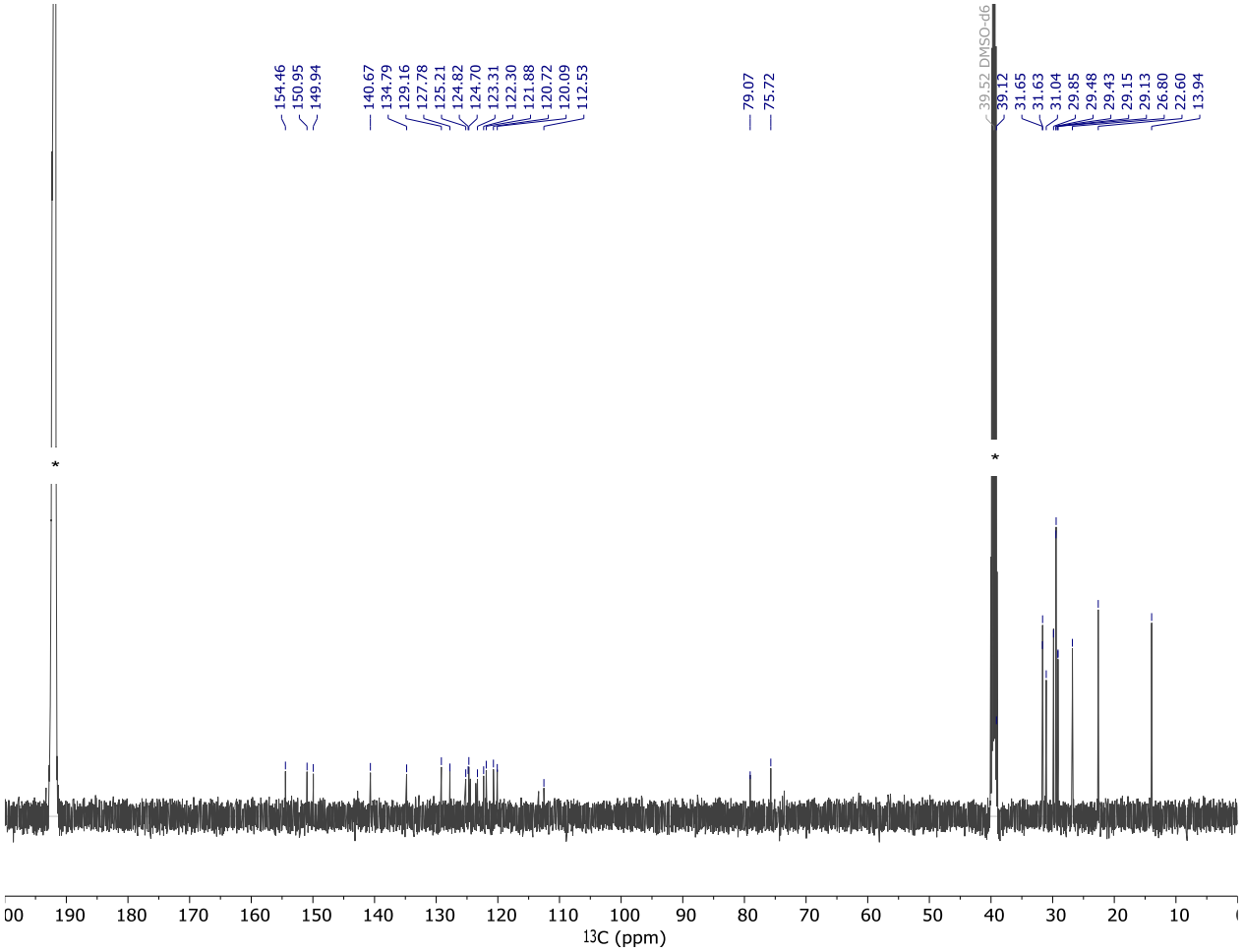

Figure S4: ^{13}C NMR spectrum of compound **4** in carbon disulfide:dimethyl sulfoxide-d_6 (4:1) at 126 MHz. Carbon disulfide peak at 191.77 ppm and dimethyl sulfoxide-d_6 at 39.52 ppm.

Compound 5

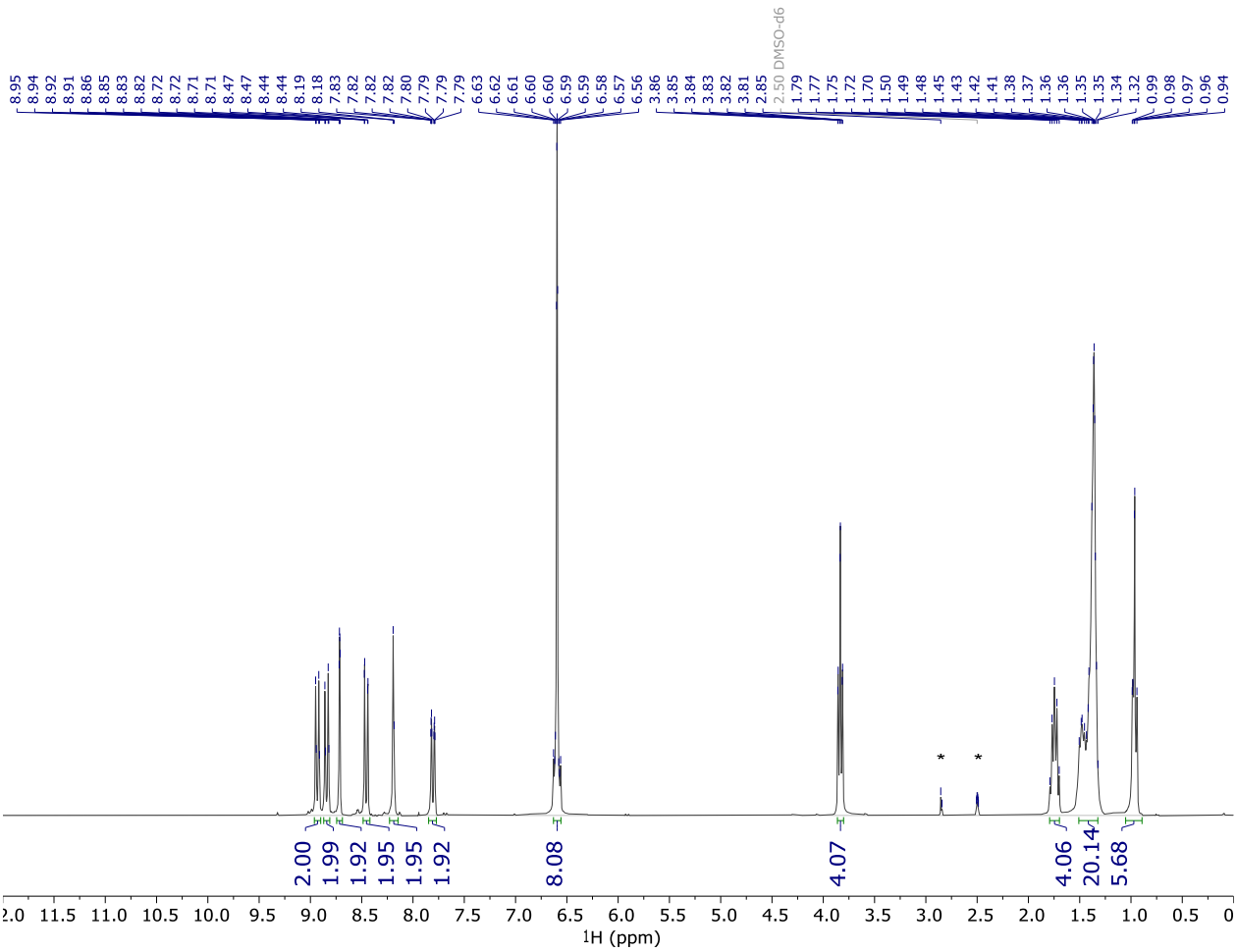

Figure S5: ^{1}H NMR spectrum of compound **5** in carbon disulfide:dimethyl sulfoxide-d_6 (4:1) at 300 MHz. Dimethyl sulfoxide-d_6 peak at 2.50 ppm and water at 2.85 ppm.

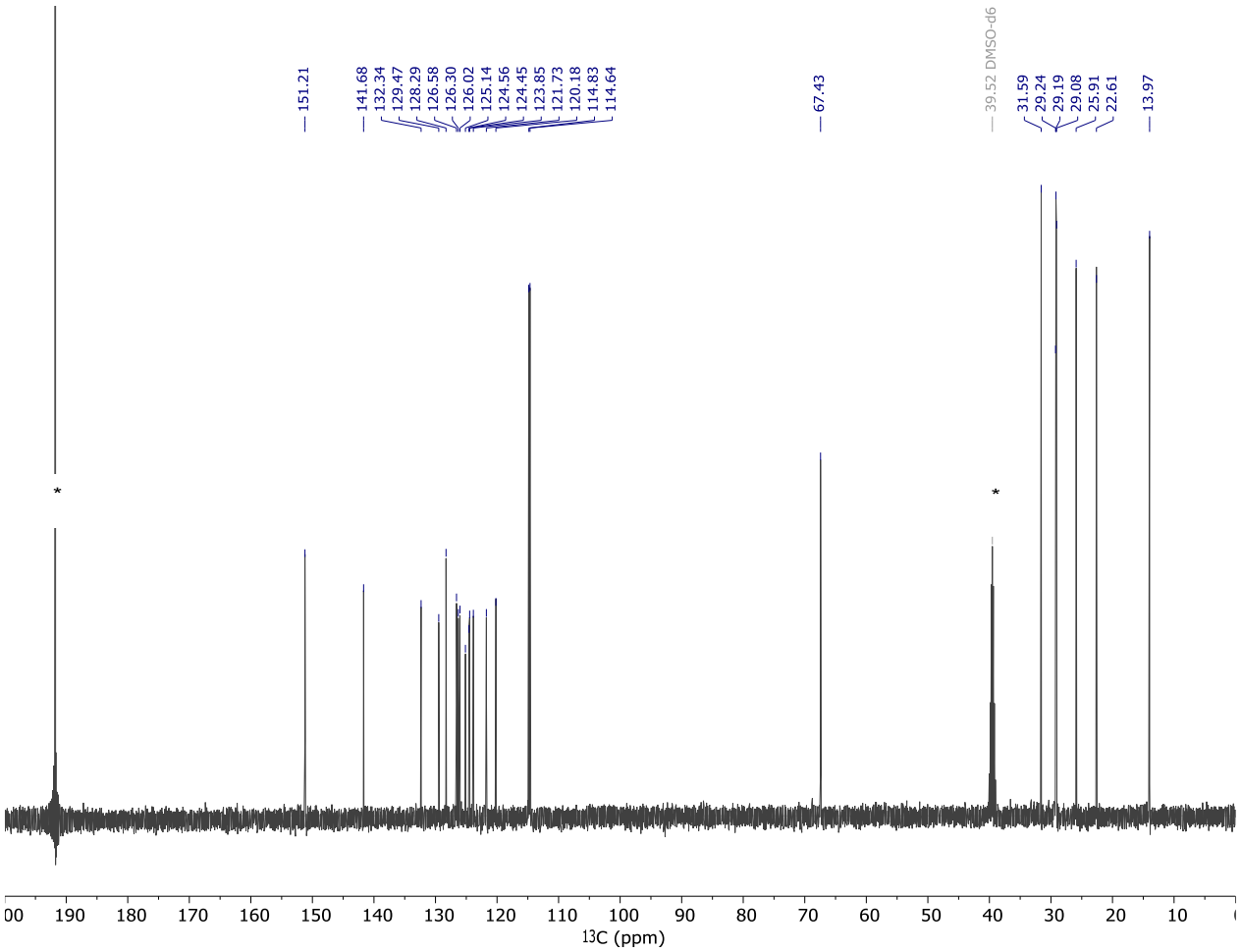

Figure S6: ^{13}C NMR spectrum of compound **5** in carbon disulfide:dimethyl sulfoxide-d_6 (4:1) at 126 MHz. Carbon disulfide peak at 191.81 ppm and dimethyl sulfoxide-d_6 at 39.52 ppm.

Compound 6

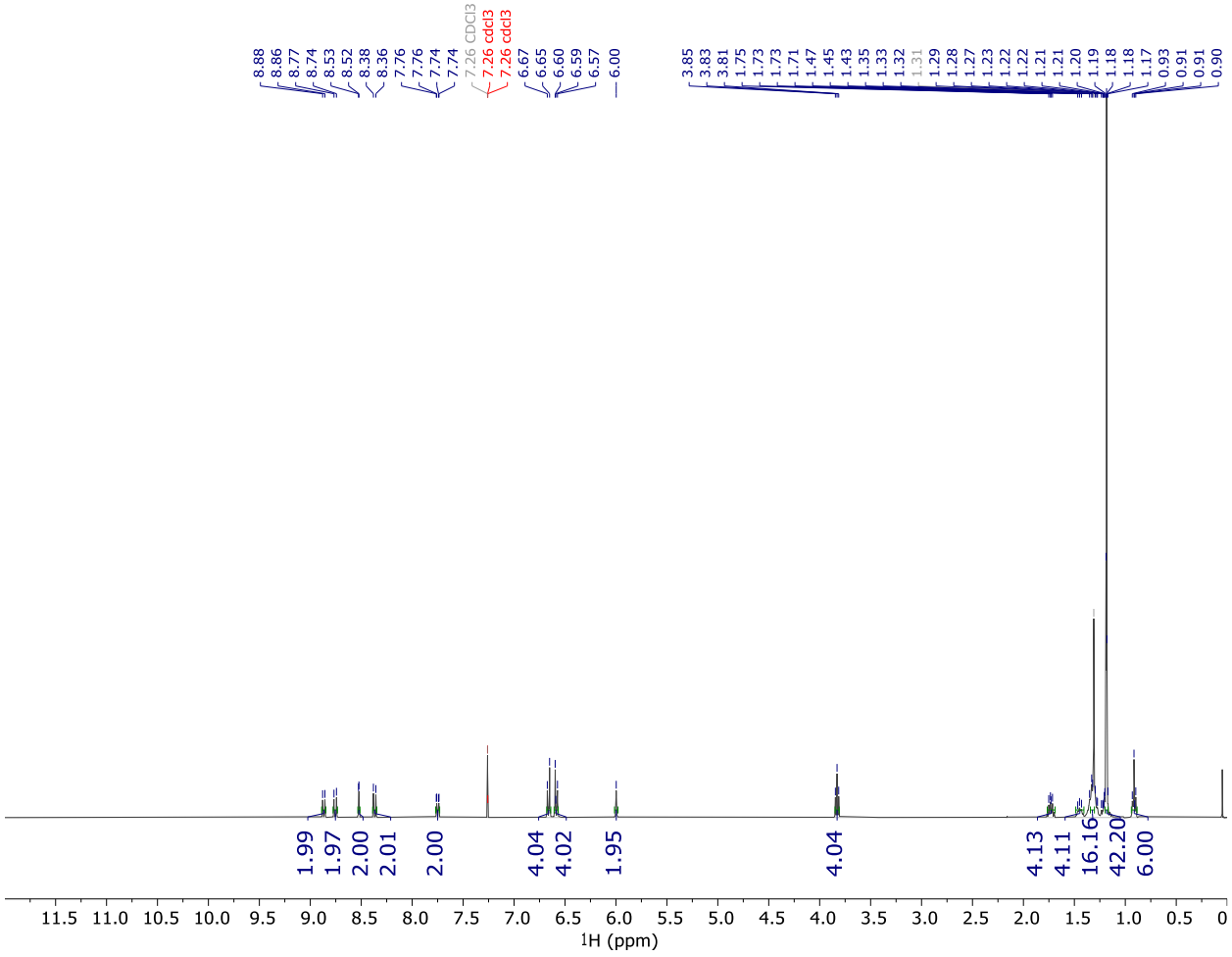

Figure S7: ^{1}H NMR spectrum of compound **6** in chloroform-*d* at 400 MHz.

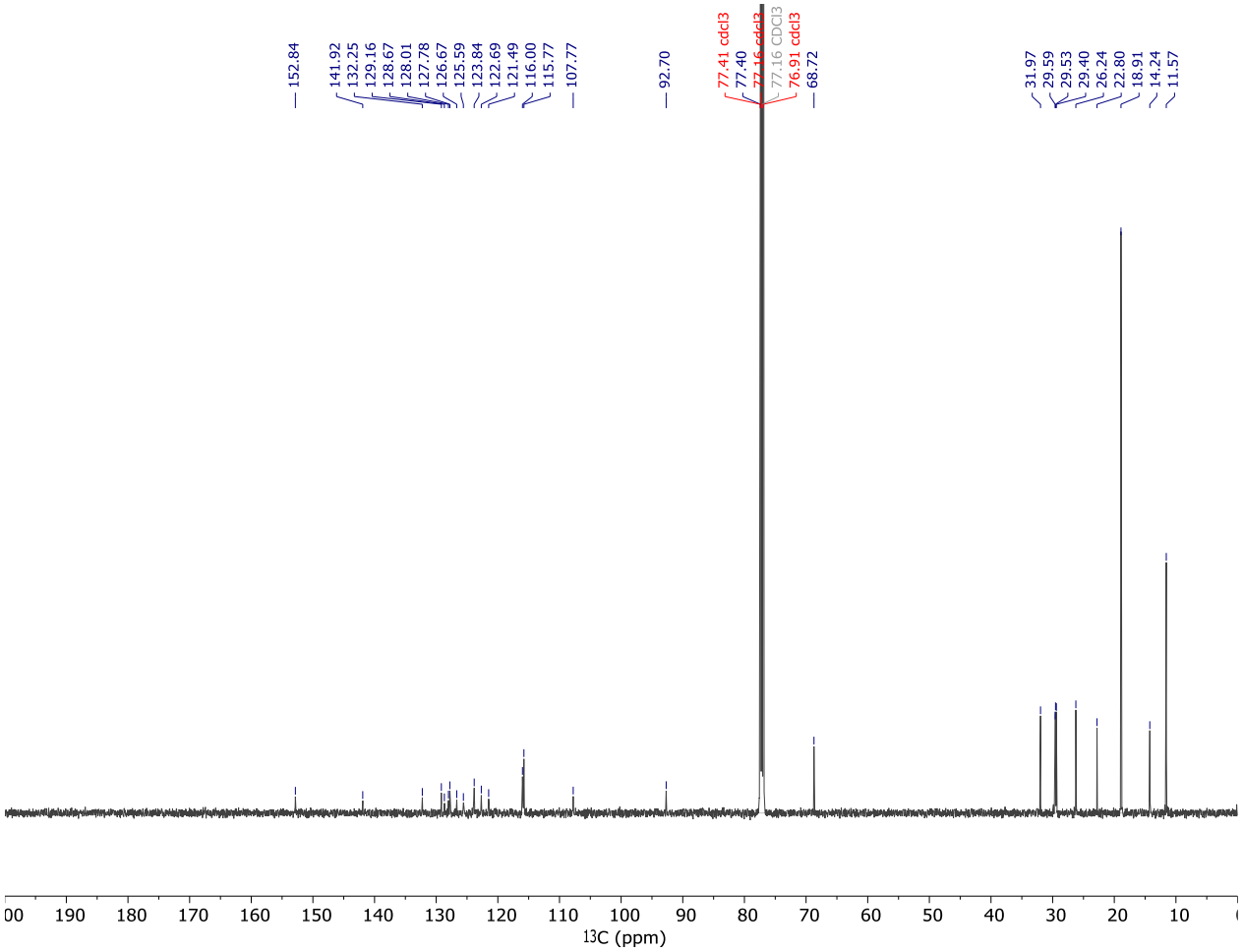

Figure S8: ^{13}C NMR spectrum of compound **6** in chloroform-*d* at 126 MHz.

Compound 7

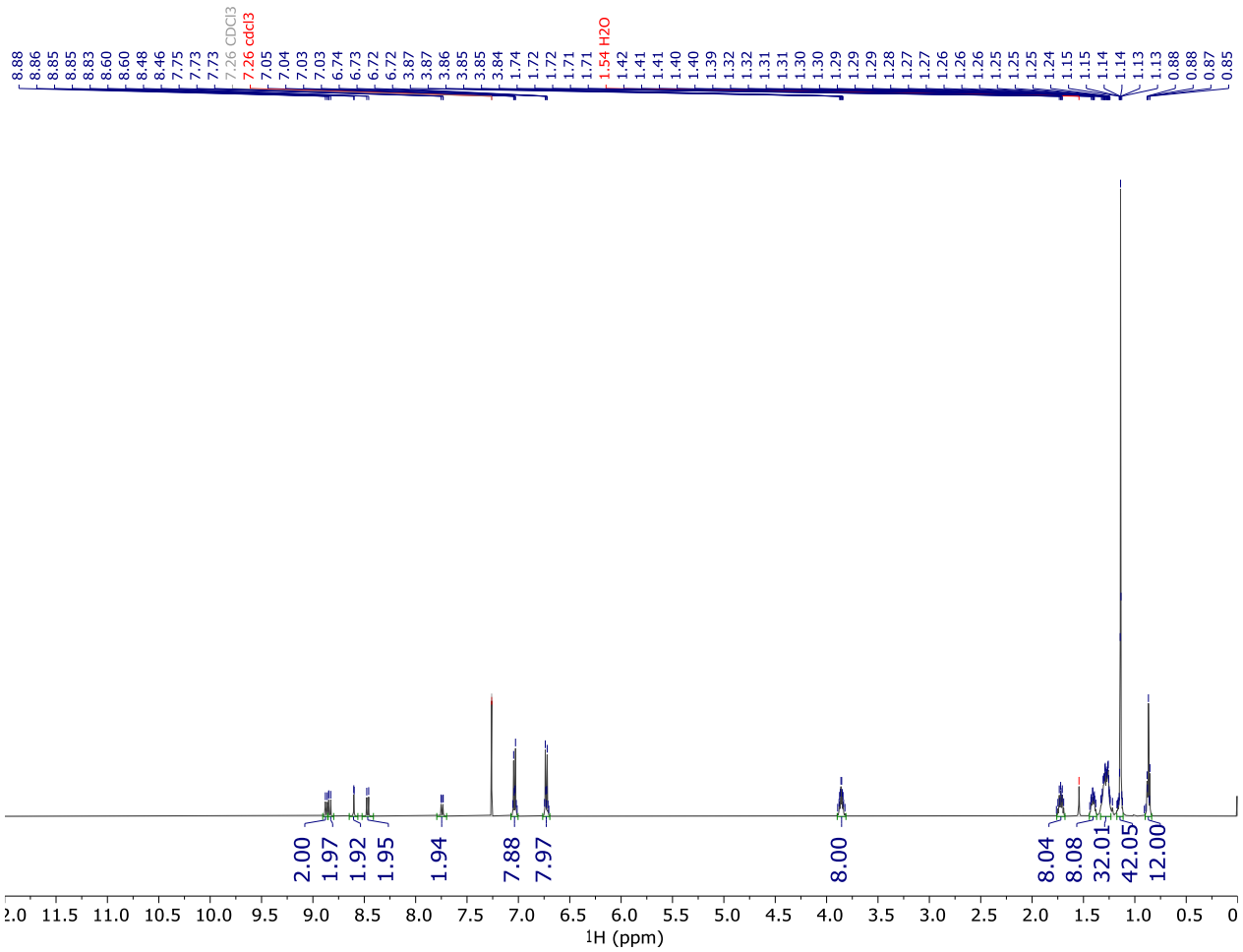

Figure S9: ^{1}H NMR spectrum of compound **7** in chloroform-*d* at 500 MHz.

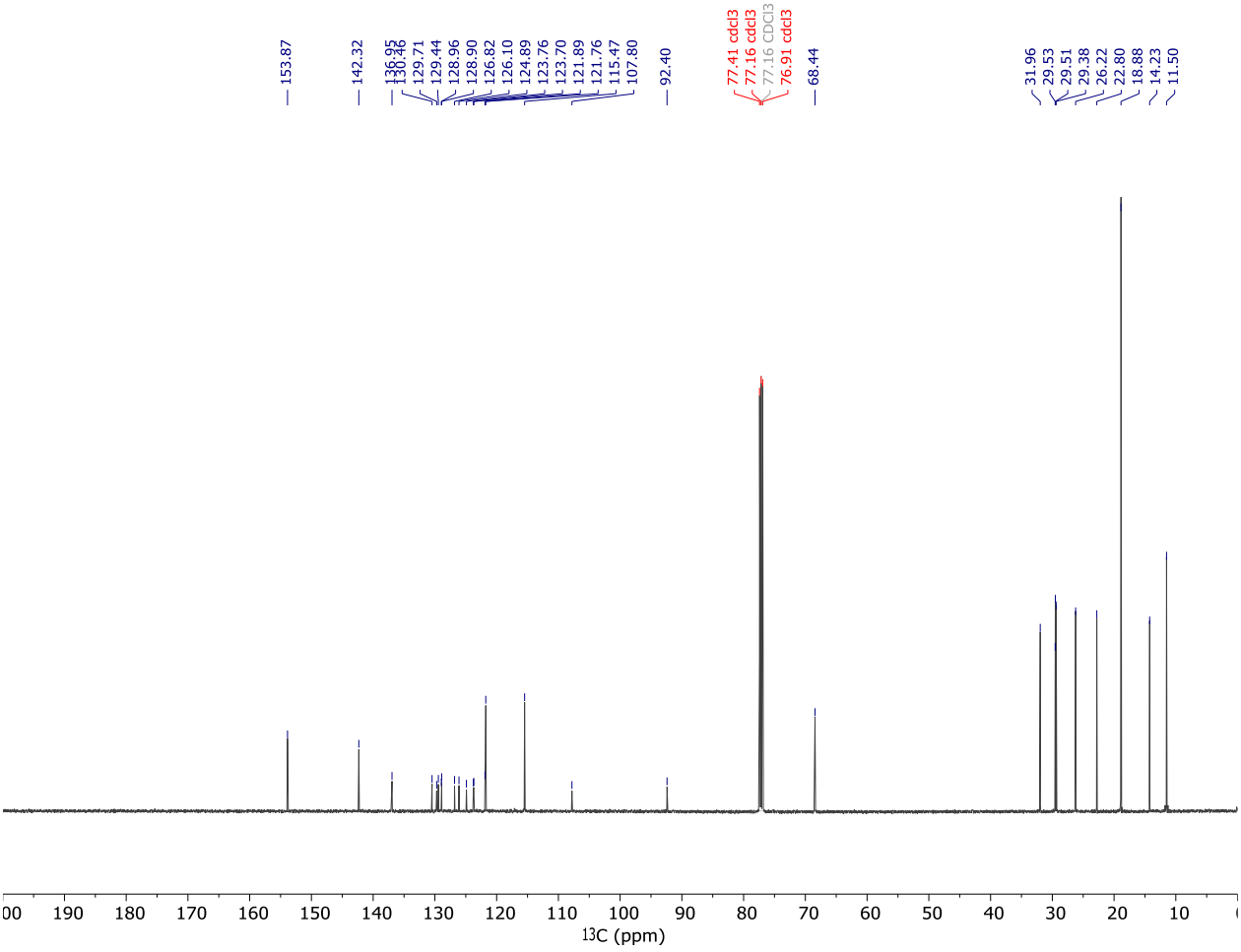

Figure S10: ^{13}C NMR spectrum of compound **7** in chloroform-*d* at 126 MHz.

Compound 8

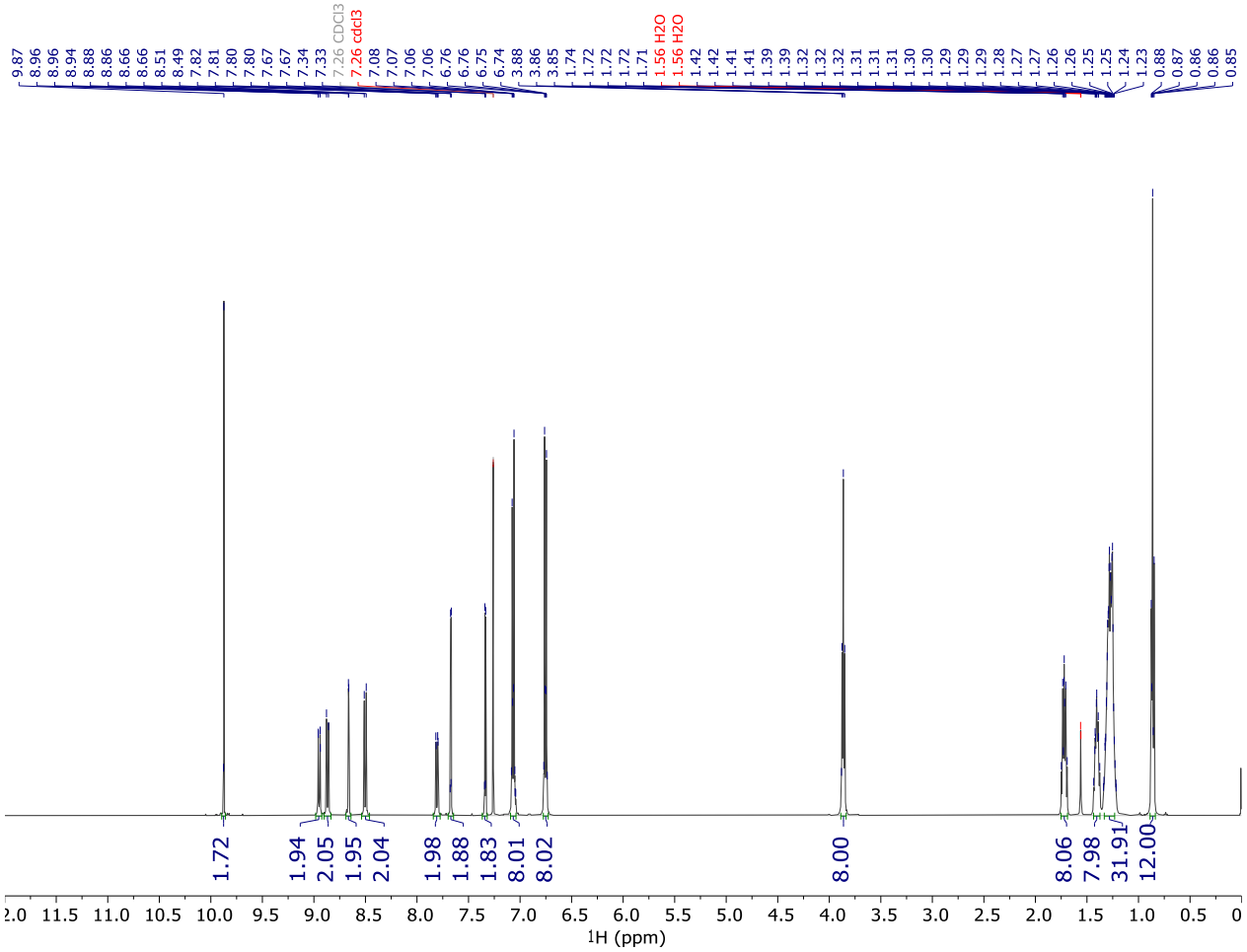

Figure S11: ^{1}H NMR spectrum of compound **8** in chloroform-*d* at 500 MHz.

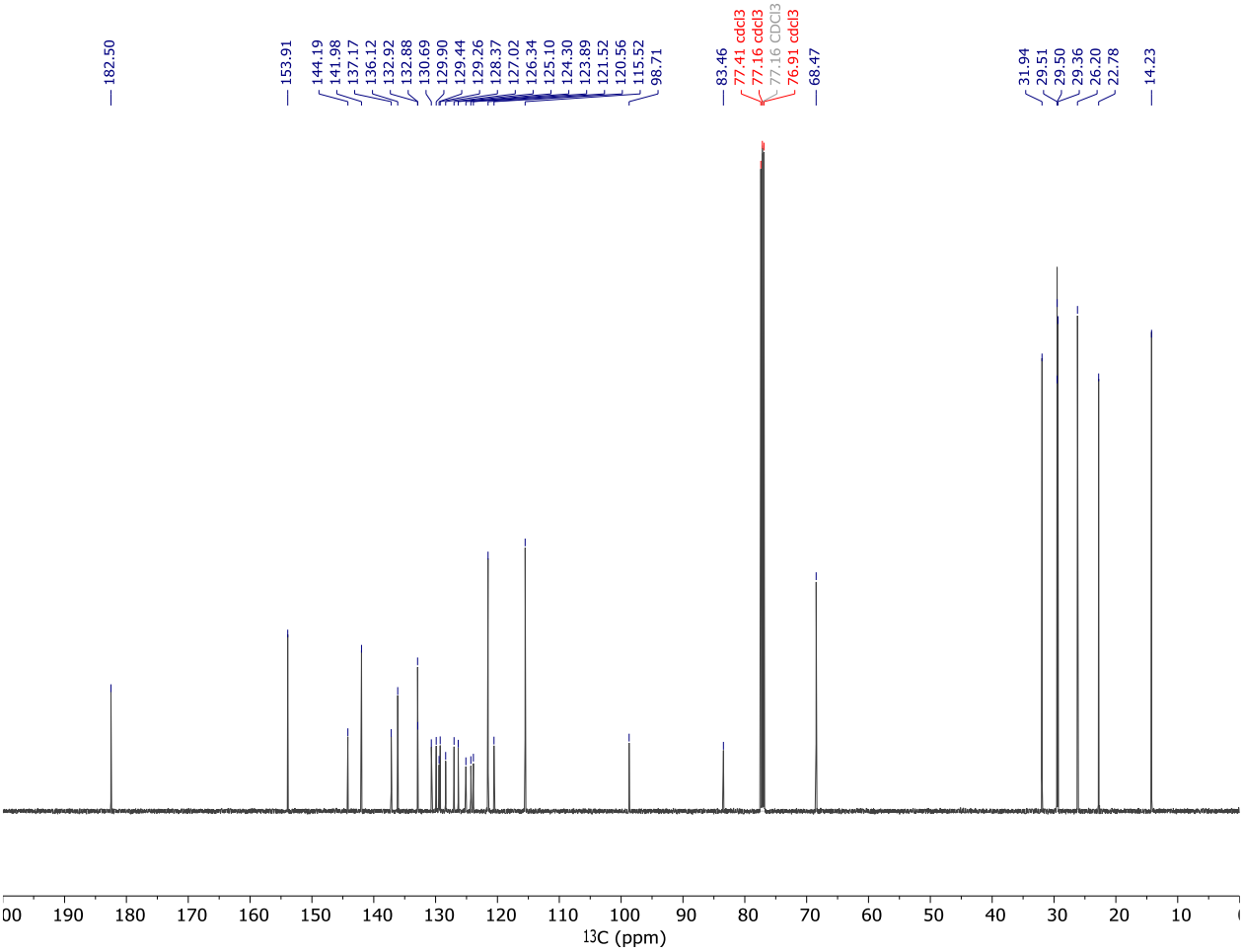

Figure S12: ^{13}C NMR spectrum of compound **8** in chloroform-*d* at 126 MHz.

Compound 9

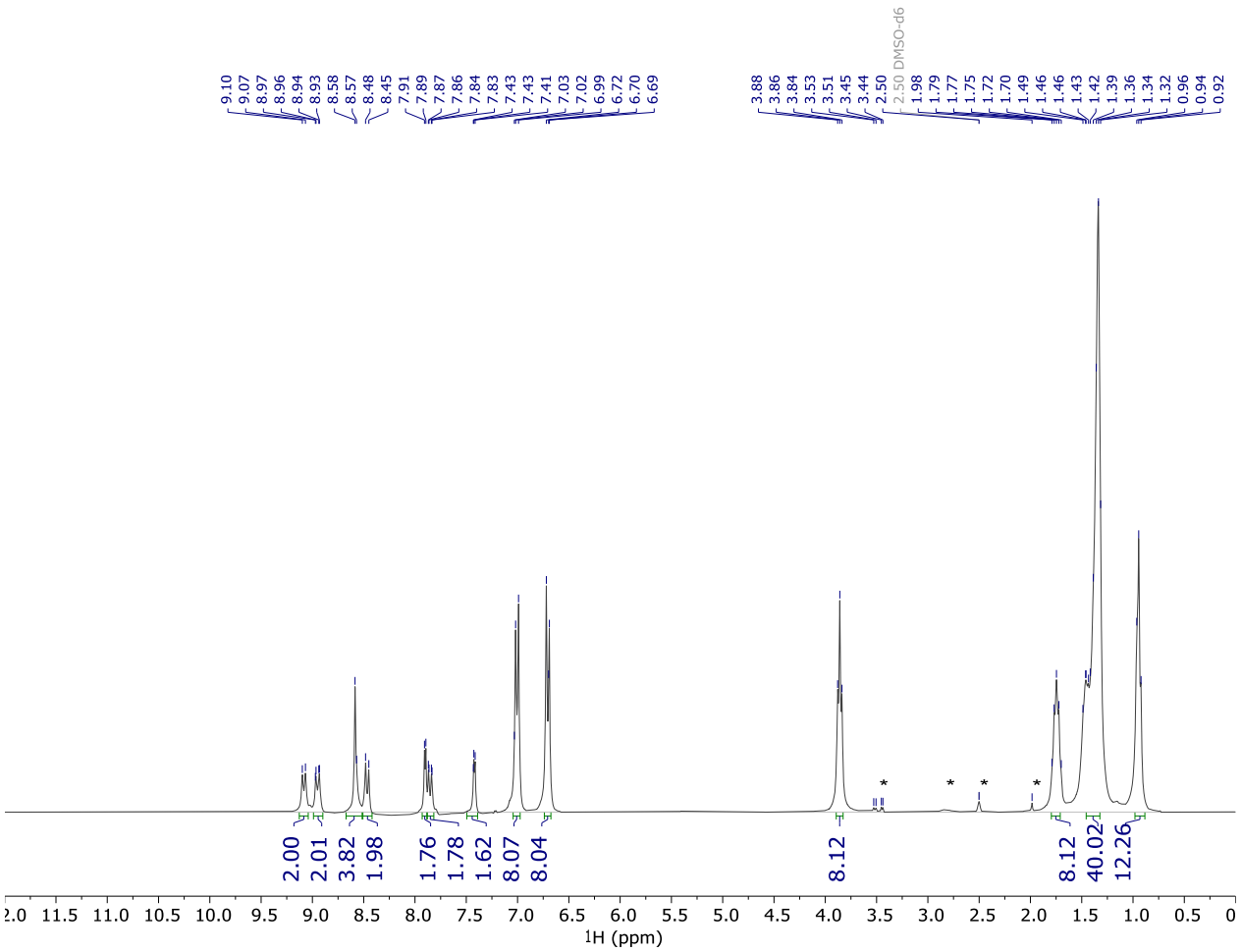

Figure S13: ^{1}H NMR spectrum of compound **9** in carbon disulfide:dimethyl sulfoxide-d_6 (4:1) at 300 MHz. Dimethyl sulfoxide-d_6 peak at 2.50 ppm and water at 2.91 ppm.f

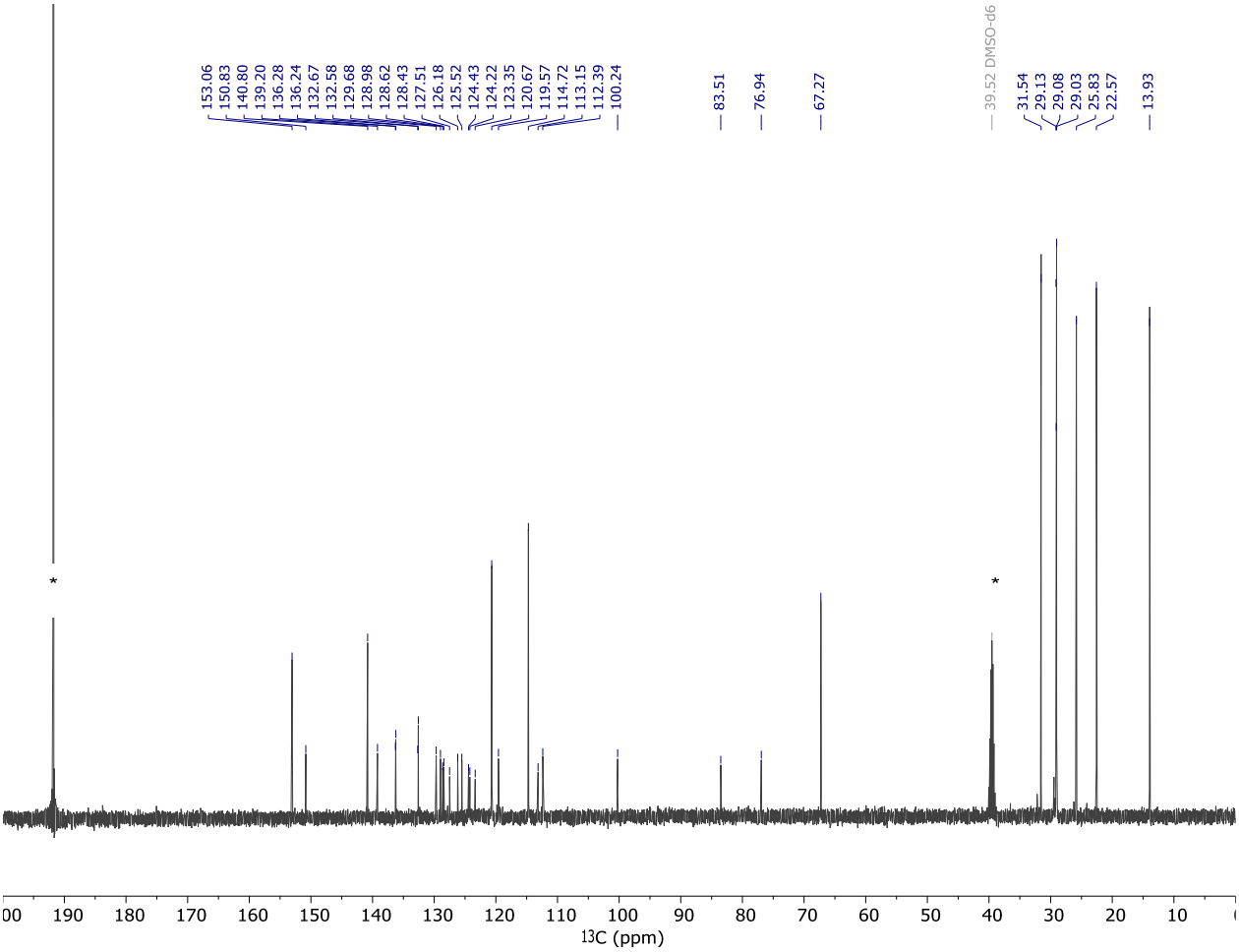

Figure S14: ^{13}C NMR spectrum of compound **9** in carbon disulfide:dimethyl sulfoxide-d_6 (4:1) at 126 MHz. Carbon disulfide peak at 191.80 ppm and dimethyl sulfoxide-d_6 at 39.52 ppm.

Compound 10

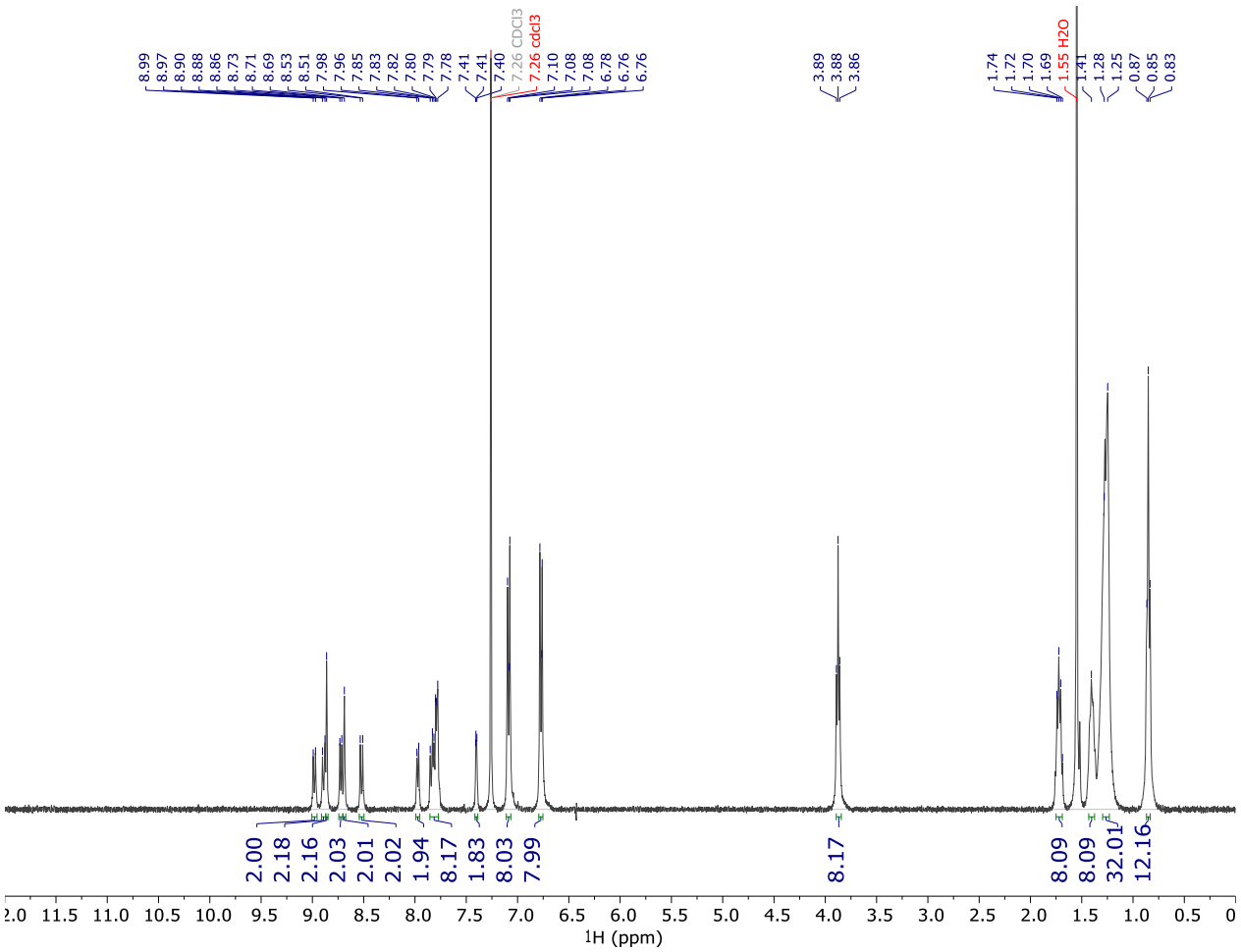

Figure S15: ^{1}H NMR spectrum of compound **10** in chloroform-*d* at 400 MHz.

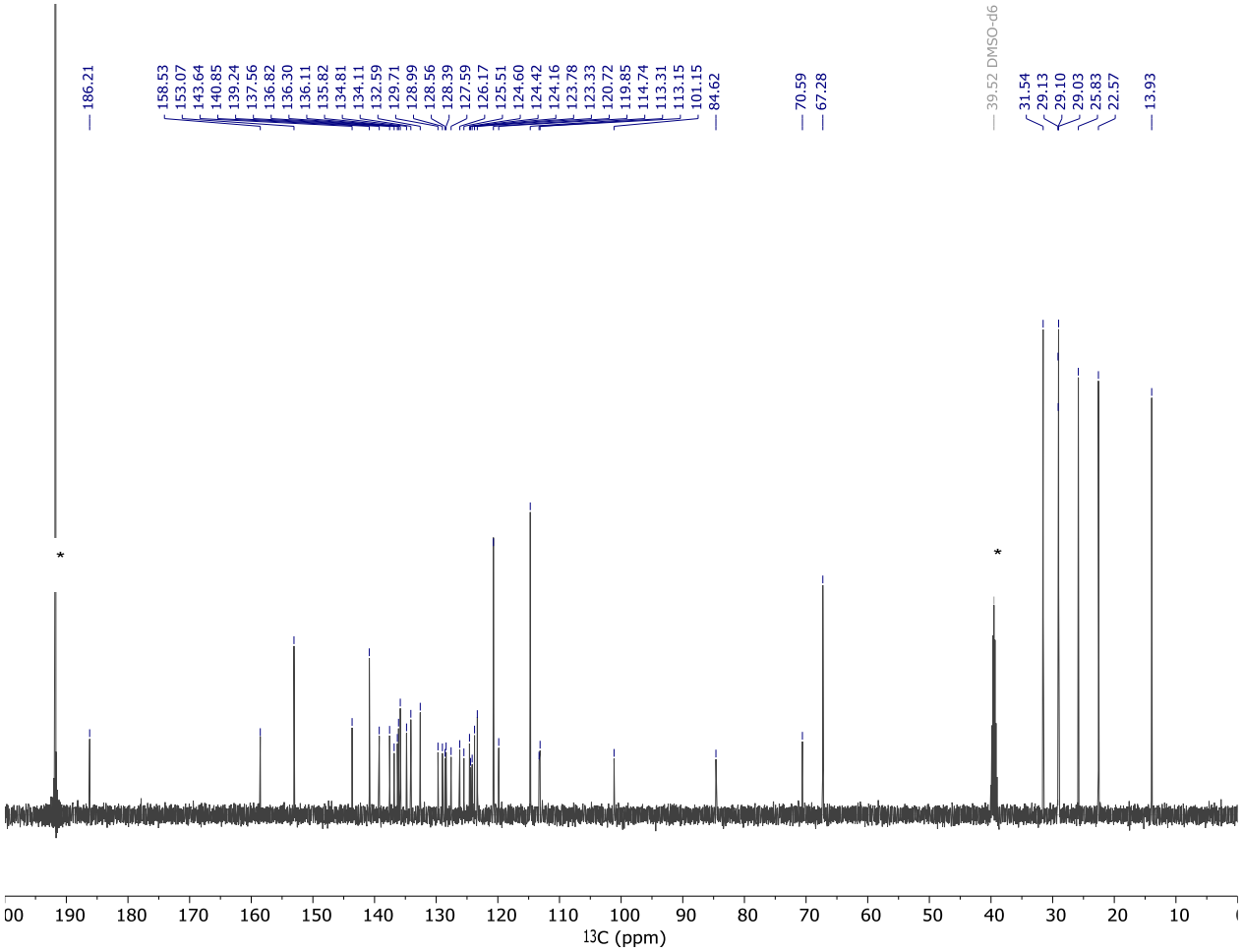

Figure S16: ^{13}C NMR spectrum of compound **10** in carbon disulfide:dimethyl sulfoxide-d_6 (4:1) at 126 MHz. Carbon disulfide peak at 191.80 ppm and dimethyl sulfoxide-d_6 at 39.52 ppm.

Compound 11

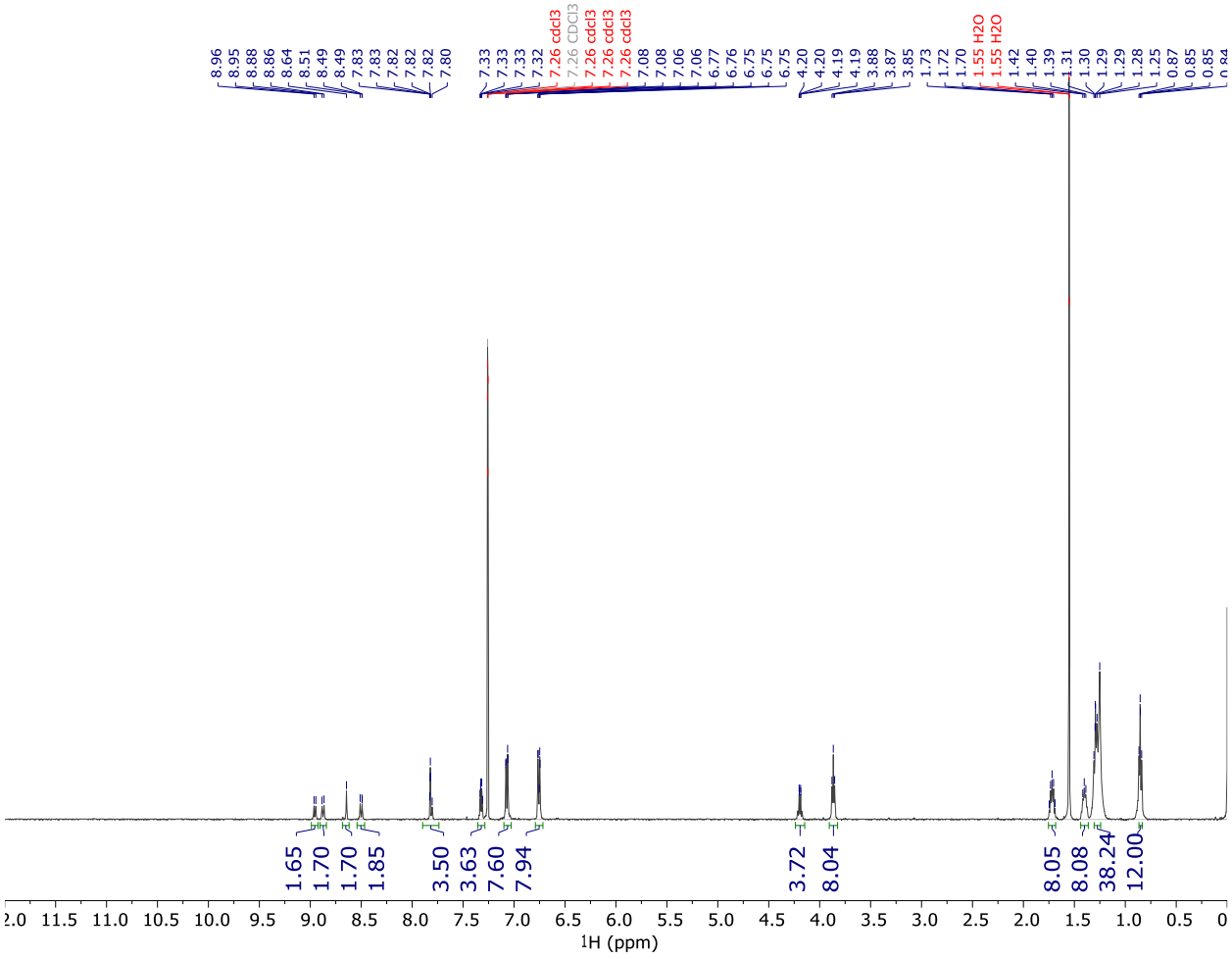

Figure S17: ^{1}H NMR spectrum of compound **11** in chloroform-*d* at 500 MHz.

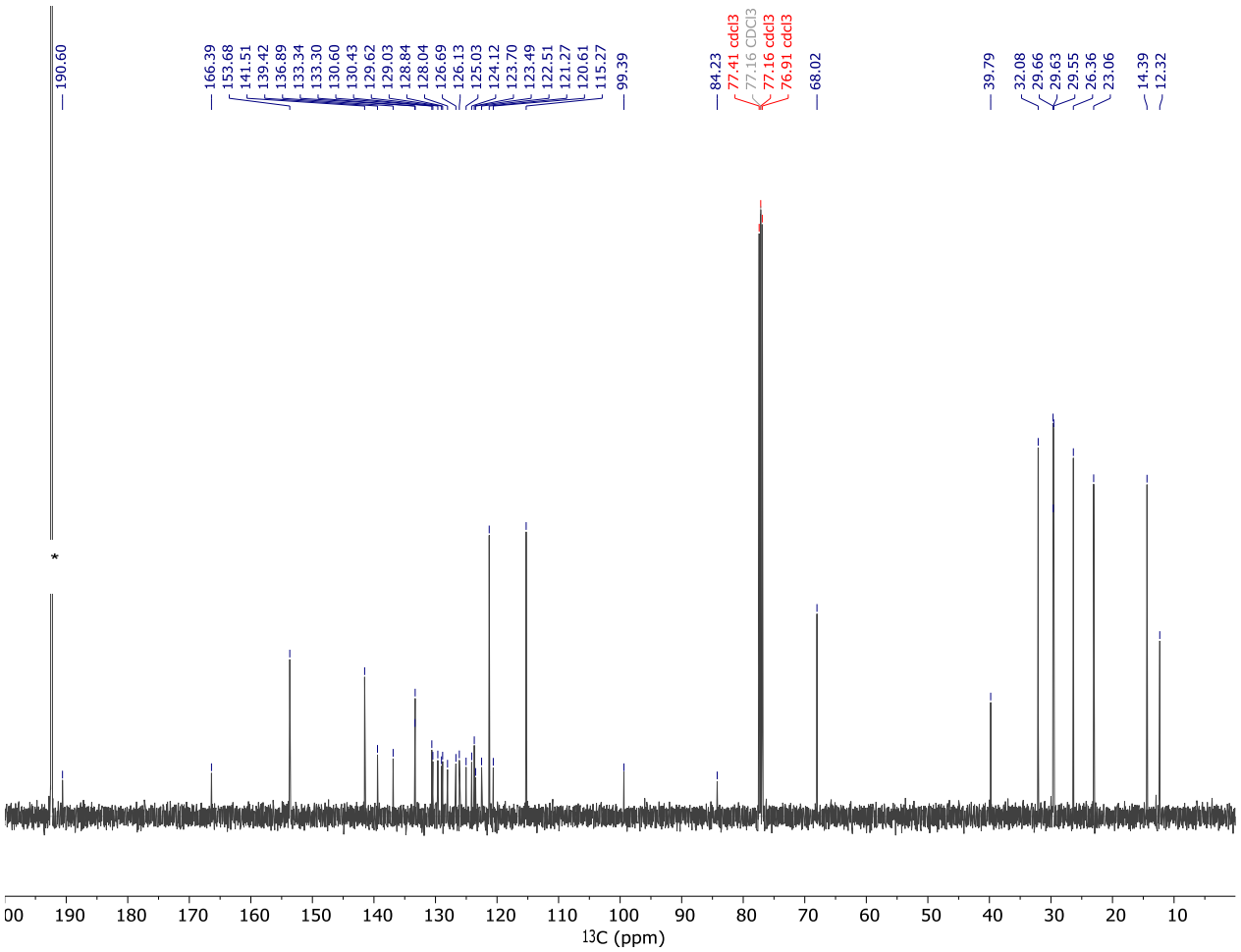

Figure S18: ^{13}C NMR spectrum of compound **11** in carbon disulfide:chloroform-*d* (3:1) at 126 MHz. Carbon disulfide peak at 192.39 ppm.

UV-Vis Spectroscopy

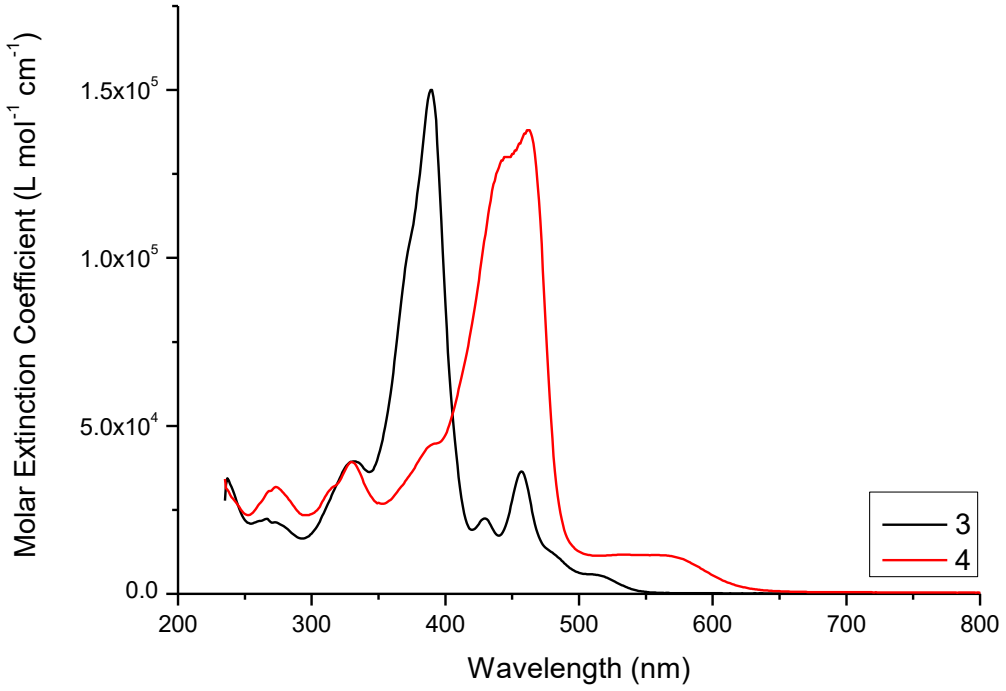

Figure S19: UV-Vis spectra of compounds **3-4** in chloroform solution.

Table S1: Absorption and emission properties of compounds **3-4** and **13-16**.

COMPOUND	$\lambda_{max}^{solution}$ / λ_{max}^{film} [a] (nm)	$\varepsilon_{max}^{solution}$ (10^4 L mol^{-1} cm^{-1})	$\lambda_{onset}^{solution}$ / λ_{onset}^{film} [b] (nm)	$E_g^{solution}$ / E_g^{film} [c] (eV)	λ_{max}^{fluo} (nm)
3	389 (510) / N/A	150	545 / N/A	2.28 / N/A	N/A
4	462 (550) / N/A	138	627 / N/A	1.98 / N/A	N/A
8	375 (579) / 382 (596)	11.5	641 / 664	1.93 / 1.87	674
9	457 (590) / 462	11.9	667 / 707	1.86 / 1.75	N/A
10	541 / 548	11.1	728 / 797	1.70 / 1.55	N/A
11	471 (585) / 494	14.2	648 / 709	1.91 / 1.75	N/A

[a] Center of the lower energy transition bands are reported in parentheses. [b] Determined using tangential curves with R^2 values over 0.93. [c] $E_g = 1240 \div \lambda_{onset}$

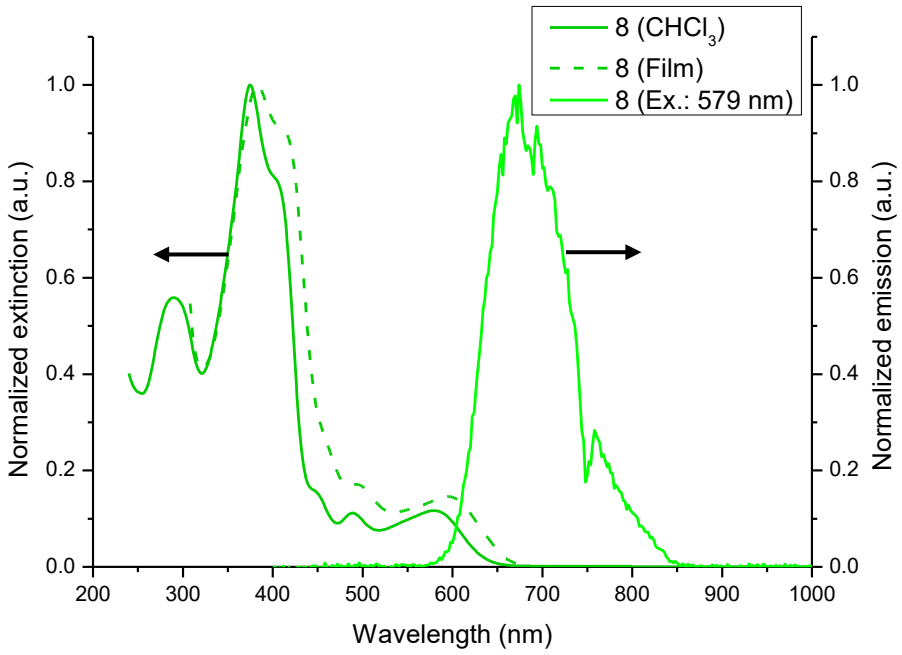

Figure S20: Normalized UV-Vis spectra in chloroform (solid line) and in thin film (dashed line), and normalized emission spectrum (pale solid line) of compound **8**.

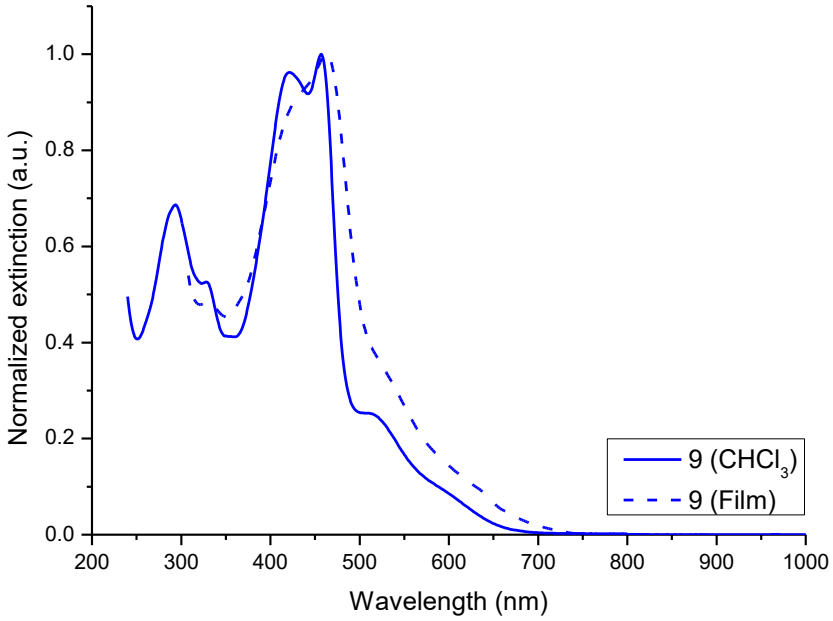

Figure S21: Normalized UV-Vis spectra in chloroform (solid line) and in thin film (dashed line) of compound **9**.

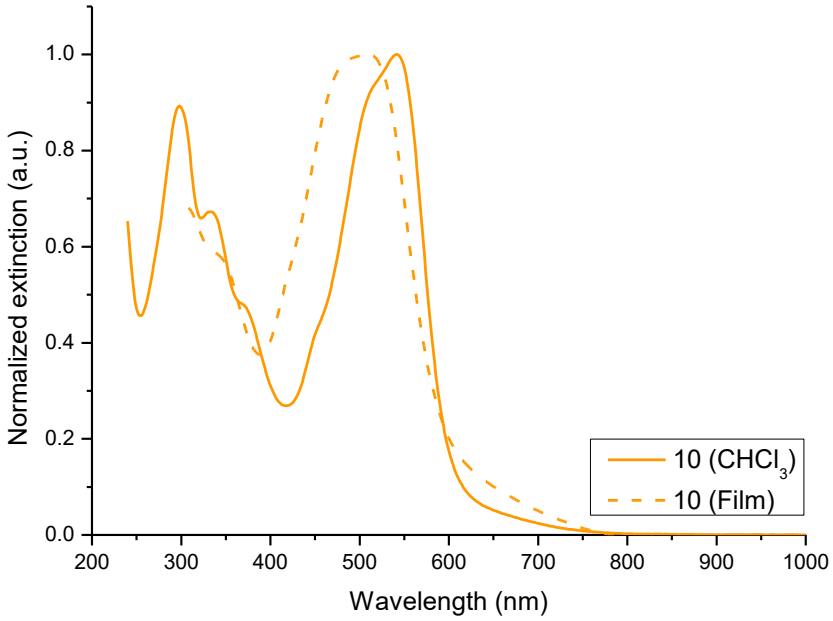

Figure S22: Normalized UV-Vis spectra in chloroform (solid line) and in thin film (dashed line) of compound **10**.

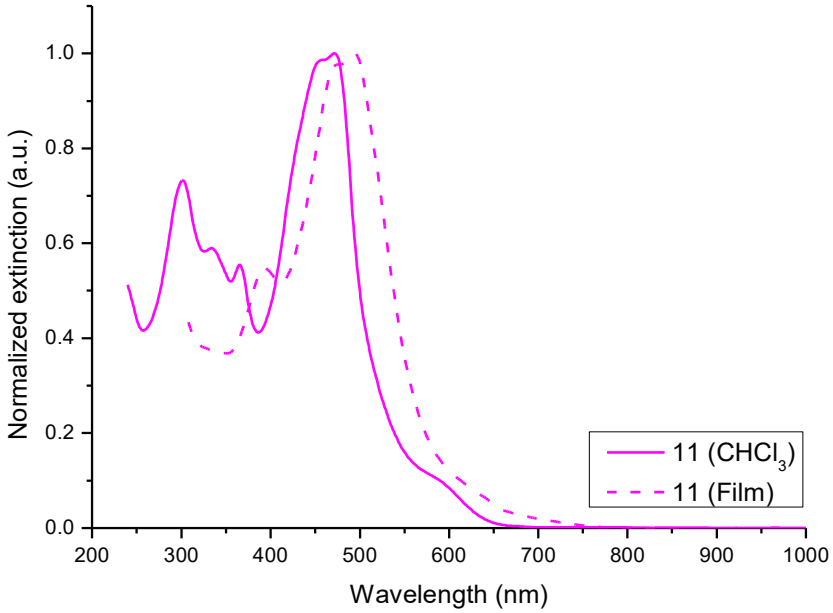

Figure S23: Normalized UV-Vis spectra in chloroform (solid line) and in thin film (dashed line) of compound **11**.

Electrochemistry

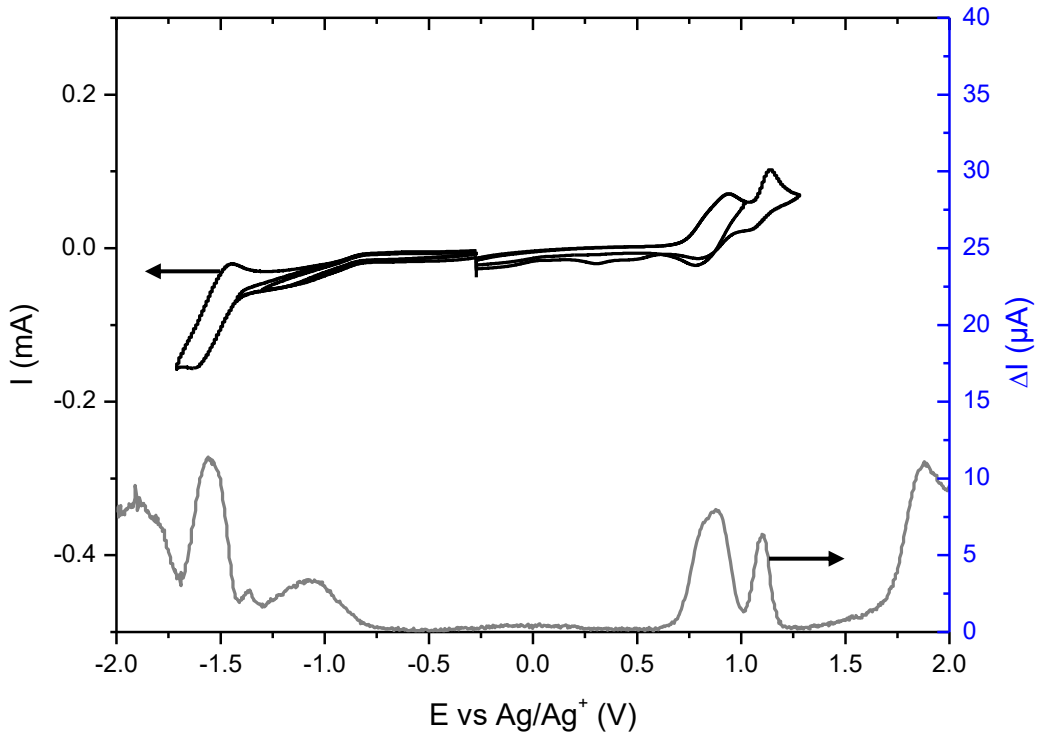

Figure S24: Cyclic Voltammetry (black curves) of compound **3** in dichloromethane solution with 0.1M [*n*-Bu_4N][PF_6] as the supporting electrolyte with a scan rate of 50 $mV \cdot s^{-1}$. Differential Pulse Voltammetry (gray curve) with a scan rate of 10 $mV\ s^{-1}$ using platinum wires as working and counter electrodes.

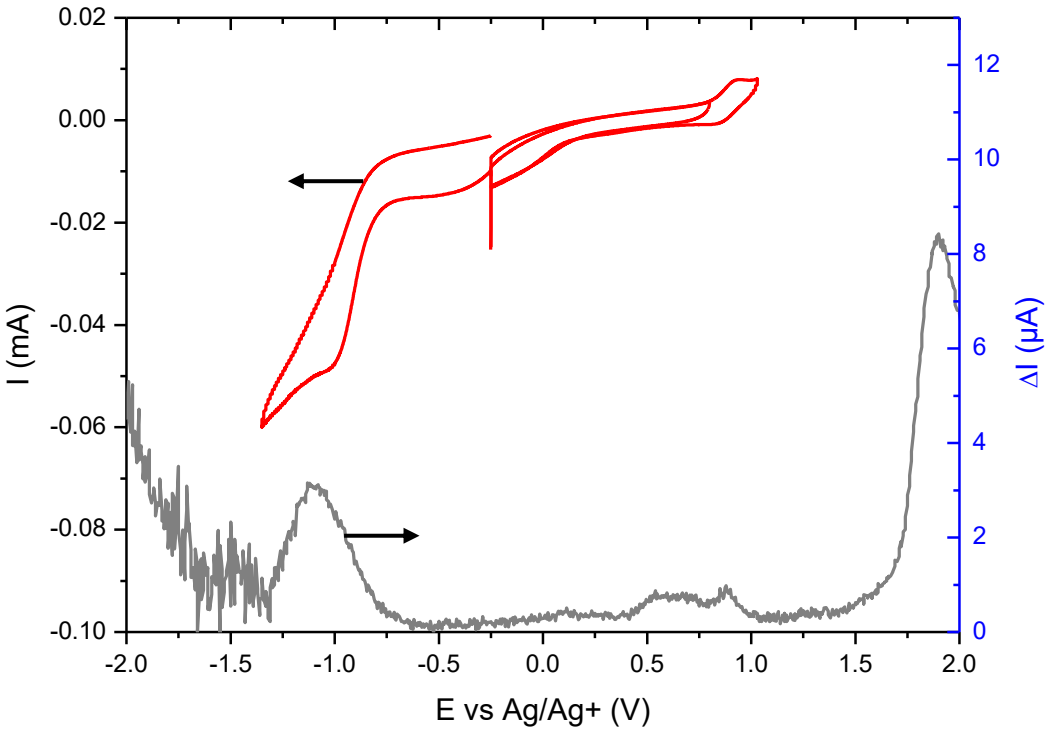

Figure S25: Cyclic Voltammetry (red curves) of compound **4** in dichloromethane solution with 0.1M [*n*-Bu_4N][PF_6] as the supporting electrolyte with a scan rate of 50 $mV \cdot s^{-1}$. Differential Pulse Voltammetry (gray curve) with a scan rate of 10 mV s^{-1} using platinum wires as working and counter electrodes. The results shown in this figure should be interpreted with caution, as compound **4** exhibits poor solubility.

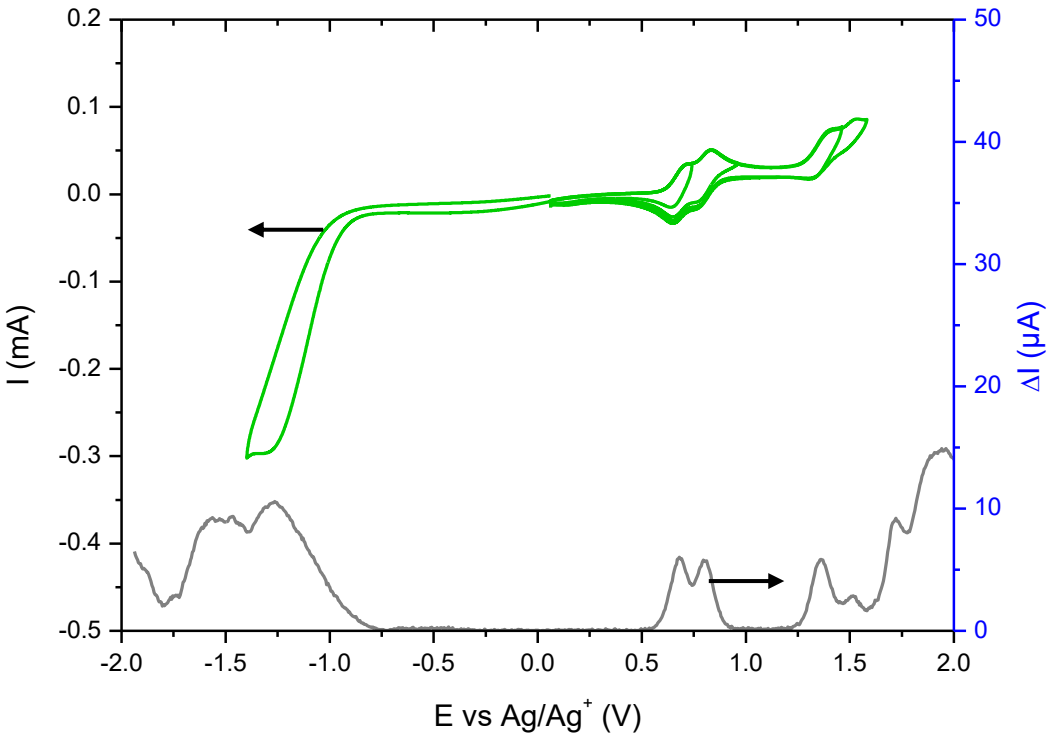

Figure S26: Cyclic Voltammetry (green curves) of compound **8** in dichloromethane solution with 0.1M [*n*-Bu_4N][PF_6] as the supporting electrolyte with a scan rate of 50 $mV \cdot s^{-1}$. Differential Pulse Voltammetry (gray curve) with a scan rate of 10 mV s^{-1} using platinum wires as working and counter electrodes.

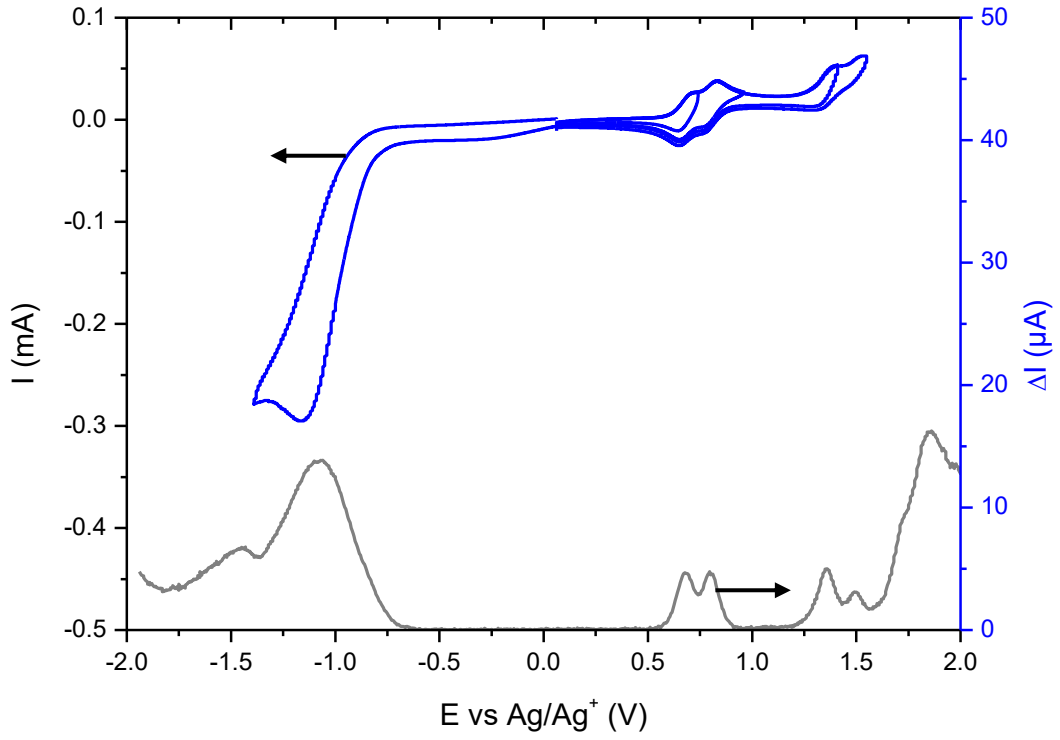

Figure S27: Cyclic Voltammetry (blue curves) of compound **9** in dichloromethane solution with 0.1M [*n*-Bu_4N][PF_6] as the supporting electrolyte with a scan rate of 50 $mV \cdot s^{-1}$. Differential Pulse Voltammetry (gray curve) with a scan rate of 10 $mV\ s^{-1}$ using platinum wires as working and counter electrodes.

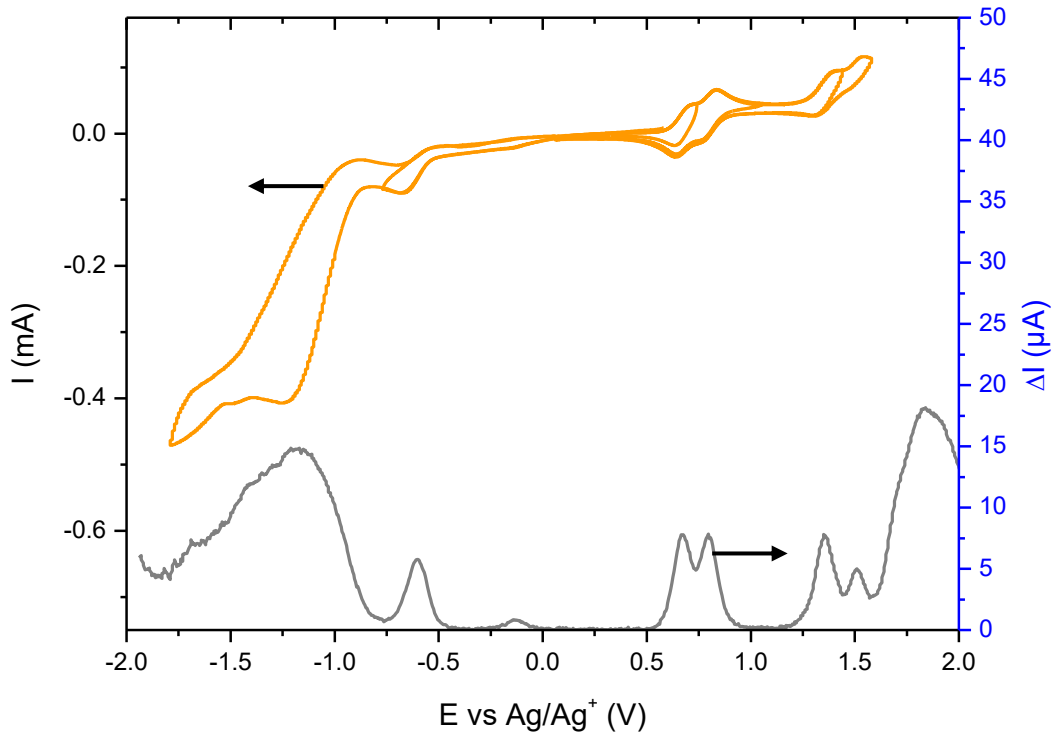

Figure S28: Cyclic Voltammetry (orange curves) of compound **10** in dichloromethane solution with 0.1M [*n*-Bu_4N][PF_6] as the supporting electrolyte with a scan rate of 50 $mV \cdot s^{-1}$. Differential Pulse Voltammetry (gray curve) with a scan rate of 10 $mV\ s^{-1}$ using platinum wires as working and counter electrodes.

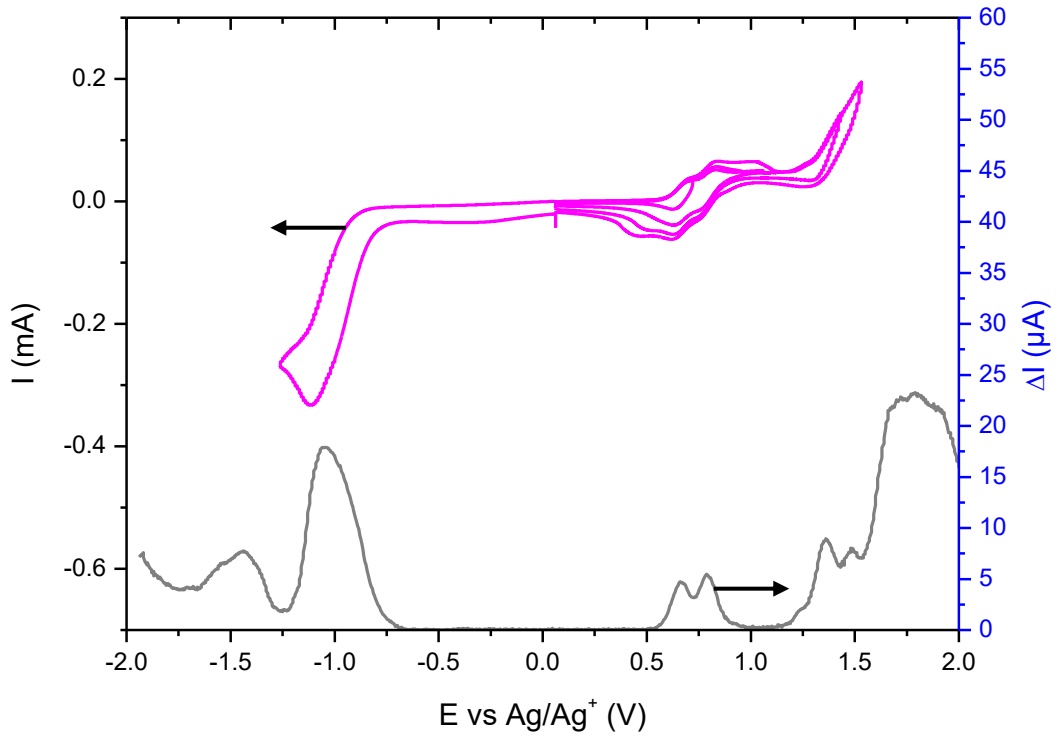

Figure S29: Cyclic Voltammetry (pink curves) of compound **11** in dichloromethane solution with 0.1M [*n*-Bu_4N][PF_6] as the supporting electrolyte with a scan rate of 50 $mV \cdot s^{-1}$. Differential Pulse Voltammetry (gray curve) with a scan rate of 10 $mV\ s^{-1}$ using platinum wires as working and counter electrodes.

Table S2: Differential pulse voltammetry (DPV)[a] reduction and oxidation peaks summary for compounds **3-4** and **8-11**.

Compound	2nd reduction (V vs Ag/Ag+)[b]	1st reduction (V vs Ag/Ag+)	1st oxidation (V vs Ag/Ag+)	2nd oxidation (V vs Ag/Ag+)	3rd oxidation (V vs Ag/Ag+)	4th oxidation (V vs Ag/Ag+)
3	-1.36	-1.08	0.88	1.10	---	---
4	---	-1.13	0.54	0.88	---	---
8	---	-1.26	0.68	0.80	1.36	1.52
9	---	-1.06	0.68	0.80	1.36	1.50
10	-1.21	-0.60	0.67	0.80	1.35	1.51
11	-1.44	-1.04	0.66	0.79	1.36	---

[a] Scan rate: 10 mV s^{-1} in dichloromethane solution with 0.1M [*n*-Bu_4N][PF_6] as the supporting electrolyte using platinum wires as working and counter electrodes. [b] The ferrocene peak were adjusted to 0.475 V versus Ag/Ag^+.[1]

Table S3: Frontier orbitals (HOMO and LUMO) energy levels and band gap (E_g) of compounds **3-4** and **8-11** calculated from electrochemical measurements.

Compound	HOMO (eV)	LUMO (eV)	Eg (eV)
3	-5.20	-3.24	1.96
4	-4.86	-3.20	1.67
8	-5.01	-3.06	1.94
9	-5.00	-3.26	1.74
10	-4.99	-3.73	1.26
11	-4.99	-3.28	1.71

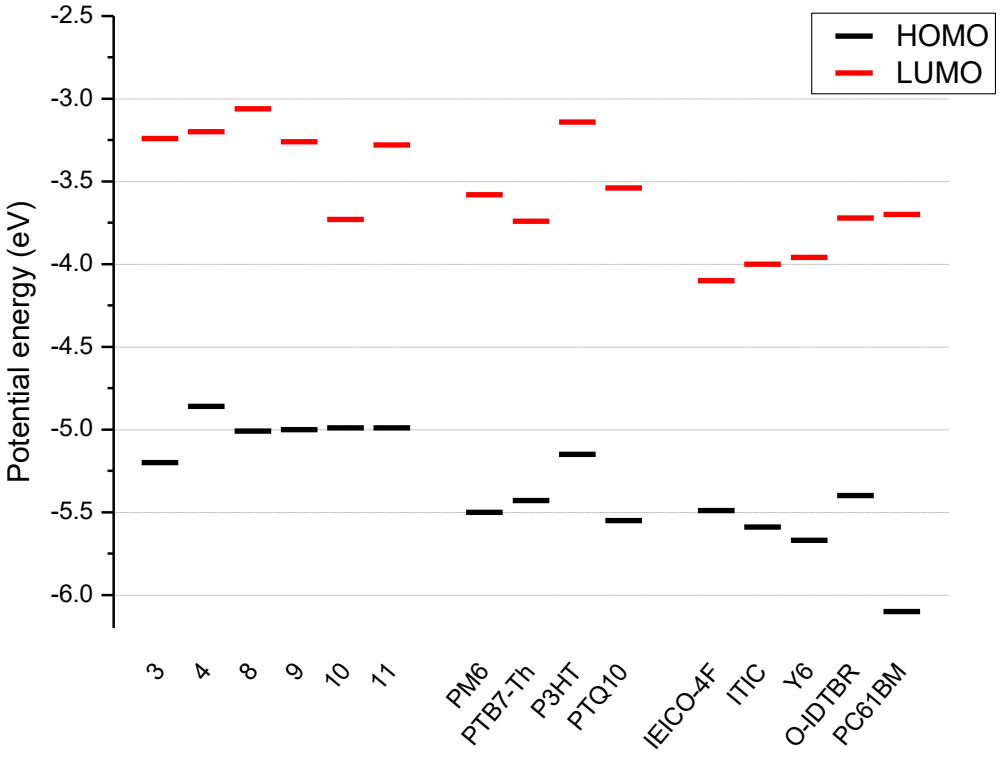

Figure S30: Ionisation potential (IP) and electron affinity (EA) of compounds **3-4** and **8-11** as calculated from CV measurements and state-of-the-art materials for OSC applications.[11]

Thermogravimetric analysis

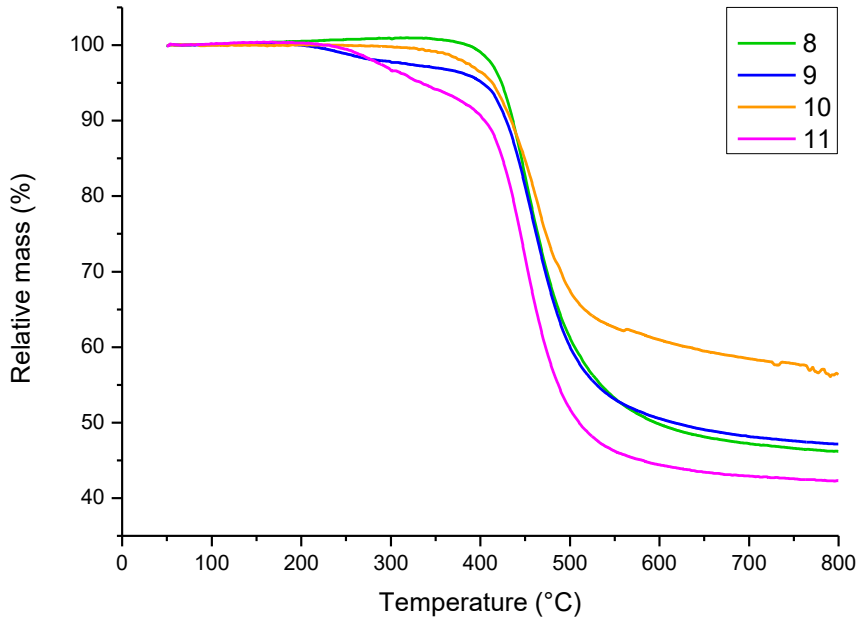

Figure S31: Thermogravimetric analysis curves for compounds **8-11** at a scan rate of 20 °C/minute and protected by a constant PP nitrogen flow of 20 mL/minute.

Table S4: Decomposition temperature of **8-11**.

COMPOUND	DECOMPOSITION TEMPERATURE[a] (°C)
8	420 – 424
9	387 – 402
10	405 – 413
11	318 – 334

[a] 5 % weight loss

Differential scanning calorimetry

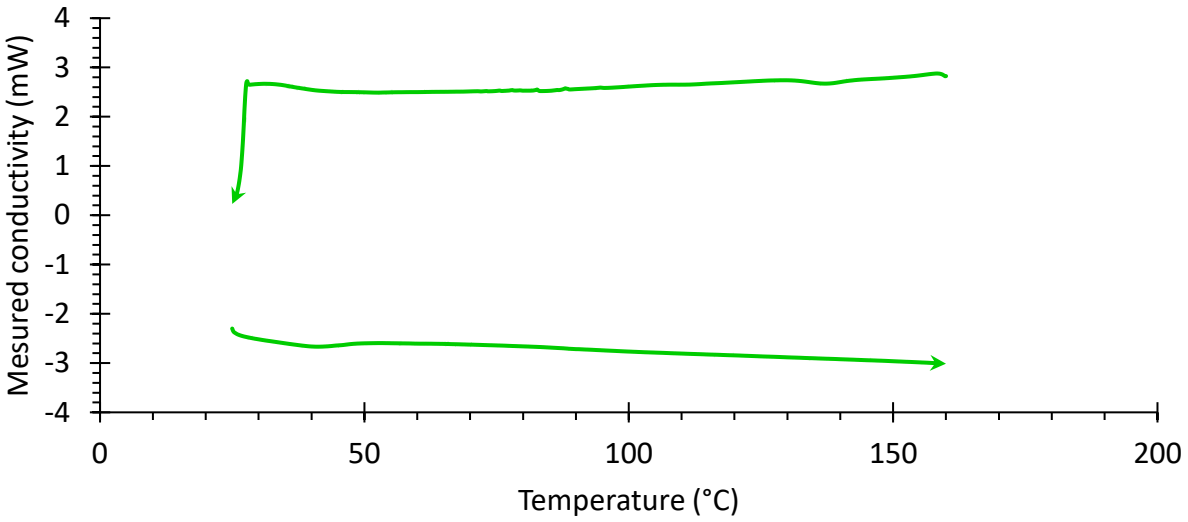

Figure S32: Differential scanning calorimetry plots of compound **8** after the thermal history was erased by heating at a rate of 20 °C/minute. Scan rate of ±10 °C/minute with 1 minute of stabilization between cooling and heating.

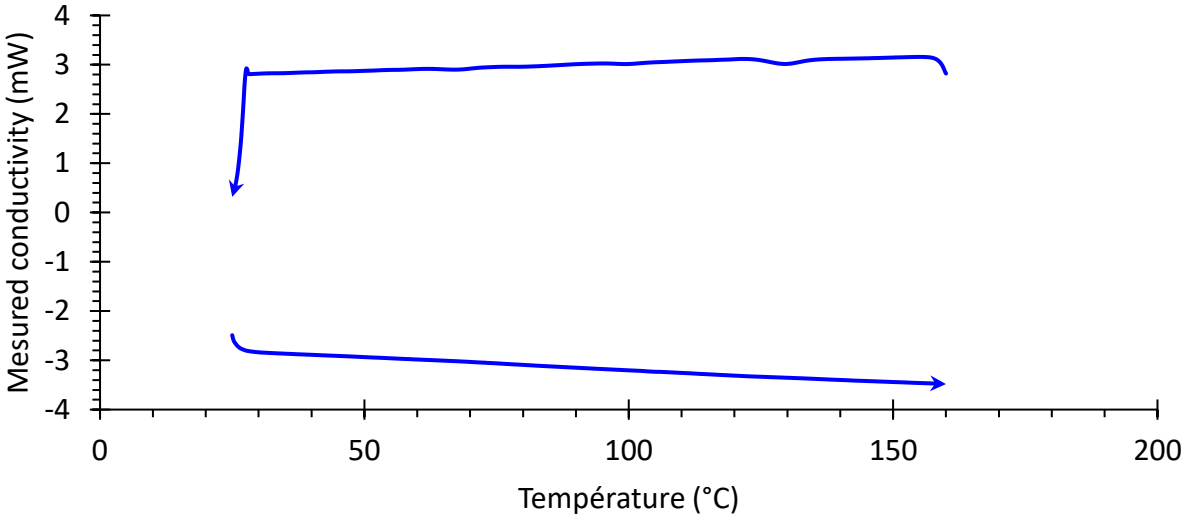

Figure S33: Differential scanning calorimetry plots of compound **9** after the thermal history was erased by heating at a rate of 20 °C/minute. Scan rate of ±10 °C/minute with 1 minute of stabilization between cooling and heating.

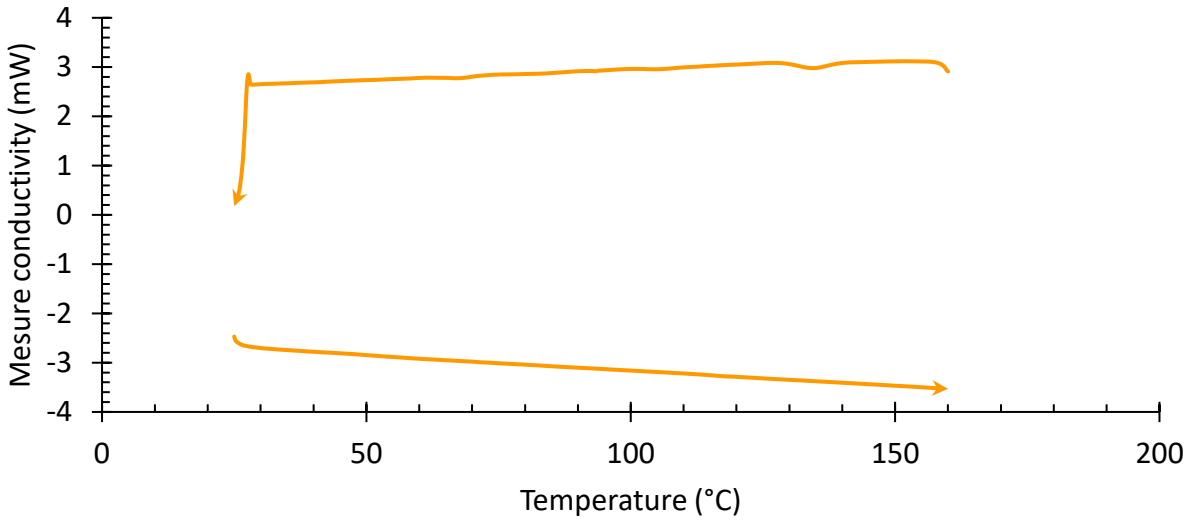

Figure S34: Differential scanning calorimetry plots of compound **10** after the thermal history was erased by heating at a rate of 20 °C/minute. Scan rate of ±10 °C/minute with 1 minute of stabilization between cooling and heating.

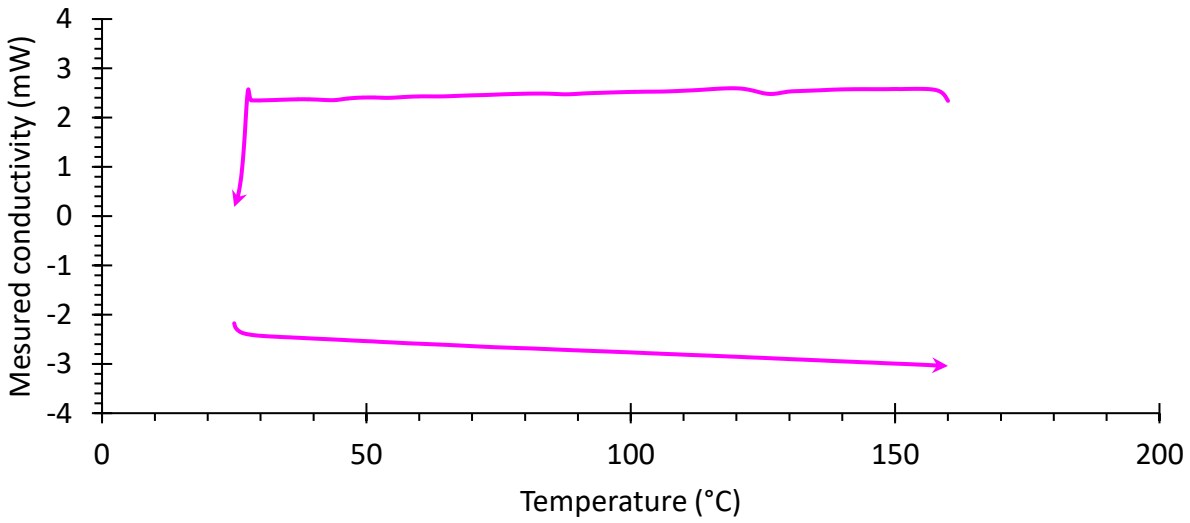

Figure S35: Differential scanning calorimetry plots of compound **11** after the thermal history was erased by heating at a rate of 20 °C/minute. Scan rate of ±10 °C/minute with 1 minute of stabilization between cooling and heating.

Computational Chemistry

Table S5: Dihedral angles of diphenylamine groups with VO1-core (DPA), thiophene units with VO1-core through the alkyne π-bridge (alkyne) and thiophene with vinyl-bridge of end-groups (end-group) of optimized geometry of compound **8-11** and **8'-11'** based on calculation at B3LYP/6-31+G(d,p) level using the PCM solvation model in chloroform with a superfine integration grid.

COMPOUND	DPA (°)	ALKYNE (°)	END-GROUP (°)
8	70 – 71	0	0
9	70 – 71	0	0
10	70 – 71	0 – 2	1 – 3
11	71	1	0
8'	25 – 31	1	0
9'	24 – 31	1	1
10'	22 – 31	1 – 4	1 – 3
11'	22 – 33	1 – 8	0 – 1

Table S6: Dihedral angles of diphenylamine groups with VO1-core (DPA), thiophene units with VO1-core through the alkyne π-bridge (alkyne) and thiophene with vinyl-bridge of end-groups (end-group) of optimized geometry of compound **8-11** and **8'-11'** based on calculation at ωB97xD/6-31+G(d,p) level using the PCM solvation model in chloroform with a superfine integration grid.

COMPOUND	DPA (°)	ALKYNE (°)	END-GROUP (°)
8	70 – 72	4	0
9	71 – 72	1	0
10	70 – 72	0 – 7	5 – 10
11	70 – 72	1 – 2	0
8'	14 – 30	43 – 52	1
9'	15 – 28	39 – 49	0 – 1
10'	14 – 31	9 – 39	5 – 11
11'	14 – 36	26 – 32	0 – 6

Table S7: Dihedral angles of diphenylamine groups with VO1-core (DPA), thiophene units with VO1-core through the alkyne π-bridge (alkyne) and thiophene with vinyl-bridge of end-groups (end-group) of optimized geometry of compound **8-11** and **8'-11'** based on calculation at HF/6-31+G(d,p) level using the PCM solvation model in chloroform with a superfine integration grid.

COMPOUND	DPA (°)	ALKYNE (°)	END-GROUP (°)
8	74 – 76	0 – 5	0
9	74 – 76	0 – 2	0 – 1
10	74 – 76	1 – 5	12 – 18
11	74 – 76	1 – 2	3 – 4
8'	19 – 36	1	0
9'	18 – 35	0	1 – 2
10'	17 – 35	1	9 – 16
11'	18 – 38	3 – 26	1 – 5

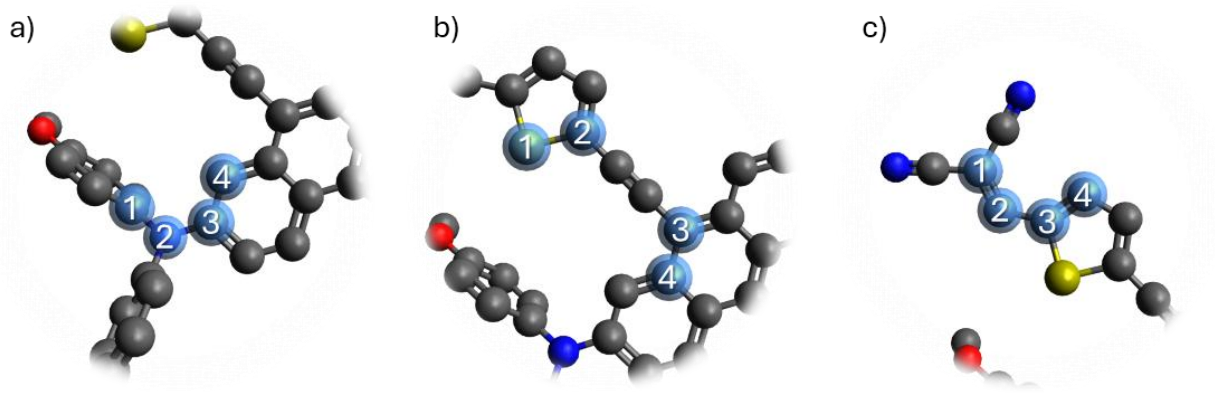

Figure S36: Representations of the mesured of dihedral angles of (a) diphenylamine groups with VO1-core (DPA), (b) thiophene units with VO1-core through the alkyne π-bridge (alkyne) and (c) thiophene with vinyl-bridge of end-groups (end-group) of optimized geometry of compound **8-11** and **8'-11'**. The dihedral angle correspond to the angle between the plane in which the atoms 1, 2 and 3 are and a second plane formed by the atoms 2, 3 and 4. The bond between atoms 2 and 3 being a part of both planes throught a segment.

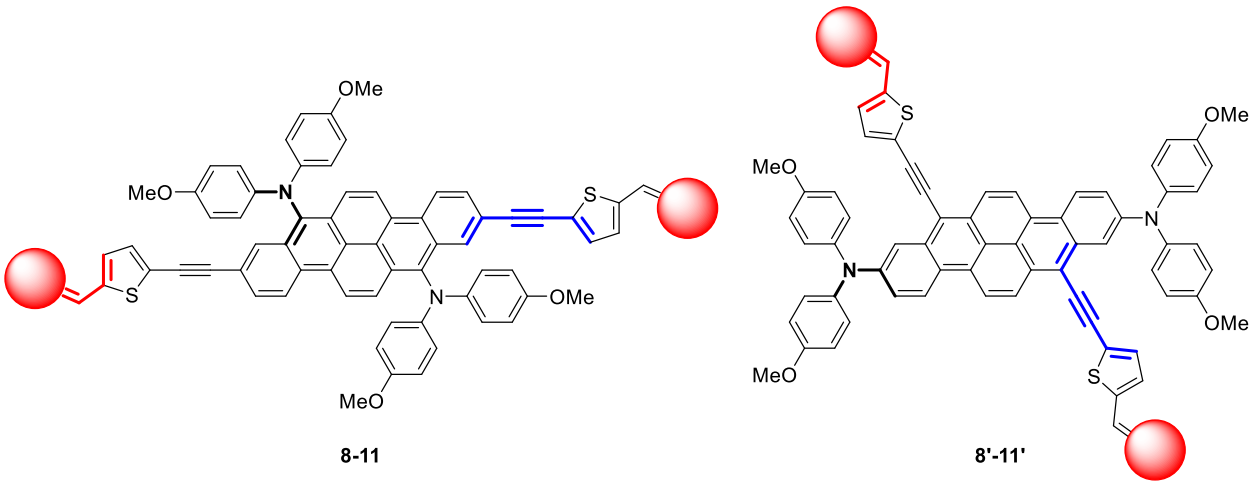

Figure S37: Representations of the mesured of dihedral angles of diphenylamine groups with VO1-core (DPA, in black), thiophene units with VO1-core through the alkyne π-bridge (alkyne, in blue) and thiophene with vinyl-bridge of end-groups (end-group, in red) of optimized geometry of compound **8-11** and **8'-11'**.

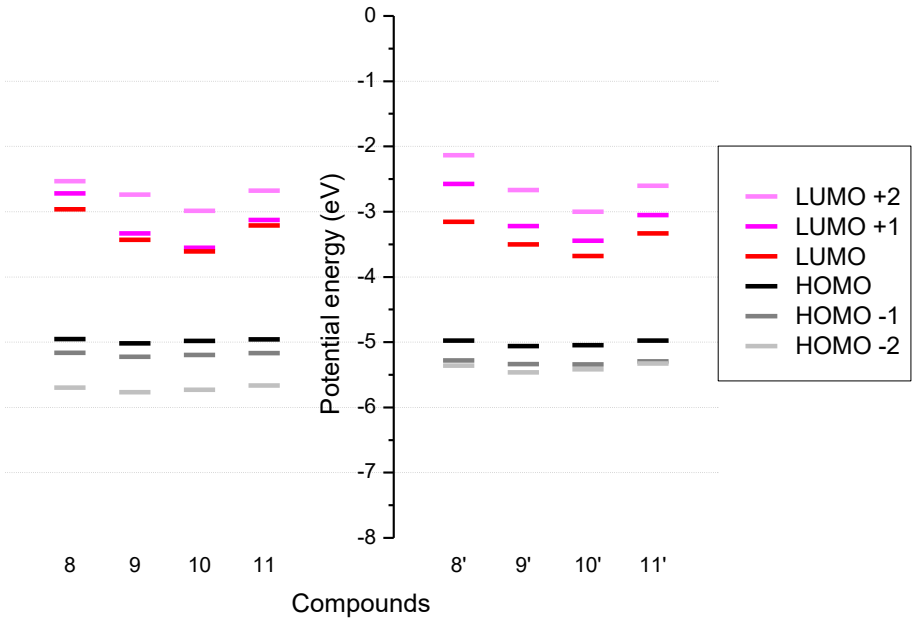

Figure S38: Frontier molecular orbital energy diagram of compounds **8-11** and **8'-11'** based on calculation at B3LYP/6-31+G(d,p) level using the PCM solvation model in chloroform with a superfine integration grid.

Table S8: Frontier molecular orbital energy and band gap of compounds **8-11** and **8'-11'** based on calculation at B3LYP/6-31+G(d,p) level using the PCM solvation model in chloroform with a superfine integration grid.

COMPOUND	HOMO -2 (eV)	HOMO -1 (eV)	HOMO (eV)	LUMO (eV)	LUMO +1 (eV)	LUMO +2 (eV)	E_g (eV)
8	-5.70	-5.17	-4.95	-2.97	-2.72	-2.53	1.99
9	-5.77	-5.23	-5.02	-3.43	-3.34	-2.74	1.59
10	-5.73	-5.19	-4.98	-3.61	-3.55	-2.99	1.37
11	-5.66	-5.17	-4.96	-3.21	-3.13	-2.68	1.75
8'	-5.36	-5.28	-4.98	-3.16	-2.57	-2.14	1.82
9'	-5.46	-5.34	-5.06	-3.50	-3.22	-2.67	1.56
10'	-5.41	-5.34	-5.05	-3.68	-3.45	-3.00	1.37
11'	-5.33	-5.30	-4.97	-3.33	-3.05	-2.61	1.64

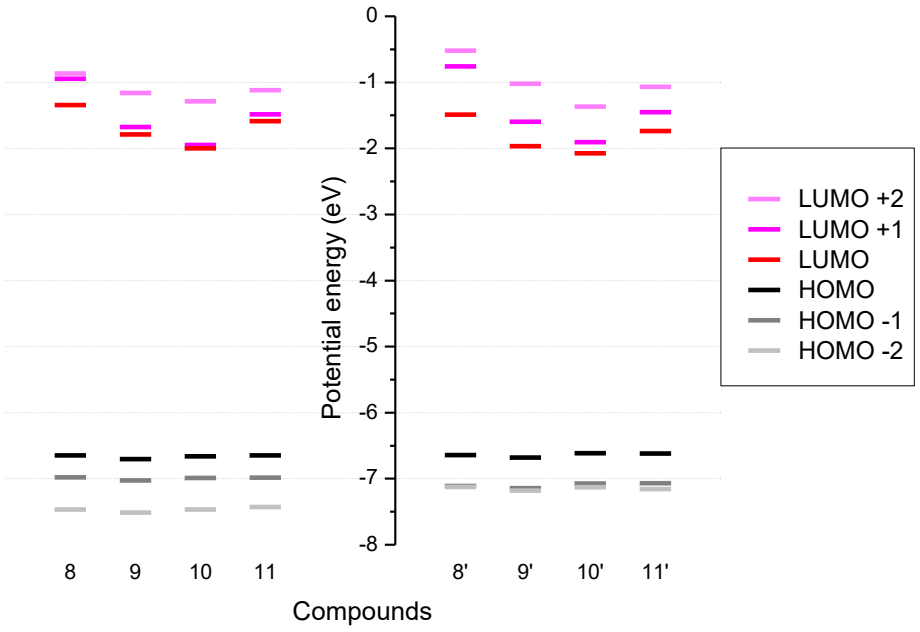

Figure S39: Frontier molecular orbital energy diagram of compounds **8-11** and **8'-11'** based on calculation at ωB97xD/6-31+G(d,p) level using the PCM solvation model in chloroform with a superfine integration grid.

Table S9: Frontier molecular orbital energy and band gap of compounds **8-11** and **8'-11'** based on calculation at ωB97xD/6-31+G(d,p) level using the PCM solvation model in chloroform with a superfine integration grid.

COMPOUND	HOMO -2 (eV)	HOMO -1 (eV)	HOMO (eV)	LUMO (eV)	LUMO +1 (eV)	LUMO +2 (eV)	E_g (eV)
8	-7.47	-6.98	-6.65	-1.34	-0.94	-0.87	5.30
9	-7.51	-7.03	-6.70	-1.79	-1.68	-1.16	4.91
10	-7.47	-6.99	-6.66	-2.00	-1.95	-1.29	4.66
11	-7.43	-6.98	-6.65	-1.59	-1.49	-1.12	5.06
8'	-7.12	-7.11	-6.64	-1.49	-0.76	-0.52	5.16
9'	-7.18	-7.14	-6.68	-1.97	-1.60	-1.02	4.71
10'	-7.13	-7.07	-6.61	-2.08	-1.91	-1.37	4.54
11'	-7.16	-7.07	-6.62	-1.74	-1.45	-1.07	4.88

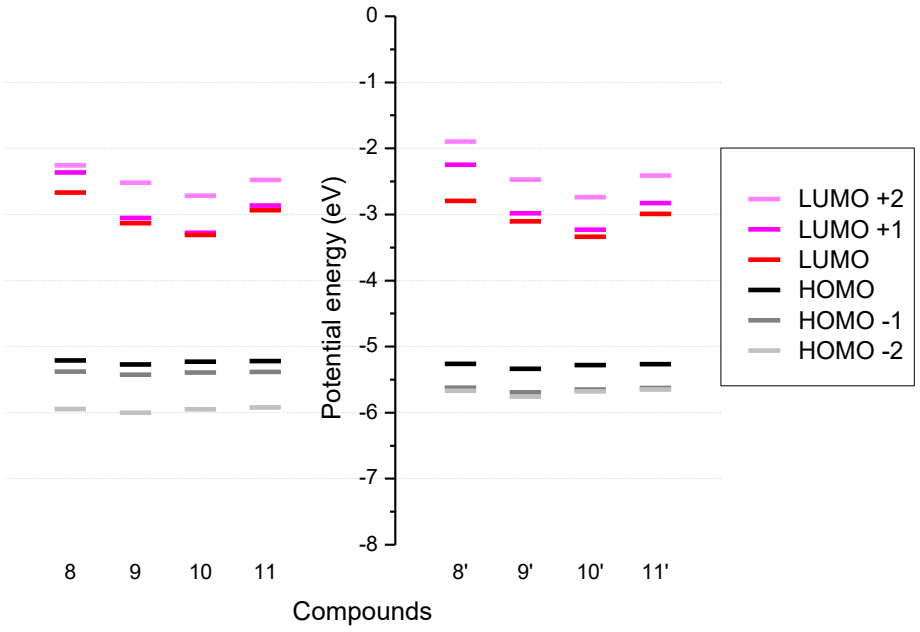

Figure S40: Frontier molecular orbital energy diagram of compounds **8-11** and **8'-11'** based on geometry optimization at HF/6-31+G(d,p) level and energy calculation at PBE0/6-31+G(d,p) level using the PCM solvation model in chloroform with a superfine integration grid.

Table S10: Frontier molecular orbital energy and band gap of compounds **8-11** and **8'-11'** based on geometry optimization at HF/6-31+G(d,p) level and energy calculation at PBE0/6-31+G(d,p) level using the PCM solvation model in chloroform with a superfine integration grid.

COMPOUND	HOMO -2 (eV)	HOMO -1 (eV)	HOMO (eV)	LUMO (eV)	LUMO +1 (eV)	LUMO +2 (eV)	E_g (eV)
8	-5.94	-5.38	-5.21	-2.67	-2.36	-2.26	2.54
9	-6.00	-5.43	-5.27	-3.13	-3.05	-2.52	2.14
10	-5.95	-5.39	-5.23	-3.31	-3.28	-2.72	1.92
11	-5.92	-5.39	-5.22	-2.93	-2.87	-2.48	2.29
8'	-5.67	-5.62	-5.26	-2.80	-2.25	-1.90	2.46
9'	-5.76	-5.69	-5.34	-3.11	-2.98	-2.47	2.23
10'	-5.68	-5.65	-5.28	-3.34	-3.23	-2.74	1.94
11'	-5.65	-5.63	-5.27	-2.99	-2.83	-2.41	2.28

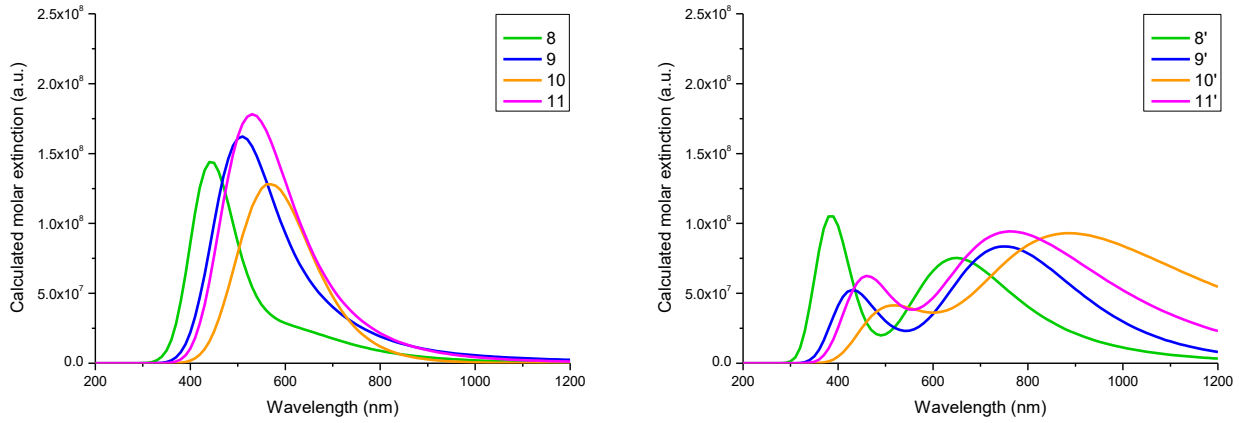

Figure S41: Simulated UV–Vis absorption spectra of compounds **8-11** (left) and **8'-11'** (right) based on calculation at B3LYP/6-31+G(d,p) level using the PCM solvation model in chloroform with a superfine integration grid for the 20 first excitation energies using a value of 0.4 eV for the standard deviation.

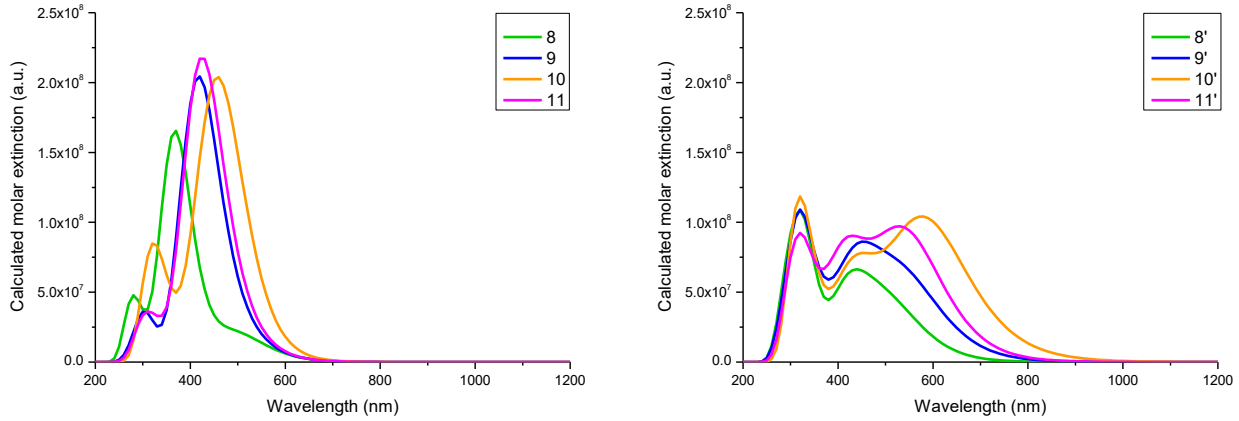

Figure S42: Simulated UV–Vis absorption spectra of compounds **8-11** (left) and **8'-11'** (right) based on calculation at ωB97xD/6-31+G(d,p) level using the PCM solvation model in chloroform with a superfine integration grid for the 20 first excitation energies using a value of 0.4 eV for the standard deviation.

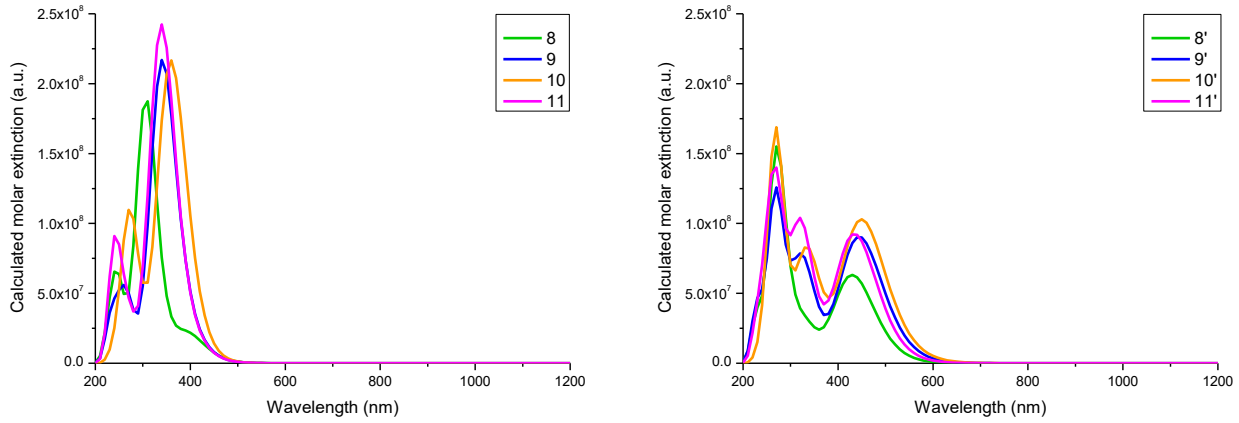

Figure S43: Simulated UV–Vis absorption spectra of compounds **8-11** (left) and **8'-11'** (right) based on geometry optimization at HF/6-31+G(d,p) level, energy calculation at PBE0/6-31+G(d,p) level and TD calculation at HF/6-31+G(d,p) level using the PCM solvation model in chloroform with a superfine integration grid for the 20 first excitation energies using a value of 0.4 eV for the standard deviation.

Table S11: Absolute maximum extinction wavelength (λ_{max}) of compound **8-11** and **8'-11'** based on calculation using different methods on the same basis set (6-31+G(d,p)) using the PCM solvation model in chloroform with a superfine integration grid. Graph has been plotted with 10 nm steps.

COMPOUND	λ_{max} B3LYP (nm)	λ_{max} ωB97xD (nm)	λ_{max} HF/PBE0/HF (nm)
8	440	370	310
9	510	420	340
10	560	460	360
11	530	420	340
8'	390	320	270
9'	750	320	270
10'	890	320	270
11'	760	530	270

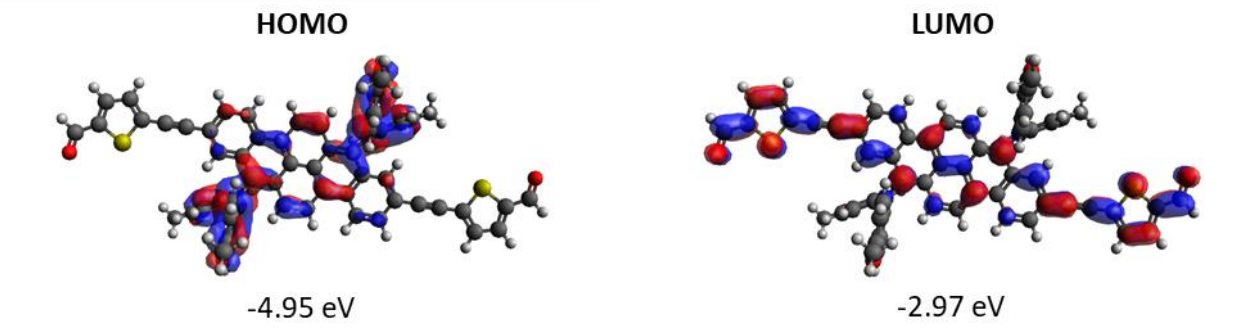

Figure S44: Kohn–Sham molecular orbitals of compound **8** based on calculation at B3LYP/6-31+G(d,p) level using the PCM solvation model in chloroform with a superfine integration grid.

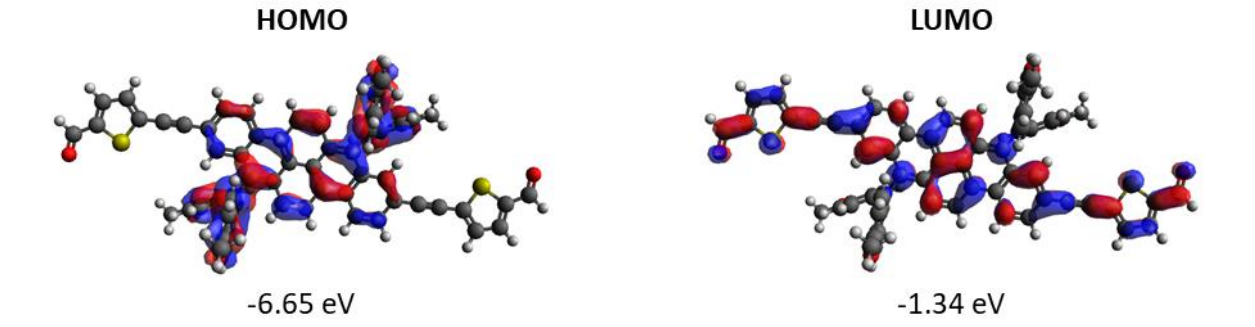

Figure S45: Kohn–Sham molecular orbitals of compound **8** based on calculation at ωB97xD/6-31+G(d,p) level using the PCM solvation model in chloroform with a superfine integration grid.

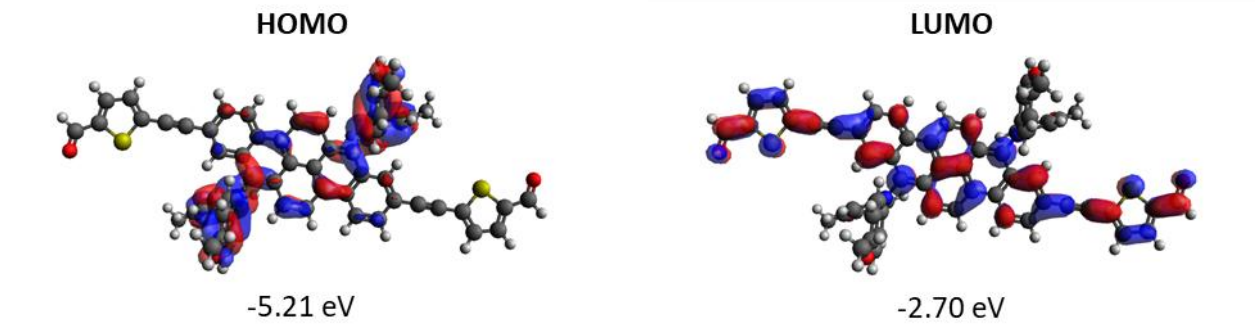

Figure S46: Kohn–Sham molecular orbitals of compound **8** based on geometry optimization at HF/6-31+G(d,p) level and energy calculation at PBE0/6-31+G(d,p) level using the PCM solvation model in chloroform with a superfine integration grid.

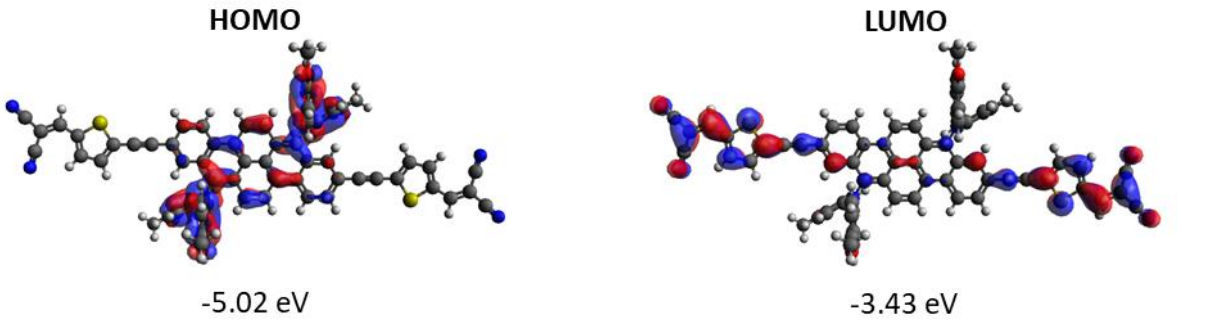

Figure S47: Kohn–Sham molecular orbitals of compound **9** based on calculation at B3LYP/6-31+G(d,p) level using the PCM solvation model in chloroform with a superfine integration grid.

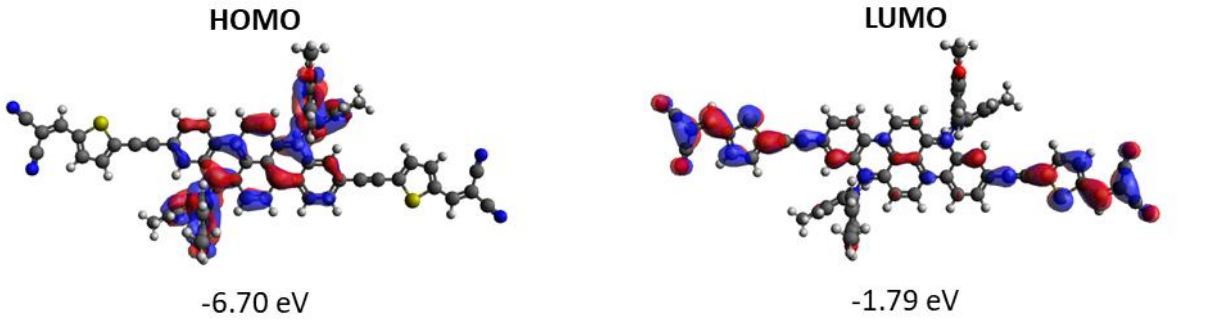

Figure S48: Kohn–Sham molecular orbitals of compound **9** based on calculation at ωB97xD/6-31+G(d,p) level using the PCM solvation model in chloroform with a superfine integration grid.

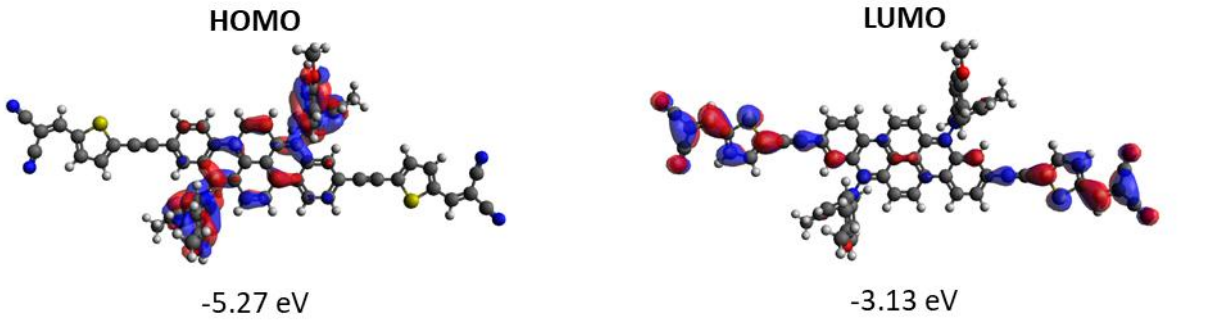

Figure S49: Kohn–Sham molecular orbitals of compound **9** based on geometry optimization at HF/6-31+G(d,p) level and energy calculation at PBE0/6-31+G(d,p) level using the PCM solvation model in chloroform with a superfine integration grid.

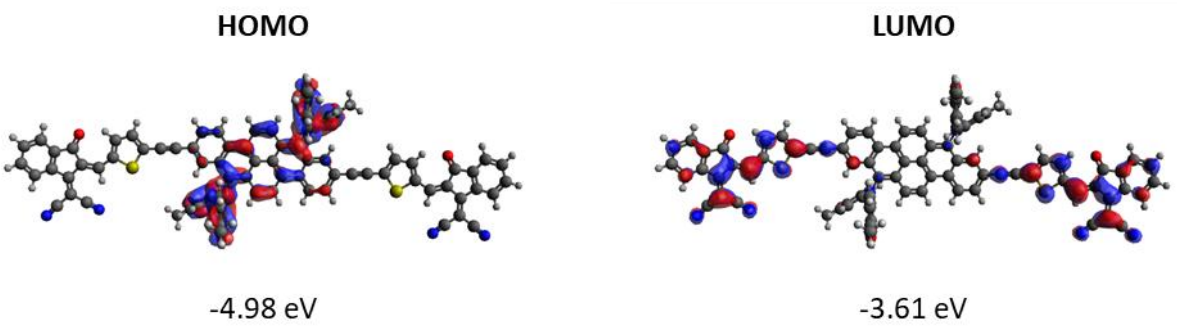

Figure S50: Kohn–Sham molecular orbitals of compound **10** based on calculation at B3LYP/6-31+G(d,p) level using the PCM solvation model in chloroform with a superfine integration grid.

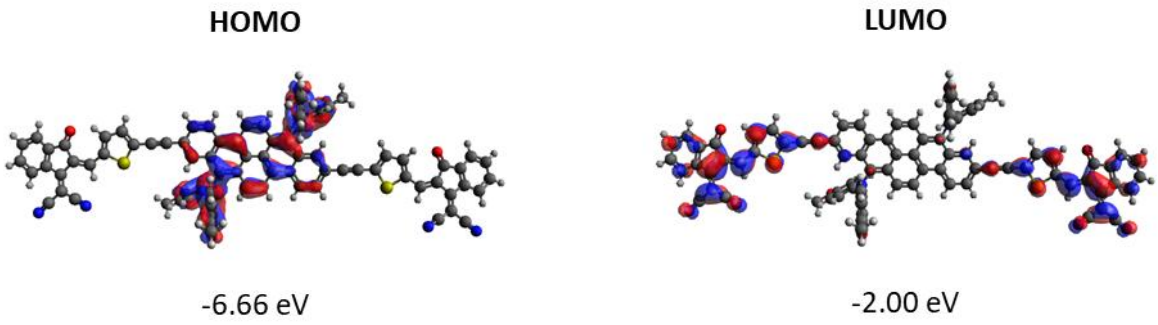

Figure S51: Kohn–Sham molecular orbitals of compound **10** based on calculation at ωB97xD/6-31+G(d,p) level using the PCM solvation model in chloroform with a superfine integration grid.

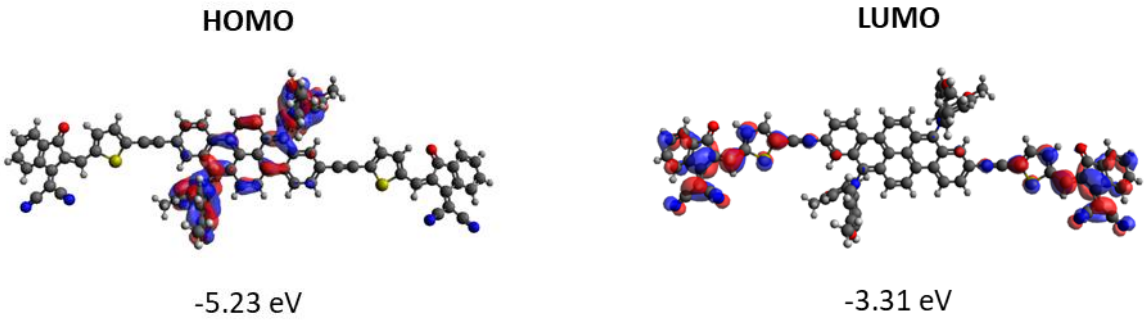

Figure S52: Kohn–Sham molecular orbitals of compound **10** based on geometry optimization at HF/6-31+G(d,p) level and energy calculation at PBE0/6-31+G(d,p) level using the PCM solvation model in chloroform with a superfine integration grid.

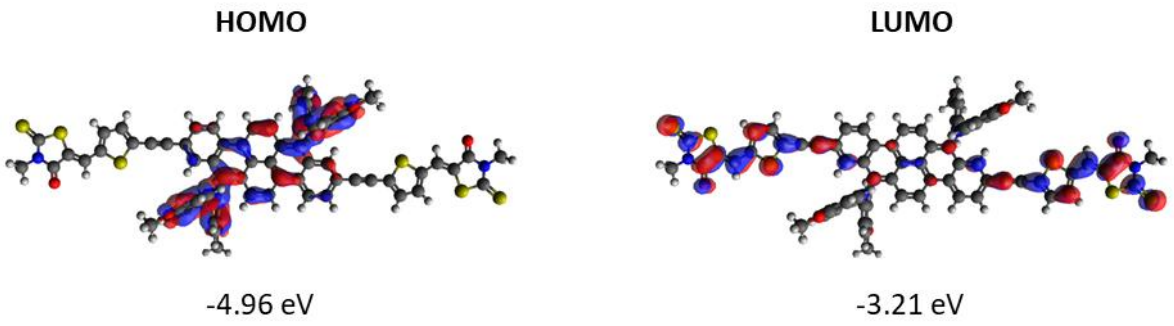

Figure S53: Kohn–Sham molecular orbitals of compound **11** based on calculation at B3LYP/6-31+G(d,p) level using the PCM solvation model in chloroform with a superfine integration grid.

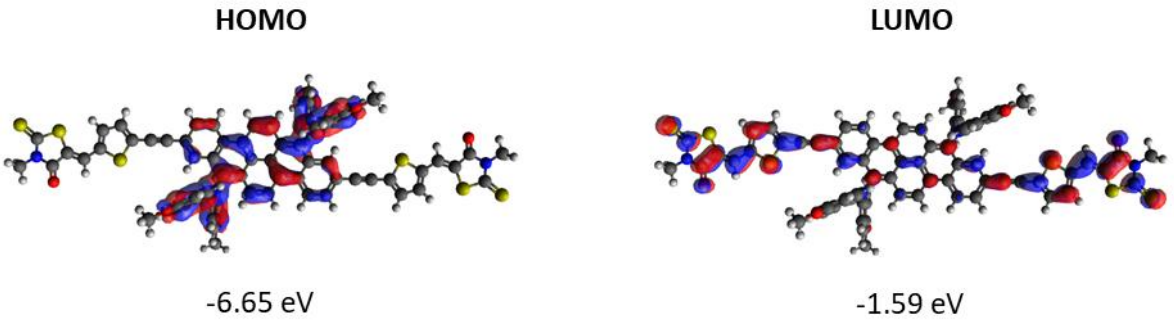

Figure S54: Kohn–Sham molecular orbitals of compound **11** based on calculation at ωB97xD/6-31+G(d,p) level using the PCM solvation model in chloroform with a superfine integration grid.

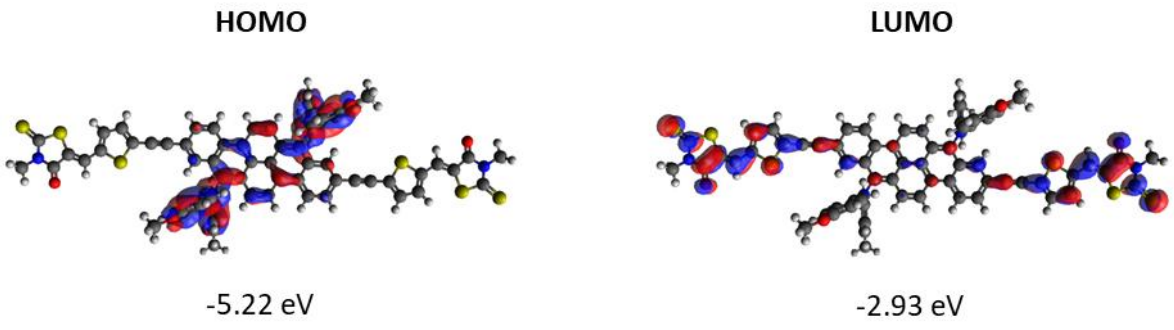

Figure S55: Kohn–Sham molecular orbitals of compound **11** based on geometry optimization at HF/6-31+G(d,p) level and energy calculation at PBE0/6-31+G(d,p) level using the PCM solvation model in chloroform with a superfine integration grid.

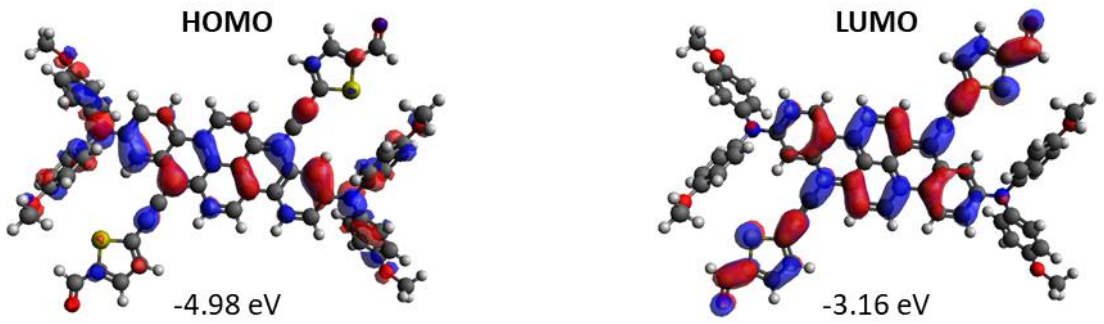

Figure S56: Kohn–Sham molecular orbitals of compound **8'** based on calculation at B3LYP/6-31+G(d,p) level using the PCM solvation model in chloroform with a superfine integration grid.

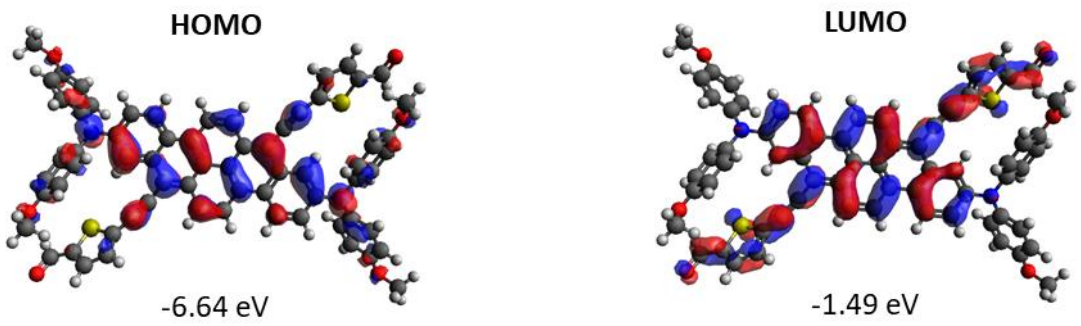

Figure S57: Kohn–Sham molecular orbitals of compound **8'** based on calculation at ωB97xD/6-31+G(d,p) level using the PCM solvation model in chloroform with a superfine integration grid.

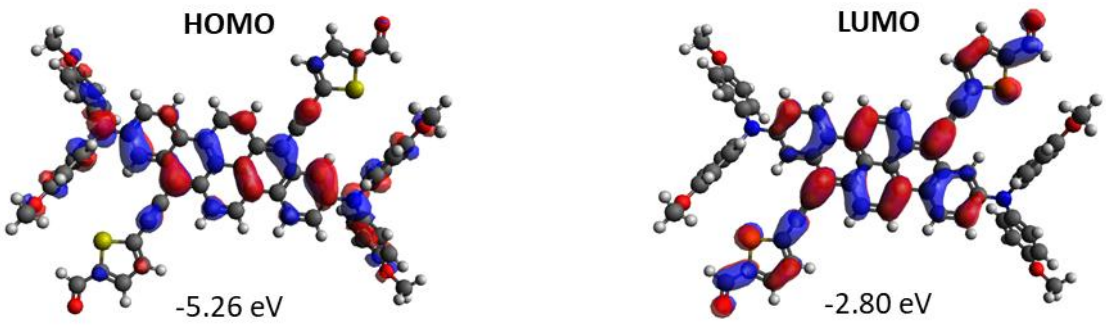

Figure S58: Kohn–Sham molecular orbitals of compound **8'** based on geometry optimization at HF/6-31+G(d,p) level and energy calculation at PBE0/6-31+G(d,p) level using the PCM solvation model in chloroform with a superfine integration grid.

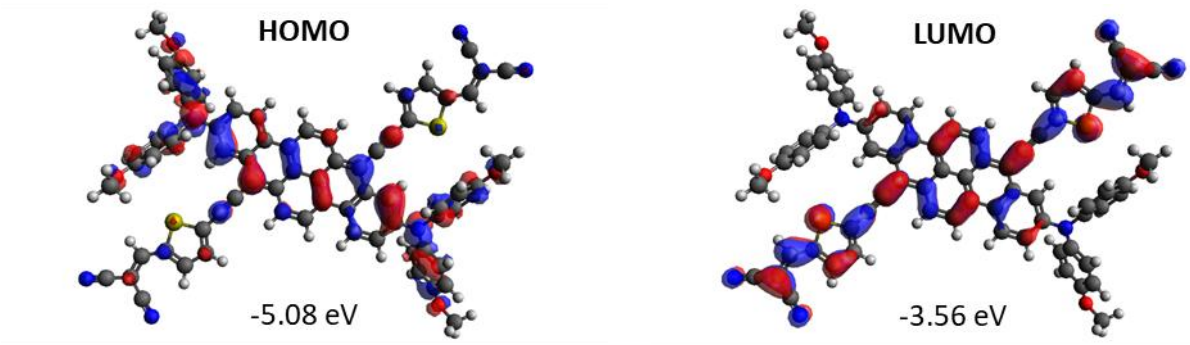

Figure S59: Kohn–Sham molecular orbitals of compound **9'** based on calculation at B3LYP/6-31+G(d,p) level using the PCM solvation model in chloroform with a superfine integration grid.

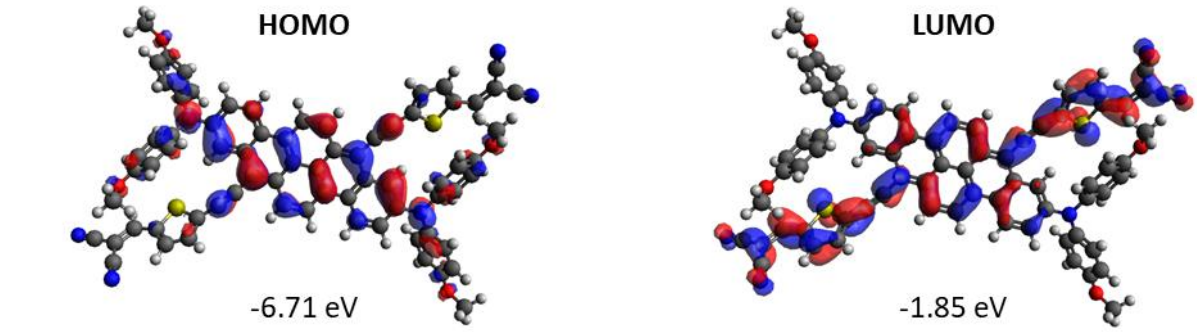

Figure S60: Kohn–Sham molecular orbitals of compound **9'** based on calculation at ωB97xD/6-31+G(d,p) level using the PCM solvation model in chloroform with a superfine integration grid.

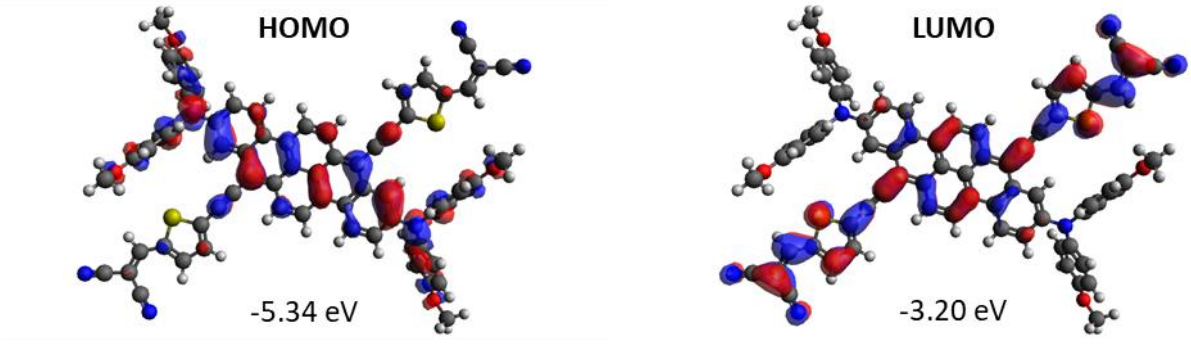

Figure S61: Kohn–Sham molecular orbitals of compound **9'** based on geometry optimization at HF/6-31+G(d,p) level and energy calculation at PBE0/6-31+G(d,p) level using the PCM solvation model in chloroform with a superfine integration grid.

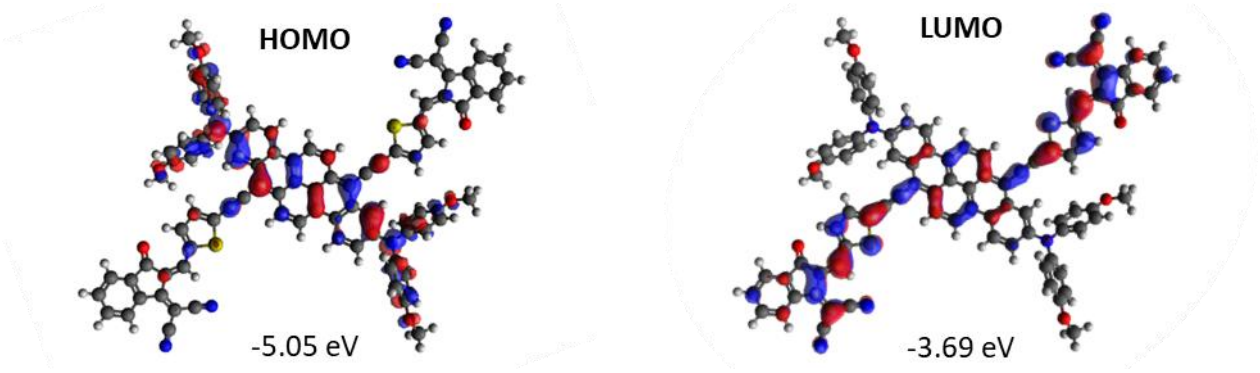

Figure S62: Kohn–Sham molecular orbitals of compound **10'** based on calculation at B3LYP/6-31+G(d,p) level using the PCM solvation model in chloroform with a superfine integration grid.

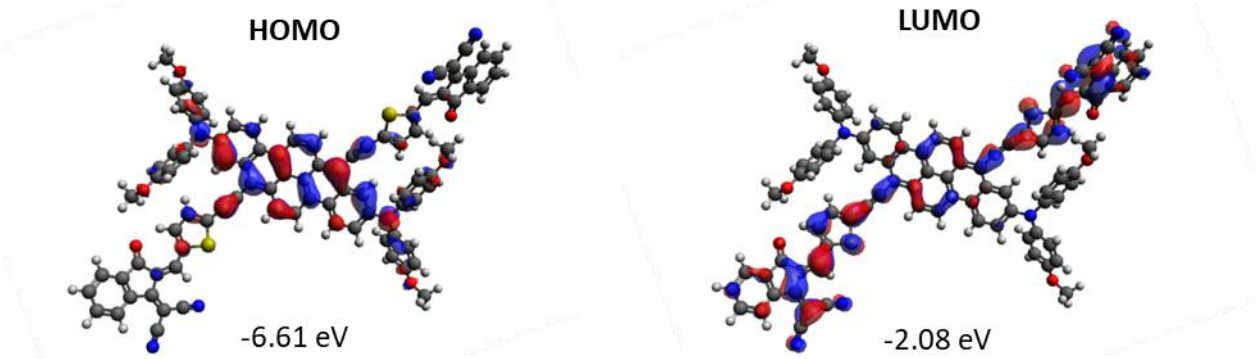

Figure S63: Kohn–Sham molecular orbitals of compound **10'** based on calculation at ωB97xD/6-31+G(d,p) level using the PCM solvation model in chloroform with a superfine integration grid.

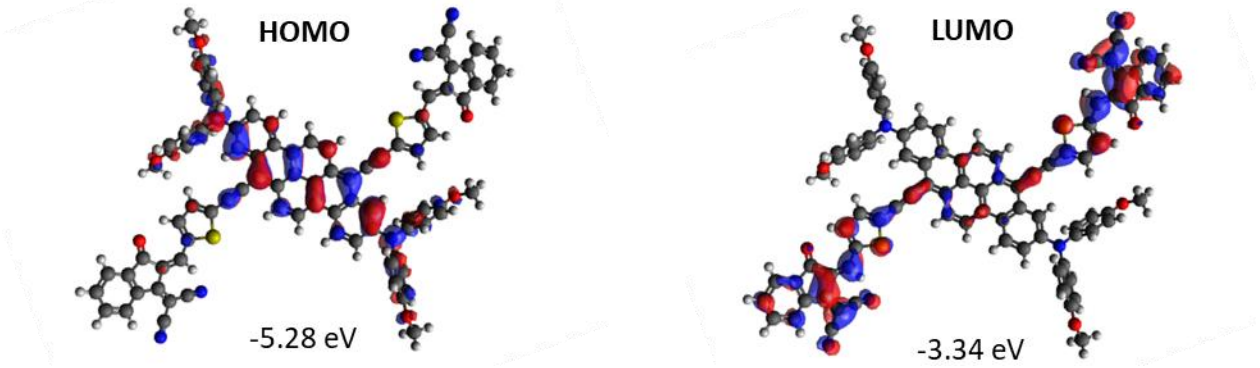

Figure S64: Kohn–Sham molecular orbitals of compound **10'** based on geometry optimization at HF/6-31+G(d,p) level and energy calculation at PBE0/6-31+G(d,p) level using the PCM solvation model in chloroform with a superfine integration grid.

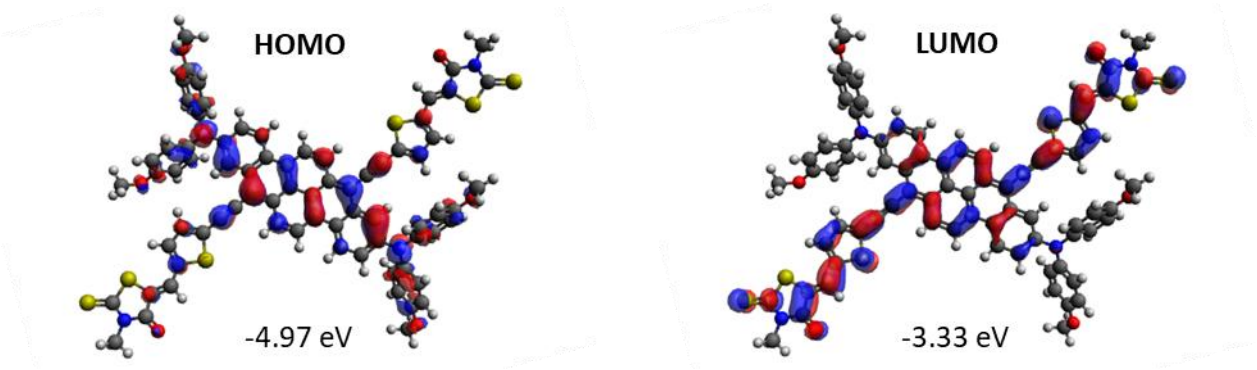

Figure S65: Kohn–Sham molecular orbitals of compound **11'** based on calculation at B3LYP/6-31+G(d,p) level using the PCM solvation model in chloroform with a superfine integration grid.

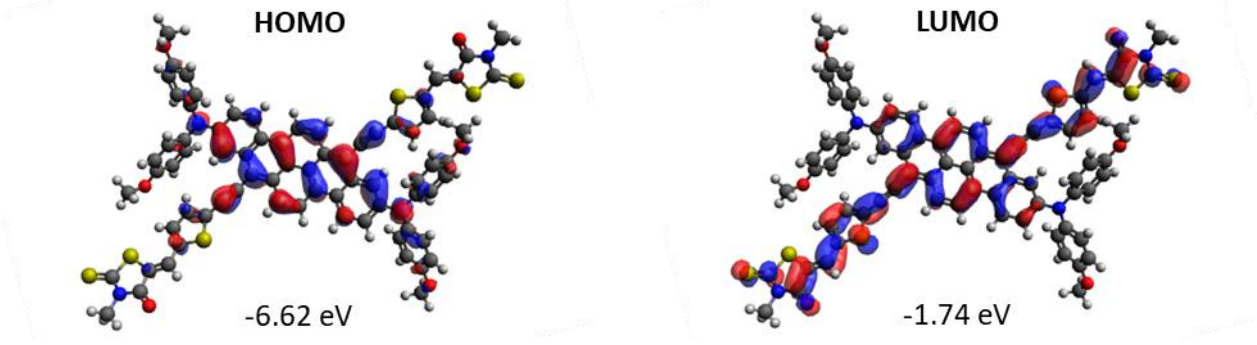

Figure S66: Kohn–Sham molecular orbitals of compound **11'** based on calculation at ωB97xD/6-31+G(d,p) level using the PCM solvation model in chloroform with a superfine integration grid.

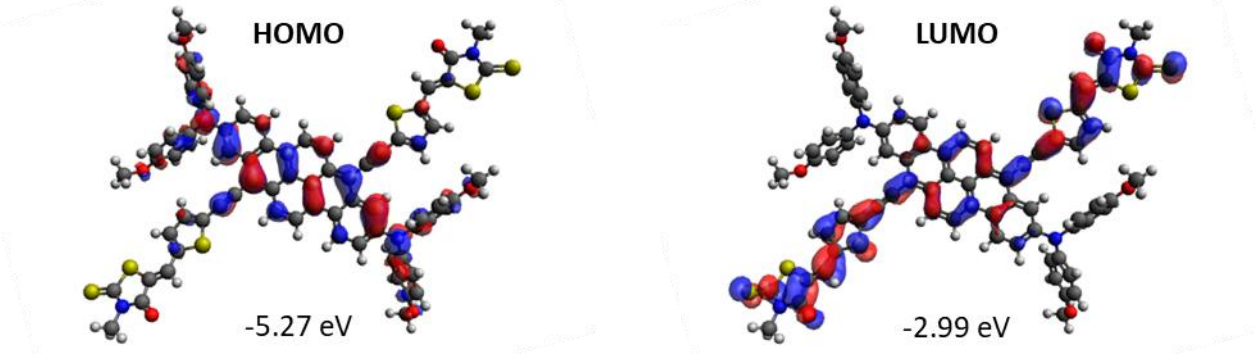

Figure S67: Kohn–Sham molecular orbitals of compound **11'** based on geometry optimization at HF/6-31+G(d,p) level and energy calculation at PBE0/6-31+G(d,p) level using the PCM solvation model in chloroform with a superfine integration grid.

Organic Solar Cells Devices

Organic Solar Cells (OSC) Fabrication: The devices were prepared in a direct and inverted architectures. The direct structure was ITO/PEDOT:PSS/Active layer/Ca/Al and the inverted one was ITO/ZnO/Active layer/MoO_3/Ag. The devices were prepared using commercial ITO-coated glass substrates (1.5 × 1.5 cm^2, 10 Ω□, VisionTek). The substrates were scrubbed with Q-tip using cleanroom detergent water and cleaned using a sequence of sonic baths: i. cleanroom detergent water (15 minutes), ii. deionized water (3 x 5 minutes), iii. acetone (5 minutes), and iv. isopropanol (5 minutes). The ITO glass substrates were then treated in a UV-Ozone chamber for 15 minutes. For the direct architecture, PEDOT:PSS solution (AI4083) was filtered over 0.45 μm (PTFE) and spin-coated at 5000 rpm onto the ITO, patterned with Q-tip using water and annealed at 150 °C for 15 minutes under ambient atmosphere. For the inverted architecture, the sol-gel ZnO solution (0.1995 g (908.89 μmol) of zinc(II) diacetate dihydrate and 55.5 μL (917.67 μmol) of 2-aminoethanol were added to 5.895 mL of absolute ethanol and stirred overnight) was spin-coated at 2000 rpm onto the ITO, patterned with Q-tip using isopropanol and annealed at 180 °C for 30 minutes under ambient atmosphere. The active layer solutions were prepared the day before the deposition as follow: the donor (8-11, P3HT) and acceptor (PCBM, 8-11) materials were mixed in a 20 mg/mL 1:1 D:A weight ratio in chlorobenzene and left to stir overnight at 90 °C. This solution was then spin-coated at 90 °C, with a spin speed of 900 rpm in a nitrogen-filled glovebox. No annealing process was performed. Finally, the substrates were taken to a vacuum-deposition chamber and placed under a high vacuum at $1x10^{-6}$ mm Hg. In direct architecture, 80 nm of calcium and 80 nm of aluminum were evaporated through a shadow mask. In inverted architecture, 7 nm of molybdenum trioxide and 70 nm of silver were evaporated through a shadow mask. The shadow

mask defined 4 devices with an active area of 10.5 mm^2 each. To perform the measurements under ambient atmosphere (External Quantum Efficiencies, EQE), the devices were encapsulated using half-cutted microscope coverslip glued with Delo® Katiobond® LP655 epoxy photo resin cured 40 seconds under UV irradiation.

OSC Characterization: The current density-voltage curves (J-V) were measured using a Keithley 2400 source meter in a nitrogen-filled glovebox. The AM 1.5 spectrum was reproduced with a light intensity of 100 mW cm^{-2} using a Xenon source with the Newport LCS-100 filter and calibrated silicon reference cell from Newport Co. Data and parameters were obtained from a LabVIEW program. The External Quantum Efficiencies (EQE) spectra were measured using a PVE300 Photovoltaic EQE from Bentham Co. under ambient atmosphere in a range of 300 to 800 nm with 5 nm step. The active layer thicknesses were measured with an MFP-3D Origin AFM from Asylum Research in tapping mode under ambient atmosphere using a AC160TS-R3 probe.

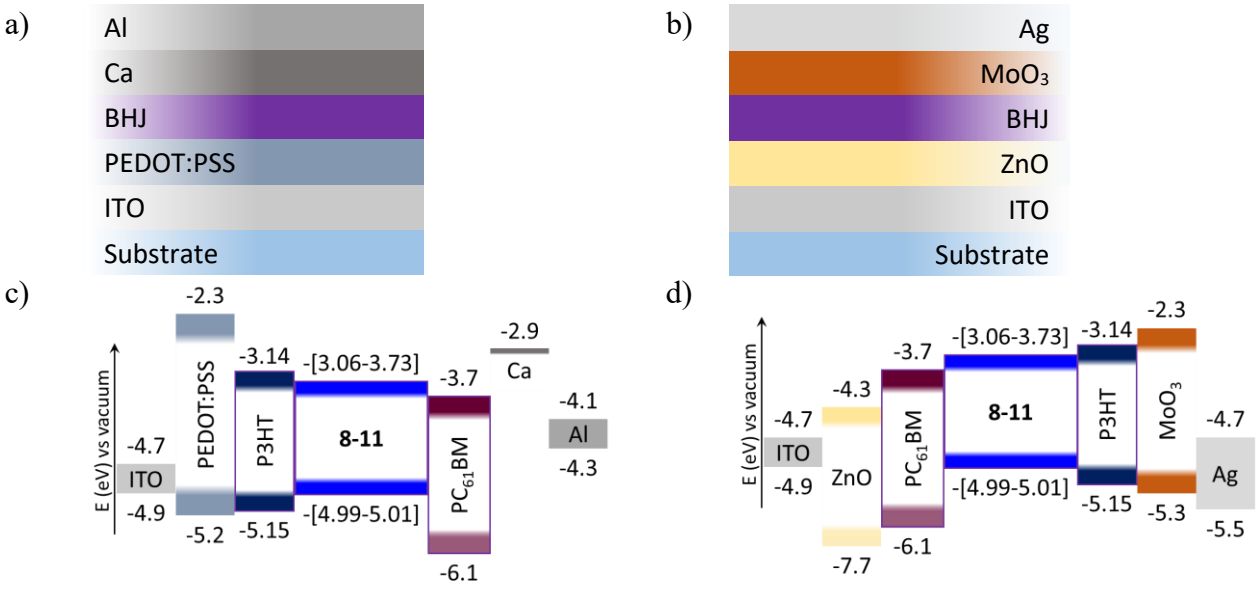

Figure S68: Solar cells configuration (a-b) and energy diagram of the solar cell components (b-d) of direct (a and c) and inverted (b and d) geometries.

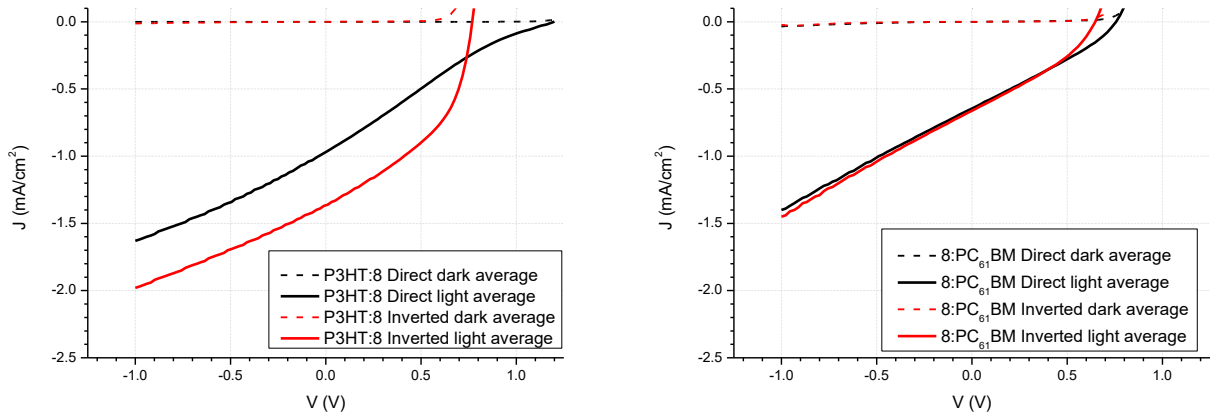

Figure S69: J-V average curves of compound **8** in direct (black) and inverted (red) geometries with P3HT (left) or $PC_{61}BM$ (right).

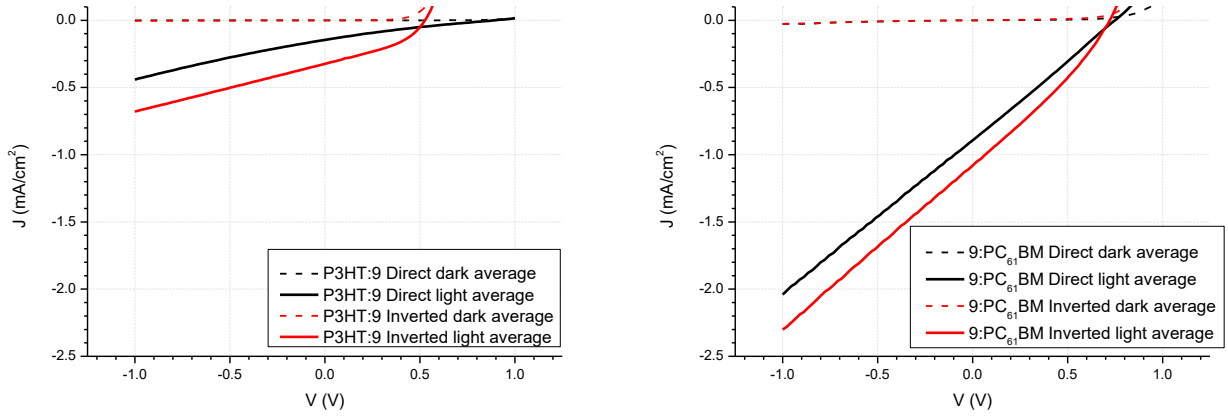

Figure S70: J-V average curves of compound **9** in direct (black) and inverted (red) geometries with P3HT (left) or $PC_{61}BM$ (right).

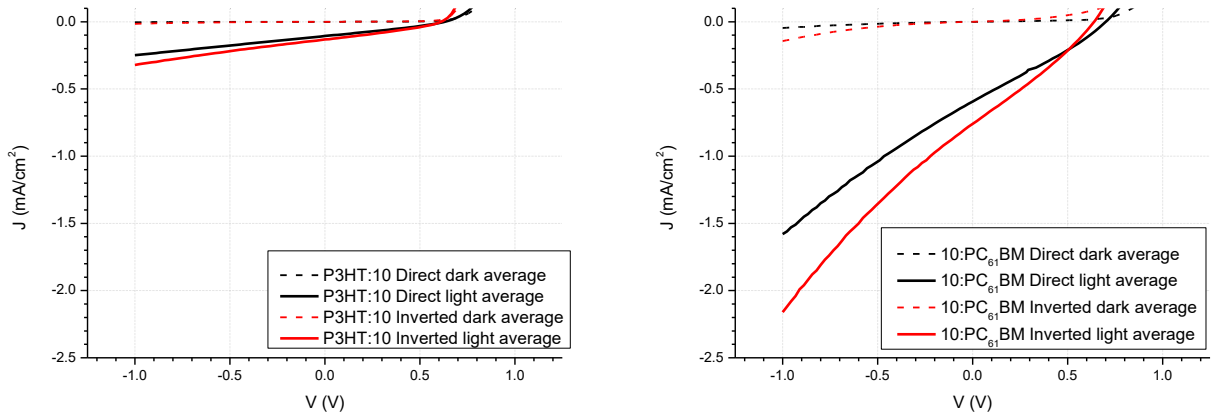

Figure S71: J-V average curves of compound **10** in direct (black) and inverted (red) geometries with P3HT (left) or $PC_{61}BM$ (right).

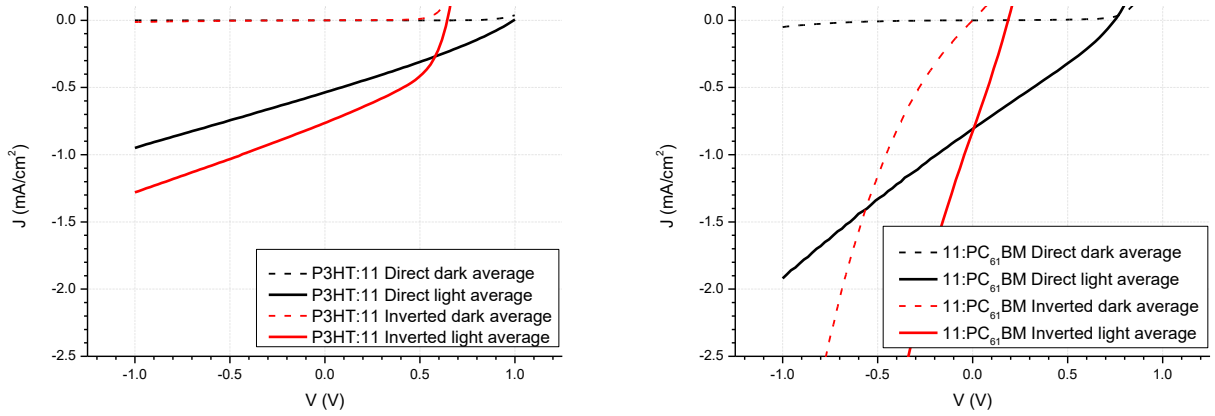

Figure S72: J-V average curves of compound **11** in direct (black) and inverted (red) geometries with P3HT (left) or $PC_{61}BM$ (right).

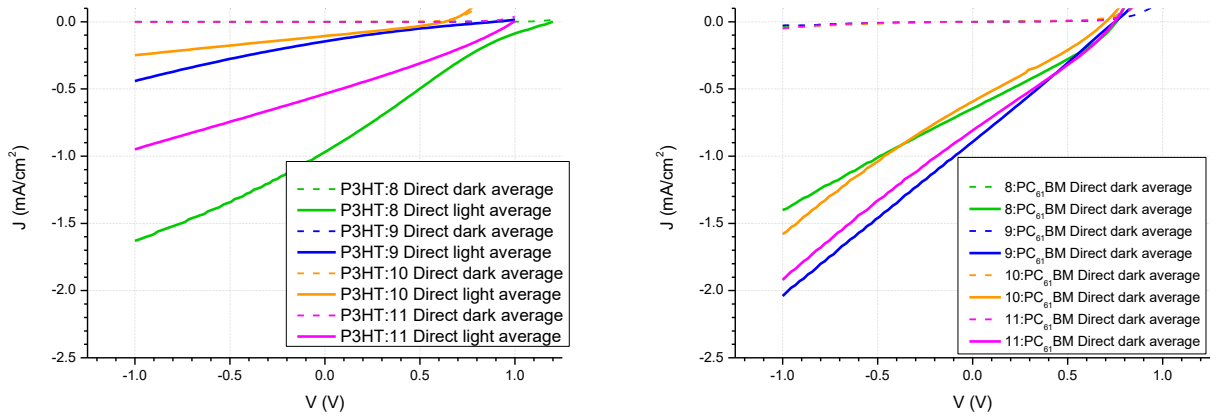

Figure S73: J-V average curves of compound **8-11** in direct architecture with P3HT (left) or $PC_{61}BM$ (right).

Table S12: Organic solar cell results (average ± standard deviation) for compound **8-11** with P3HT in direct architecture.

Compound	R - Voc (x 10 kohm)	Shunt R (x 10^2 Mohm)	J_{sc} (mA/cm²)	V_{oc} (V)	FF (%)	PCE (%)	Series R (Mohm)	BHJ Thickness (x 10 nm)
8[(a)]	1.9	0.4 ± 0.2	0.97 ± 0.05	1.198	21.0	0.26 ± 0.01	3 ± 1	7.5 ± 0.5
9	7 ± 1	0.6 ± 0.3	0.15 ± 0.01	0.90 ± 0.01	20.4 ± 0.9	0.026 ± 0.002	0.17 ± 0.05	7 ± 1
10	3 ± 2	0.03 ± 0.01	0.11 ± 0.01	0.63 ± 0.01	30 ± 2	0.021 ± 0.003	0.01 ± 0.01	8.0 ± 0.8
11	1.05 ± 0.08	2 ± 2	0.54 ± 0.04	0.8 ± 0.4	29.5 ± 0.3	0.15 ± 0.01	0.059 ± 0.005	6 ± 1

[(a)] It happened that only 1 of 16 devices had worked of the measurements over 1.00 V resulting in no standard deviation available for V_{OC} and FF values. Average values were obtained from 8 of 24 devices with measurements stopped at 1.00 V.

Table S13: Organic solar cell results (average ± standard deviation) for compound **8-11** with $PC_{61}BM$ in direct architecture.

Compound	R - Voc (kohm)	Shunt R (x 10^2 kohm)	J_{sc} (mA/cm²)	V_{oc} (V)	FF (%)	PCE (%)	Series R (kohm)	BHJ Thickness (x 10 nm)
8	3.7 ± 0.2	2.0 ± 0.2	0.645 ± 0.007	0.757 ± 0.003	29.3 ± 0.4	0.143 ± 0.001	0.21 ± 0.01	6 ± 1
9	8.1 ± 0.4	3 ± 2	0.89 ± 0.02	0.749 ± 0.005	25.70 ± 0.09	0.172 ± 0.005	3.1 ± 0.6	7 ± 3
10	6.8 ± 0.6	2.2 ± 0.8	0.59 ± 0.02	0.70 ± 0.02	28.0 ± 0.5	0.117 ± 0.006	2.1 ± 0.2	5 ± 1
11	4.5 ± 0.4	2.5 ± 0.8	0.81 ± 0.01	0.75 ± 0.02	27.9 ± 0.2	0.169 ± 0.007	0.31 ± 0.06	7.0 ± 0.8

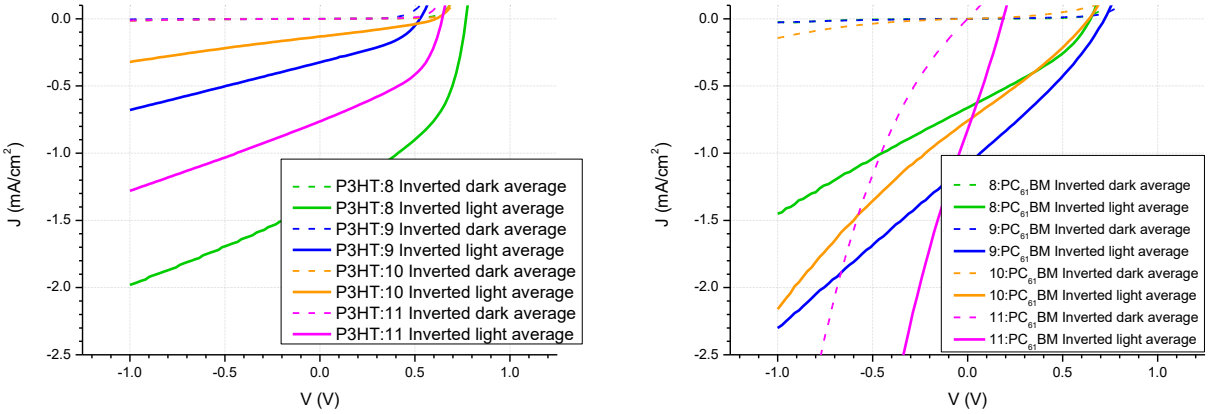

Figure S74: J-V average curves of compound **8-11** in inverted architecture with P3HT (left) or $PC_{61}BM$ (right).

Table S14: Organic solar cell results (average ± standard deviation) for compound **8-11** with P3HT in inverted architecture.

Compound	R - Voc (x 10 kohm)	Shunt R (Mohm)	J_{sc} (mA/cm²)	V_{oc} (V)	FF (%)	PCE (%)	Series R (x 10^2 ohm)	BHJ Thickness (x 10 nm)
8	0.064 ± 0.006	1.4 ± 0.9	1.36 ± 0.07	0.77 ± 0.01	45 ± 1	0.46 ± 0.03	2.2 ± 0.4	6 ± 2
9	0.36 ± 0.06	2.4 ± 0.7	0.32 ± 0.02	0.53 ± 0.03	39 ± 2	0.067 ± 0.004	2.9 ± 0.1	8 ± 1
10	1.2 ± 0.4	0.4 ± 0.3	0.137 ± 0.005	0.59 ± 0.04	30.8 ± 0.9	0.025 ± 0.003	4 ± 2	8.8 ± 0.7
11	0.11 ± 0.02	2 ± 2	0.76 ± 0.03	0.65 ± 0.03	43 ± 2	0.211 ± 0.009	4 ± 2	8 ± 1

Table S15: Organic solar cell results (average ± standard deviation) for compound **8-11** with $PC_{61}BM$ in inverted architecture.

Compound	R - Voc (kohm)	Shunt R (x 10^2 kohm)	J_{sc} (mA/cm²)	V_{oc} (V)	FF (%)	PCE (%)	Series R (x 10^2 ohm)	BHJ Thickness (x 10 nm)
8[(a)]	2.45	3.46	0.663	0.647	33.2	0.142	4.82	5 ± 2
9	3.1 ± 0.6	6 ± 5	1.08 ± 0.03	0.72 ± 0.03	29.6 ± 0.4	0.23 ± 0.01	7.7 ± 0.9	8 ± 1
10	4.3 ± 0.5	0.7 ± 0.3	0.76 ± 0.03	0.65 ± 0.07	28.6 ± 0.5	0.140 ± 0.008	1.2 ± 0.1	5 ± 1
11	1.8 ± 0.3	0.024 ± 0.001	0.8 ± 0.2	0.18 ± 0.04	27 ± 1	0.04 ± 0.02	0.8 ± 0.6	6 ± 2

[(a)] It happened that only 1 of 16 devices had worked of the measurements resulting in no standard deviation available.

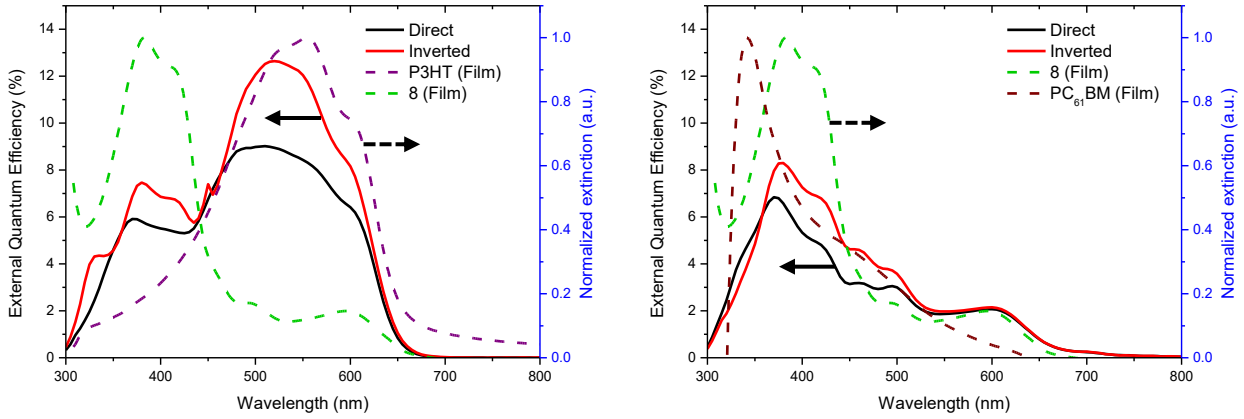

Figure S75: Comparison between the UV-vis spectra of single materials (dashed lines) and EQE spectra in direct (solid dark line) or inverted (solid red line) architectures of the P3HT:**8** (left) and **8**:$PC_{61}BM$ (right) blends.

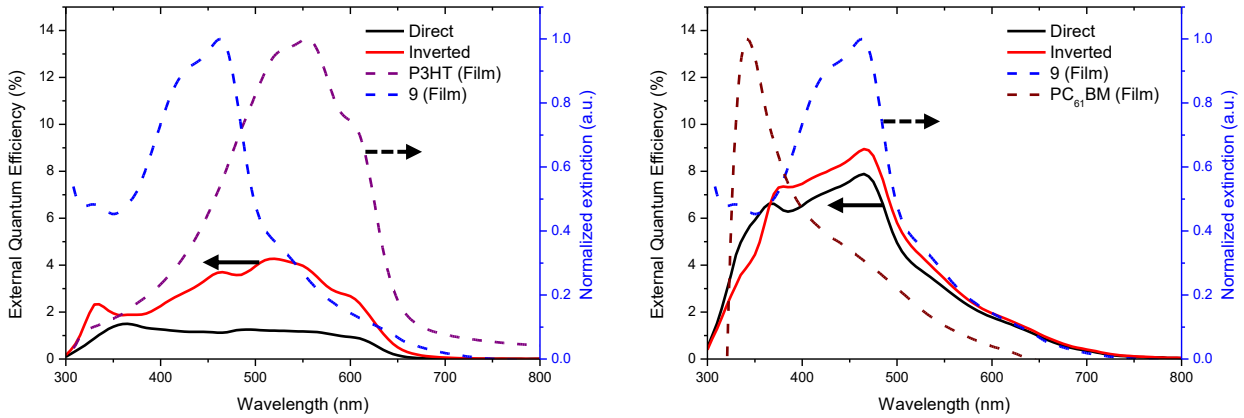

Figure S76: Comparison between the UV-vis spectra of single materials (dashed lines) and EQE spectra in direct (solid dark line) or inverted (solid red line) architectures of the P3HT:**9** (left) and **9**:$PC_{61}BM$ (right) blends.

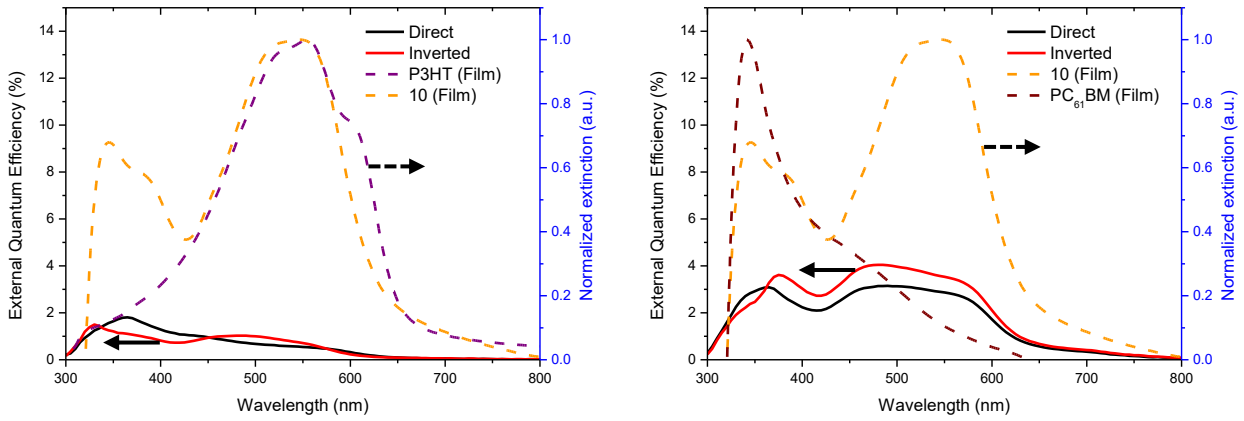

Figure S77: Comparison between the UV-vis spectra of single materials (dashed lines) and EQE spectra in direct (solid dark line) or inverted (solid red line) architectures of the P3HT:**10** (left) and **10**:$PC_{61}BM$ (right) blends.

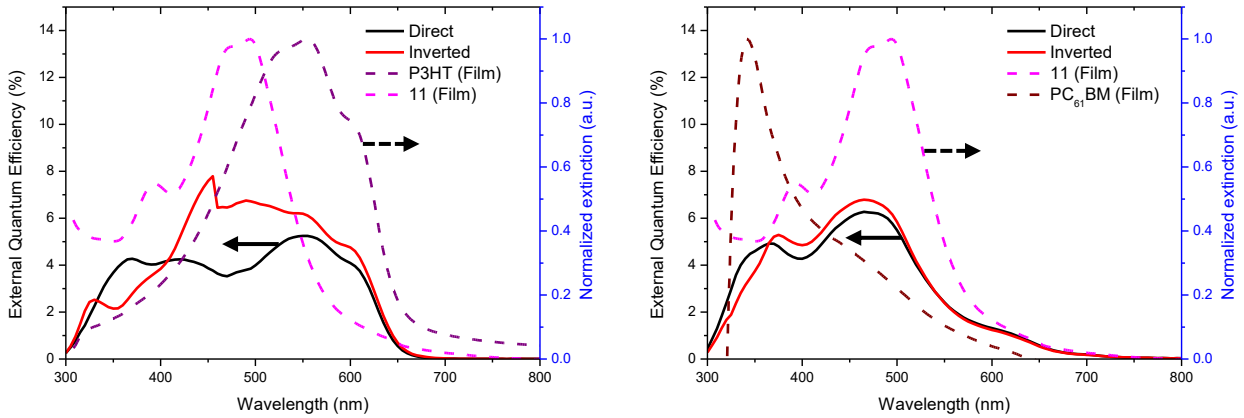

Figure S78: Comparison between the UV-vis spectra of single materials (dashed lines) and EQE spectra in direct (solid dark line) or inverted (solid red line) architectures of the P3HT:**11** (left) and **11**:$PC_{61}BM$ (right) blends.

References

1. J. R. Aranzaes, M.-C. Daniel and D. Astruc, *Canadian Journal of Chemistry*, 2006, **84**, 288-299.
2. N. G. Connelly and W. E. Geiger, *Chemical Reviews*, 1996, **96**, 877-910.
3. J. Pommerehne, H. Vestweber, W. Guss, R. F. Mahrt, H. Bässler, M. Porsch and J. Daub, *Advanced Materials*, 1995, **7**, 551-554.
4. A. J. Bard, L. R. Faulkner and L. R. Faulkner, *Electrochemical methods : fundamentals and applications*, J. Wiley, New York, 2nd ed. edn., 2001.
5. C. M. Cardona, W. Li, A. E. Kaifer, D. Stockdale and G. C. Bazan, *Advanced Materials*, 2011, **23**, 2367-2371.
6. G. P. Kissling, B. Ruhstaller and K. P. Pernstich, *Organic Electronics*, 2023, **122**, 106888.
7. F. Gagnon, V. Tremblay, A. Soldera, M. U. Ocheje, S. Rondeau-Gagné, M. Leclerc and J.-F. Morin, *Materials Advances*, 2022, **3**, 599-603.
8. B. Sambathkumar, P. S. V. Kumar, K. Saurav, S. S. K. Iyer, V. Subramanian and N. Somanathan, *New Journal of Chemistry*, 2016, **40**, 3803-3811.
9. Y. Hu, W. Cai, L. Ying, D. Chen, X. Yang, X.-F. Jiang, S. Su, F. Huang and Y. Cao, *Journal of Materials Chemistry C*, 2018, **6**, 2690-2695.
10. J. Grolleau, *Synthesis*, 2015, **47**, 3901-3906.
11. J. Bertrandie, J. Han, C. S. P. De Castro, E. Yengel, J. Gorenflot, T. Anthopoulos, F. Laquai, A. Sharma and D. Baran, *Advanced Materials*, 2022, **34**, 2202575.